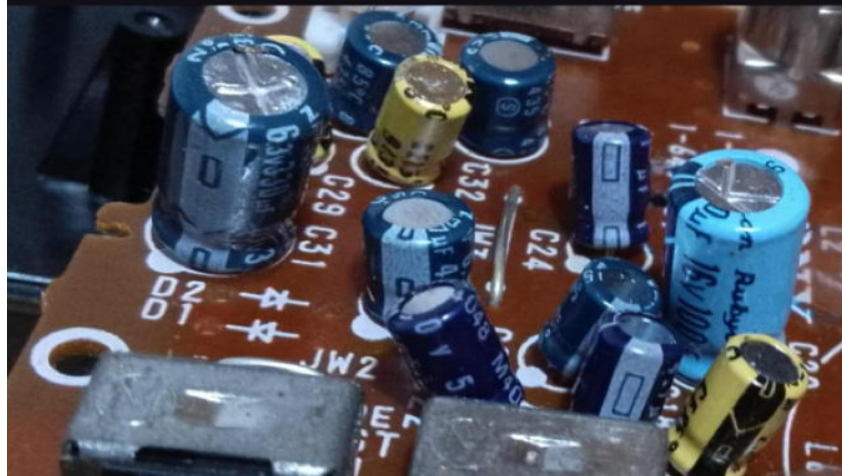


Functional materials

An introduction with worked examples

Haixue Yan & Harshad Bhadeshia



Functional materials

An introduction with worked examples

Haixue Yan

Harshad K. D. H. Bhadeshia

Queen Mary University of London
School of Engineering and Materials Science

FUNCTIONAL MATERIALS – an introduction with worked examples

PUBLISHED INDEPENDENTLY BY THE AUTHORS
Mile End Road
London E1 4NS United Kingdom

<https://www.sems.qmul.ac.uk/>

© Haixue Yan and Harshad K. D. H. Bhadeshia, 2025

This publication is in copyright. Subject to statutory exception and to the provision of the relevant collective licensing agreements, no reproduction of any part may take place without the written permission of the authors.

First published 2025

Functional materials – an introduction with worked examples
written by Haixue Yan and Harshad K. D. H. Bhadeshia
Includes index
ISBN 9798289772268 Paperback

The publishers bear no responsibility for the persistence or accuracy of URLs for external or third-party internet websites referred to in this publication and do not guarantee that any content on such websites is, or will remain, accurate or appropriate.

Typeset in Computer Modern font
by the authors

Preface

Functional materials represent those specifically designed to exhibit unique and often tuneable physical or chemical properties in response to external stimuli. They are valued for their ‘function’ – their ability to perform a specific task or change their behaviour under certain conditions. They can change their shape, electrical conductivity, magnetic properties, colour, or other characteristics when exposed to temperature, pressure, electric fields, magnetic fields, light, or chemical changes. Materials with electrical conductivity between that of a metal and an insulator are the basis of electronics. Long-chain molecules too have functionalities, including flexibility and charge mobility. Ordered arrangements of molecules can be useful in optics. Inorganic, non-metallic solids such as ceramics can be exploited for properties like piezoelectricity, and for elevated temperature service.

Some functional materials can exhibit several of these properties simultaneously, leading to sophisticated applications. Variety can be nurtured by controlled synthesis, doping, or structuring over a range of length scales.

This short book serves as an *introduction*, providing sufficient and complete coverage of concepts suitable for a final year undergraduate course. It includes worked examples to aid understanding and is designed for third-year students across a range of disciplines, including materials science, engineering, chemical engineering, physics, chemistry, Earth sciences, and general physical sciences. For those wishing to explore the topics in greater depth, references are provided at the end of each chapter.

Throughout this book, braces are used to imply a functional relationship, i.e., $f\{x\}$ means that f is a function with an argument x .

The authors also express gratitude to those who provided images and information, noting that these contributions are acknowledged within the text.

Haixue Yan and Harshad K. D. H. Bhadeshia

The year 2025
London.

Contents

Nomenclature	viii
1 Electrical conductivity and breakdown	1
1.1 Introduction	1
1.2 Electronic conductors	3
Example 1: Activation energy for electronic conduction, $\text{Sr}_2\text{Nb}_2\text{O}_7$	4
1.3 Mechanisms of conduction	5
Example 2: Metallic hydrogen	5
Example 3: Metal and titanium dioxide	8
Example 4: Resistivity and perfection	9
Example 5: Quantum dots	10
1.4 More on ionic conduction	10
1.5 Semiconductors: p - n junctions	12
1.6 Varistors	14
1.7 Thermistors	15
1.8 Electrical breakdown of insulators	17
1.9 North Hyde 275 kV electricity substation failure	20
Example 6: Spark machining	20
Example 7: Varistor heating by lightning strike	21
Example 8: Artificial muscles	22
<i>Bibliography</i>	
2 Dielectrics	25
2.1 Introduction	25
2.2 Fundamentals of dielectric materials	26
2.2.1 Polarisation	27
Example 9: Polarisation of tetragonal barium titanate	28
2.3 Variety of polarisations	30
2.4 Capacitor subjected to alternating voltage	32
2.4.1 Very large permittivity	36
2.4.2 Multilayered ceramic capacitors	36
2.4.3 Dielectric resonator	36
2.4.4 Terahertz probes	37
Example 10: Sintering and dielectrics	38
Example 11: Temperature coefficient of resonant frequency	40
Example 12: Strange dielectric	40
Example 13: Variation in Curie point	41
<i>Bibliography</i>	
3 Ferroelectric oxides	43
3.1 Introduction	43
3.2 Domain structures	45

3.3	Characterisation	48
3.3.1	Alumina	49
3.3.2	Bismuth ferrite	50
3.3.3	Sodium potassium niobate	51
3.4	Poling	53
3.5	Relaxor ferroelectrics	54
3.6	Antiferroelectrics	55
	Example 14: Permittivity as a function of temperature	57
	Example 15: Poling conditions for ferroelectric ceramics	57
3.7	Electrocaloric effect	58
	Example 16: Electrocaloric material selection	58
<i>Bibliography</i>		
4	Piezoelectrics	61
4.1	Introduction	61
4.2	Crystallography	62
4.3	Anisotropy	65
	Example 17: Piezoelectric response	67
4.3.1	Piezoelectric efficiency	68
4.3.2	Measurement of efficiency	69
4.3.3	Bank of properties	70
	Example 18: Medical transducer	72
4.4	Typical piezoelectric materials	72
4.4.1	Some non-ferroelectric piezoelectrics	72
	Example 19: Rise time	74
	Example 20: Tourmaline device	75
4.5	Ferroelectrics as piezoelectric materials	77
4.5.1	Lead replacement	78
4.5.2	$K_{0.5}Na_{0.5}NbO_3$	79
4.5.3	$Bi_{0.5}Na_{0.5}TiO_3$	80
4.5.4	Layer-structured ferroelectrics	80
4.6	Field-induced effects in ferroelectrics	82
	Example 21: $Pb(Zr_xTi_{1-x})O_3$ polarisation versus electric field	82
	Example 22: $Pb(Zr_xTi_{1-x})O_3$ strain versus electric field	84
<i>Bibliography</i>		
5	Organic materials	87
5.1	Introduction	87
5.2	Polarisation mechanisms in polymers	88
5.3	Polymer composite dielectrics	90
	Example 23: Electrical fields in polymer composite	91
5.4	Dielectric polymers: orientational polarisation	93
5.5	Molecular ferroelectrics	95
	Example 24: Design of wearable ferroelectric device	95
5.6	Conducting polymers	96
5.7	Organic light-emitting diode	97
	Example 25: Organic light emitting diode	98
<i>Bibliography</i>		

6 Thermoelectrics	100
6.1 Seebeck effect	100
Example 26: Sign of Seebeck coefficient	102
Example 27: Broken thermocouple	103
Example 28: Criteria for thermoelectric performance assessment	104
Example 29: Efficiency of a refrigerator	105
6.2 Conflicting thermoelectric requirements	105
6.3 Peltier effect	106
6.4 Phonon-Glass Electron-Crystal	108
<i>Bibliography</i>	
7 Optical and magnetic materials	110
7.1 Optical materials	110
Example 30: Opacity	111
7.2 Metals	111
7.3 Dielectrics	112
Example 31: Absorption as a function of thickness	113
7.4 Linear optics	114
7.5 Anisotropy of refractive index	115
7.6 Non-linear optics	116
Example 32: Convergent lens	118
Example 33: Optical switch	118
7.7 Types of magnetism	120
7.7.1 Diamagnetism	121
Example 34: Graphite & magnetic field	122
7.7.2 Paramagnetism	124
7.7.3 Ferromagnetism, antiferromagnetism and ferrimagnetism	125
7.8 Magnetic domains	125
Example 35: Tetrataenite	127
<i>Bibliography</i>	
8 Two-dimensional materials, superconductors	130
8.1 Introduction	130
8.2 Hall effect	130
8.3 Graphene device	131
Example 36: Transparency of graphene	133
8.4 Superconductors	134
8.4.1 Meissner effect	136
Example 37: Estimation of T_{sc}	136
<i>Bibliography</i>	
8.5 Random questions	141
Subject index	143

Nomenclature

α_R	Temperature coefficient of resistivity
ϵ_o	Permittivity of free space, $8.854 \times 10^{-12} \text{ F m}^{-1} \equiv \text{C}^2 \text{ N}^{-1} \text{ m}^{-2}$
ϵ_r	Relative permittivity (≥ 1), same as dielectric constant
κ	Thermal conductivity, $\text{J m}^{-1} \text{ s}^{-1} \text{ K}^{-1} \equiv \text{W m}^{-1} \text{ K}^{-1}$
μ	Mobility of electrical charge, $\text{m}^2 \text{ V}^{-1} \text{ s}^{-1}$
μ^\uparrow	Dipole moment, C m
μ_o	Magnetic permittivity of free space, H m^{-1} or N A^{-2}
μ_B	Bohr magneton, $\approx 9.274 \times 10^{-24} \text{ J T}^{-1}$
μ_r	Relative magnetic permittivity
ν_o, ν_a	Resonance and antiresonance frequencies, respectively, s^{-1} , Hz
ρ	Electrical resistivity, $\Omega \text{ m}$
σ	Electrical conductivity, $\text{C s}^{-1} \text{ V}^{-1} \equiv \text{S m}^{-1} \equiv \Omega^{-1} \text{ m}^{-1}$
σ_s	Stress, Pa
τ	Relaxation time, s
χ_e	Electrical susceptibility
a, b, c	Symbols for lattice parameters, m
A	Area, m^2 , or wave amplitude
b_i	Empirical constants
B	Magnetic flux, Tesla $\equiv \text{V s m}^{-2}$
c	Speed of light in a vacuum, m s^{-1}
C	Capacitance, $\text{F} \equiv \text{C V}^{-1}$
d_{33}	Coefficient representing piezoelectric performance, C N^{-1}
\mathcal{D}	Electrical displacement (quantity of charge displaced), C m^{-2}
E	Electric field, V m^{-1}
E_{emf}	Electromotive force, V
E_F	Fermi level, eV or J
E_g	Band gap, eV
F	Faraday constant, $9.648 \times 10^4 \text{ C mol}^{-1}$
\hbar	Reduced Planck constant, $1.054 \times 10^{-34} \text{ J s}$
H	Magnetic field, A m^{-1}
I	Electrical current, A
J	Electrical current density, A m^{-2}
k	Boltzmann constant, $1.3807 \times 10^{-23} \text{ J K}^{-1}$
k_e	Efficiency of piezoelectric device in converting mechanical to electrical energy
m_e	Rest mass of electron, $9.109 \times 10^{-31} \text{ kg}$
n	Refractive index
n	Number of charge carriers per unit volume, m^{-3}
N	Number
\mathcal{P}	Polarisation field, C m^{-2}

\mathcal{P}_s	Spontaneous polarisation
q	Electrical charge, C
Q	Activation energy, J mol^{-1} or eV atom^{-1}
\mathcal{R}	Electrical resistance, Ω
R	Gas constant, $8.3143 \text{ J mol}^{-1} \text{ K}^{-1}$
S_e	Seebeck coefficient, V K^{-1}
t	Time, s
T	Temperature, K
T_B	Burns temperature for relaxor ferroelectrics, K
T_C	Curie point, K
T_f	Temperature below which polarised regions in relaxors adopt a frozen configuration
T_{sc}	Temperature below which a material becomes a superconductor
v	Drift velocity of charge, m s^{-1}
\dot{V}	Rate of change of voltage, V s^{-1}
V	Voltage, V
\mathcal{Z}	Part of the figure of merit, with ZT being dimensionless
z_t	Thickness, m
z_w	Width, m
Z	Impedance, Ω .

Chapter 1

Electrical conductivity and breakdown

1.1 INTRODUCTION

The phenomenon of electrical conductivity is fundamental to a vast array of technologies and applications that permeate our daily lives. Metals, such as copper, are exemplary conductors of electricity because of their delocalised electrons that are not tightly bound to individual atoms but rather are free to move throughout the metallic lattice. When an external electric field (E) is applied, they can drift, constituting an electrical current.

Insulating plastics have very low conductivity because the electrons within are tightly bound to their respective atoms and molecules, forming strong covalent bonds. Consequently, there is no current flow when an electric field is applied. This makes plastics ideal for insulating electrical cables and components, preventing short circuits and ensuring the safe and controlled passage of electricity.

Charged particles such as electrons or ions must be able to move within the material to achieve electrical conduction. Their response to an applied field defines electrical conduction. Riecke [1, 2] and Drude [3] treated this conduction in terms of a drift velocity v with which a charge q drifts through metal but losing all of its original momentum (vm where m is the mass of the moving charge) when colliding with a metal atom. The average momentum acquired by the charge under the influence of the electrical field is $\frac{1}{2}qEt$, where t is the time between successive collisions. By balancing these terms, it follows that flux of charged particles is expressed as a current density J across a unit cross-sectional area

$$J = nqv = \frac{nEq^2t}{2m} \equiv nq\mu E \quad (1.1a)$$

- J is the current density, A m^{-2} . An ampere is a coulomb of charge moving past a point in a second.
- q is the charge in coulombs (C) per particle, expected to be a multiple of the electronic charge $e = -1.602 \times 10^{-19} \text{ C}$.
- v is the drift velocity of the charge carrier, m s^{-1} . This can be written μE where μ ($\text{m}^2 \text{ V}^{-1} \text{ s}^{-1}$) is known as the mobility of the charge carrier under

2 CHAPTER 1. ELECTRICAL CONDUCTIVITY AND BREAKDOWN

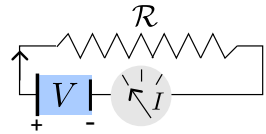
the influence of a unit applied field E (V m^{-1}).

- n is the number of charge carriers per unit volume, m^{-3} .

The electrical conductivity σ ($\text{C s}^{-1} \text{V}^{-1} \equiv \text{S m}^{-1} \equiv \Omega^{-1} \text{m}^{-1}$) is defined as

$$\sigma = nq\mu \quad (1.1b)$$

where ‘S’ stands for a ‘Siemen’ and Ω is the resistance defined by from Ohm’s law below in Equation 1.1c. The electrical conductivity of copper is $\approx 58 \text{ MS}^{-1} \text{m}^{-1}$ whereas that of polythene is $\approx 10^{-15} \text{ S m}^{-1}$. The inverse of σ is the electrical resistivity ρ which is a material property. The resistance, on the other hand, is the ratio of the voltage and current I in an arbitrary circuit



Ohm’s law [4] $\mathcal{R} = \frac{V}{I}, \quad (1.1c)$

which for a disc of thickness z_t and area A relates resistivity and resistance

$$\mathcal{R} = \rho \frac{z_t}{A}. \quad (1.1d)$$

In materials where multiple types of charge carriers contribute to electrical conduction, the overall conductivity is the sum of the conductivities of each individual charge carrier, $\sigma = \sum_{i=1}^N \sigma_i$. This principle extends beyond the simple electron-hole conduction in semiconductors to more complex systems. In intrinsic semiconductors like pure silicon, both electrons and holes contribute to conduction.¹ Both the mobile electron and the mobile hole can transport charge, and their individual contributions sum up to the total conductivity. Some of the lanthanum based perovskites have both electronic and oxygen-ion conductivity at suitably high temperatures.

Figure 1.1 shows that a mixture of zirconia with a small amount of yttria has a greater ionic conductivity than the pure variety. Zirconia contains vacancies in its oxygen sub-lattice, which means that a limited number of oxygen ions can conduct by diffusion through vacancies [6]. When yttria (Y_2O_3) is dissolved in zirconia, it forms a solid solution. The crucial aspect here is the difference in the valency of the cations:

- Zirconium in ZrO_2 is in the Zr^{4+} state.
- Yttrium in Y_2O_3 is in the Y^{3+} state.

1. When temperature provides enough energy to promote an electron from the valence band to the conduction band, it leaves behind a hole. The holes in effect carry positive charge just as mobile electrons carry a negative charge [5].

To maintain charge neutrality in the zirconia lattice when Y^{3+} ions replace some Zr^{4+} ions, extra oxygen vacancies are created. Since yttrium has a lower positive charge (Y^{3+}) than zirconium (Zr^{4+}), there's a deficit of positive charge. To compensate for this, the crystal lattice removes negatively charged oxygen ions, thereby creating more oxygen vacancies, thus increasing the ionic conductivity. A solid electrolyte based on this principle has been used in the measurement of the oxygen concentration in molten steel or copper [7].

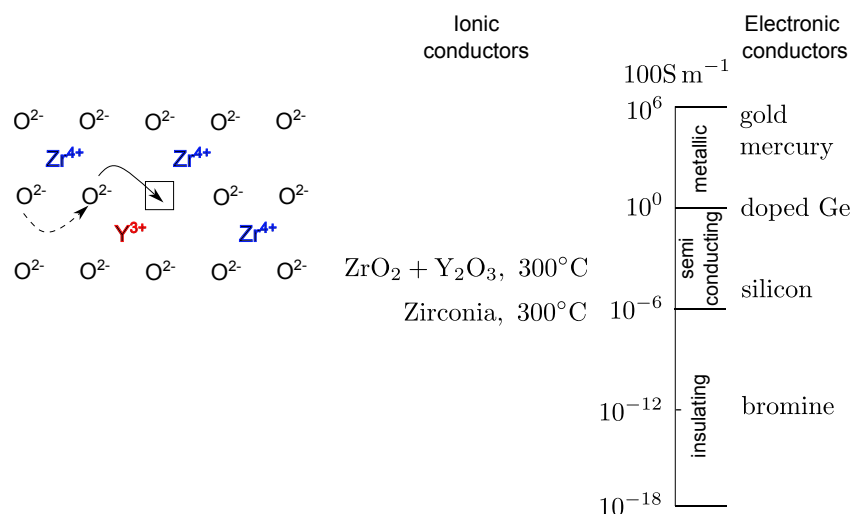


FIGURE 1.1 Approximate conductivities for a range of materials. This figure is in the style used elsewhere [8, 9]. The illustration on the left shows that the substitution of Y^{3+} for Zr^{4+} introduces a vacancy (\square) in the oxygen sub-lattice.

1.2 ELECTRONIC CONDUCTORS

Strontium niobate, $Sr_2Nb_2O_7$, exhibits several properties that make it suitable for high-temperature applications, particularly as a vibration sensor.

Strontium niobate, $Sr_2Nb_2O_7$ has an orthorhombic unit cell without a centre of symmetry [e.g., p.4, 6]; it is piezoelectric (applied mechanical stress causes electrical polarisation) and ferroelectric (has spontaneous polarisation that can be switched by an external electrical field) below its Curie point of 1615 K [10]. This means that it is extremely stable in its performance at elevated temperatures. It is mainly an electronic conductor so its resistivity ρ decreases as the temperature increases (Figure 1.2), but not so much that this causes its piezoelectric response is compromised, making the material suitable for vibration sensors that operate in hot environments.

4 CHAPTER 1. ELECTRICAL CONDUCTIVITY AND BREAKDOWN

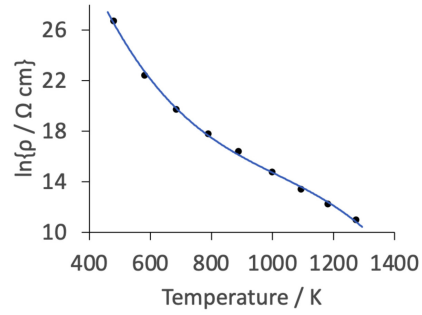


FIGURE 1.2 Direct current measurements of the resistivity of strontium niobate as a function of temperature [11]. The activation energies (Q , [p.54, 6]) derived by fitting straight line segments to $\ln\{\sigma\} = \ln\{\sigma_o\} - Q/kT$ and since $\sigma = \rho^{-1}$, to $\ln\{\rho\} = \ln\{\rho_o\} + Q/kT$ [12]. For elevated temperatures, $Q_{\text{high-}T} \approx 1.5 \text{ eV atom}^{-1}$.

Example 1: Activation energy for electronic conduction, $\text{Sr}_2\text{Nb}_2\text{O}_7$

Using the data for strontium niobate given in Figure 1.3 for an electronic conductor, determine the activation energy for the dependence of resistivity ρ on temperature.

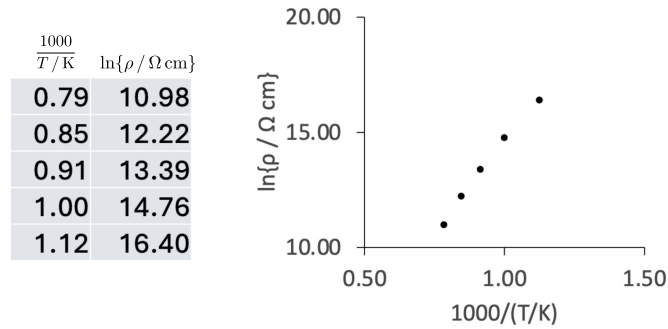


FIGURE 1.3 Data and plot for determination of the activation energy for intrinsic electronic conductivity, representing resistivity determined using direct current.

Solution 1

A best-fit straight line to the data gives

$$\ln\{\rho\} = 17.4 \times \frac{1000}{T} - \ln\{\rho_0\}.$$

Since the gradient should equal Q/k with $k = 8.617 \times 10^{-5} \text{ eV K}^{-1}$, it follows that $Q = 1000 \times 17.4 \times 8.617 \times 10^{-5} = 1.5 \text{ eV atom}^{-1}$.

Around 1900, shortly after J. J. Thompson's discovery of the electron, people became interested in understanding more about the mechanism of metallic conduction. The first work by Riecke in 1898 [1] was quickly superseded by that of Drude [3]. This explained the excellent electrical conductivity of metals like gold in terms of a free-electron model, later formalised by Lorentz [13] and Sommerfeld [14]. This model posits that metals contain a high concentration of mobile electrons, the essence of which is described next.

1.3 MECHANISMS OF CONDUCTION

We are familiar with the conventional structure of individual atoms where electrons occupy discrete, separated energy levels, with each level capable of accommodating two electrons with opposite spins. When a large number N of atoms is brought into sufficiently close proximity, say as in a crystal, the solid can be regarded as a huge molecule. Each original atomic level contributes to the formation of a *bands*, with each band containing N closely spaced crystal levels [p.113, 15].

Example 2: Metallic hydrogen

How could hydrogen become metallic?

Solution 2

The key is to force the atoms into close proximity. Hydrogen can become metallic at pressures exceeding 25 GPa [16], such as those found in the interior of Jupiter ($\approx 7.5 \text{ TPa}$) [17]. When individual hydrogen atoms are forced so close together, that their atomic orbitals overlap significantly, energy bands form resulting in metallic properties. Helium would require a pressure of 10 TPa to approach the metallic state at *low temperatures*, close to 0 K due to its tightly bound electron configuration and closed shell.

For an electron to move within the material, it must be able to enter an empty state. However, if the gap between a filled and empty band is large then the material must remain an insulator. When thermal energy can help an electron to accomplish the transition to an empty state and leave behind a hole, the material is classified as an intrinsic *semiconductor*, whose conductivity increases with temperature. If there is an overlap of filled and empty bands, then the electrons are free to move and the material exhibits electrical conduction at all temperatures. This is illustrated in Figure 1.4 to show how the electron-energy levels of an atom change into bands when large numbers of atoms cluster appropriately.

At 0 K, the Fermi level E_F for an intrinsic semiconductor is located precisely in the middle of the band gap. This is because at 0 K, the valence band is completely filled and the conduction band is completely empty, meaning the probability of finding an electron in the conduction band is zero, and the probability of finding a hole in the valence band is also zero. At finite temperatures, the Fermi level still represents the energy at which the probability of finding an electron occupying an available state is exactly 0.5. For an intrinsic semiconductor, it continues to act as the midpoint of the energy distribution for electrons and holes, balancing their equal concentrations.

For an *n*-type semiconductor at 0 K, the donor impurity levels are occupied, and the Fermi level is located at or very near the donor energy level (Figure 1.4b(ii)). Similarly, for a *p*-type semiconductor at 0 K, the acceptor impurity levels are empty, and the Fermi level is located at or very near the acceptor energy level (Figure 1.4b(iii)). As temperature increases, thermal energy causes more electrons to be ionised from donor levels into the conduction band (for *n*-type) or from the valence band to acceptor levels (for *p*-type). Additionally, intrinsic electron-hole pairs are generated. At higher temperatures, the semiconductor's behaviour increasingly resembles that of an intrinsic semiconductor due to the dominance of intrinsic carrier generation. Consequently, the Fermi level for both *n*-type and *p*-type semiconductors moves towards the intrinsic mid-gap position.

We have seen that the Fermi energy is defined for zero Kelvin, but at finite temperatures, the electrons close to E_F may be thermally promoted into nearby empty levels. But the number of electrons that can participate will be limited by the fact that at realistic temperatures, $kT \ll E_F$. For example, for aluminium, $E_F = 11.65$ eV; if this is set equal to the thermal energy kT , where $k = 8.617 \times 10^{-5}$ eV K⁻¹, the Fermi energy of aluminium would correspond to a temperature $E_F/k = 1.35 \times 10^5$ K! This is because the Pauli exclusion principle allows only two electrons per energy level. This close packing of electrons into available quantum states, mandated by the Pauli exclusion principle, forces the electrons to occupy very high energy levels even at absolute zero, leading to the large Fermi energy value.

In metals the valence electrons are not bound to particular ions, but because such

electrons can be scattered due to the increased amplitude of atomic vibrations at high temperature, the electrical resistance of a metal increases with temperature. This is unlike intrinsic semiconductors, where an electron can be promoted into a conduction band by thermal energy, so that conductivity actually increases with temperature.

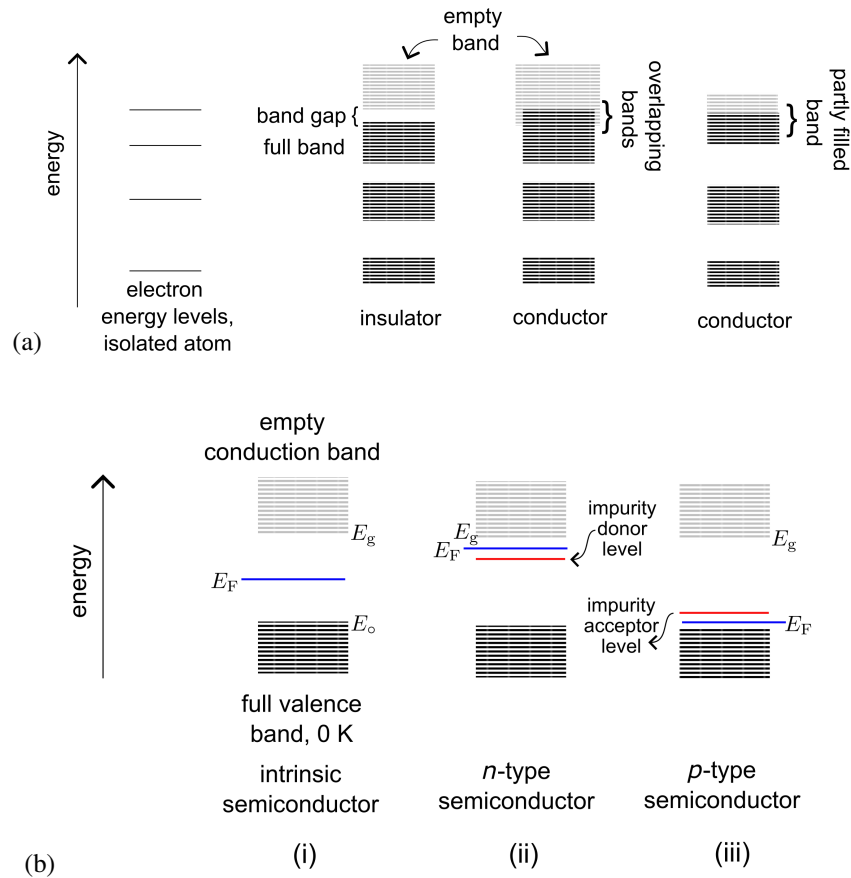


FIGURE 1.4 Schematic energy-band diagrams in which electron energy is measured vertically and position in the material, horizontally. For a crystalline material, there may be a direction dependence that is not shown here for the sake of simplicity. (a) Illustration of the formation of bands of electron-energy levels when large numbers of atoms are placed in sufficiently close proximity. Each level within a band can accommodate just two electrons of opposite spins. It is also possible to have a partly filled band depending on the type of atom. (b) Energy levels in semiconductors. (i) At 0 K, the Fermi energy (not marked) is that corresponding to the highest occupied state in the full valence band, with the Fermi level in the middle of the band gap. In (ii) E_F at 0 K corresponds to the donor impurity level, whereas in (iii) it corresponds to the impurity acceptor level.

A semiconductor such as silicon, which can be regarded as a giant, predominantly-covalently bonded crystal with each atom being tetrahedrally coordinated, consistent with its valency of four. There can be minor quantum mechanical effects that introduce a very slight degree of ‘metallic’ character due to the delocalisation of electrons. The valence band represents the energy levels of electrons in the covalent bonds. In an intrinsic semiconductor, some electrons may be thermally promoted into the conduction band, leaving behind holes – these are the free electrons, and free holes, available to conduct electricity. When an atom such as phosphorus which has a valency of 5 is added to the silicon, it bonds covalently, leaving an additional electron which is easy to ionise, in effect creating a donor level below the conduction band (Figure 1.4b). The extra electron is therefore weakly bound with each of the extra electrons from the phosphorus is a charge carrier so the conductivity does not rely solely on thermal energy as in an intrinsic semiconductor, but rather, on the phosphorus concentration. Because the phosphorus donates an extra electron, such a semiconductor is referred to as *negative type*, or *n-type* in short.

If an atom that has a valency of 3 (e.g., boron) is added to silicon, then the valence band is short of an electron, enabling charge to be carried by a positive hole (*p-type*) semiconductor.

Example 3: metal and titanium dioxide

Explain why the temperature dependence of the electrical conductivity of copper and of TiO_2 are different.

Solution 3

The electrical resistance of metals in general (copper is an example) is largely due to the scattering of electrons by the vibration of atoms in the lattice. These vibrations are known as phonons, which represent the collective excitation of atoms within the material. Such vibrations naturally increase with temperature, so there is a greater chance of electrons being scattered from the trajectories they would adopt in a perfectly periodic crystal. The resistivity therefore increases with temperature.

Titanium dioxide is an electronic conductor which unlike metals, has a large intrinsic resistivity at ambient temperature, in the range $10^3 \rightarrow 10^8 \Omega \text{ cm}$ [18]. This is because there is a significant gap E_g between the valence and conduction bands, with the activation energy of charge carriers $E_a = 0.5E_g$. Temperature has the effect of promoting more electrons into the conduction band:

$$\sigma \propto \exp\left\{-\frac{E_a}{kT}\right\}$$

thereby increasing conductivity at elevated temperatures, because as indicated in Equation 1.1b, the conductivity varies directly with the number n of charge carriers. In the case of extrinsic conduction, $E_a \ll E_g$.

Example 4: Resistivity and perfection

Why does the electrical conductivity of a metal that has undergone plastic deformation, increase on annealing (i.e., heat treatment without phase transformation)?

Solution 4

The implicit assumption in the discussion of metals so far has been that they are perfect single-crystals. However, defects such as vacancies, interstitials, and dislocations disrupt the long-range periodicity of the crystal, causing electrons to be scattered. This leads to an increase in the residual resistivity, which is largely independent of temperature. Separately, when a cold-worked or deformed metal is heated to sufficiently high temperatures, it undergoes processes like recovery and recrystallisation. These processes reduce the density of defects introduced by deformation, thereby reducing the component of electrical resistance associated with those defects. It is important to note, however, that the overall electrical resistance of a metal still generally increases with temperature due to enhanced phonon scattering.

Figure 1.5 shows how the resistivity (which is the reciprocal of the conductivity) decreases as the temperature at which it is annealed is increased. The annealing drives the copper towards a lower number density of defects.

Another example of the role of defects in altering the resistivity of metals is that when iron and its alloys are irradiated by neutrons in a nuclear reactor, or by bombardment with a flux of energetic electrons, their electrical resistivity increases due to the damage caused by the displacement of atoms. In fact, the changes in resistivity can be used to monitor the defect concentration [19], useful because the defects also cause the hardening and embrittlement of the alloys [20]. This problem is greater for the proposed fusion reactors where not only are the neutron fluxes expected to be much greater, but the neutrons have significantly higher energies (14 MeV versus ≈ 2 MeV for fusion). These more energetic and numerous neutrons are expected to cause even more severe radiation damage to structural materials [21], posing a major hurdle for long-term component integrity and reactor viability. Material scientists are actively researching and developing new radiation-resistant alloys for this specific challenge [22].

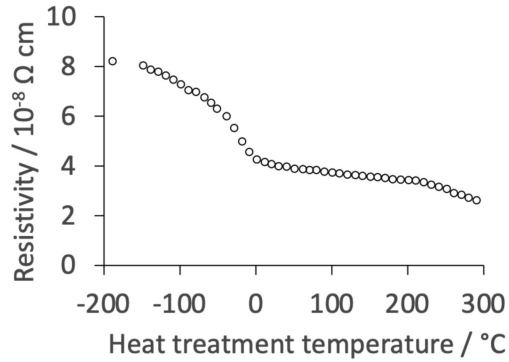


FIGURE 1.5 Copper (99.00% pure) deformed using cyclic torsion at -196°C , and then held at each heat-treatment temperature for 10 min. Its resistivity is in each case, measured at liquid-nitrogen temperature. Selected data from Polak [23].

Example 5: Quantum dots

The band gap of bulk crystals of cadmium selenide (CdSe) is typically 1.74 eV at ambient temperature. However, for CdSe nanocrystals is about $2 \rightarrow 2.5$ eV. Why is that?

Solution 5

When the size of the crystal decreases, the energy levels become more widely spaced. This is because the motion of charge carriers such as electrons and holes becomes limited by the dimensions of the crystal, leading to boundary conditions that the wave functions must satisfy, i.e., the wave functions must fit within the boundaries of the crystal. Theory associated with this *quantum confinement* phenomenon states that the band gap varies with the inverse square of the size.

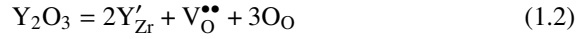
Visible light can be emitted during electronic transitions when the band gap is in the range $1.65 \rightarrow 3.1$ eV corresponding to red light and violet light respectively. So minute crystals of CdSe (known as *quantum dots*) can emit visible light of high colour purity and efficiency, making them useful in displays.

1.4 MORE ON IONIC CONDUCTION

Zirconia has three stable allotropes, monoclinic, tetragonal and cubic. Transformation between these allotropes are accompanied by volume changes that can compromise the mechanical integrity of the solid. The solution of 0.07 \rightarrow

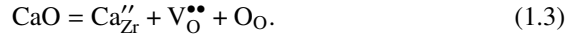
0.55 moles of yttria can stabilise the cubic phase when cooled from 2000 °C [24], although the monoclinic allotrope can appear under equilibrium conditions at ambient temperatures [25], it is unlikely to do so given kinetic limitations. Tetragonal zirconia is obtained in partially stabilised varieties; it has chemical stability, strength and the largest anion diffusivity of all allotropes [26].

But the solution of yttria in zirconia has other consequences. On page 2, the addition of a small amount of yttria to zirconia was stated to lead to an increase in vacancies on the oxygen sites, thereby increasing the ionic conductivity of zirconia, Figure 1.1. This is because the cation in yttria (Y^{3+}) has a smaller valency than Zr^{4+} so to maintain charge balance, there must be a corresponding loss of the negative oxygen ions. The effect can be written formally as follows,



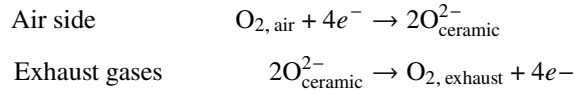
where in the Kröger-Vink notation [p.432, 27], Y'_{Zr} stands for a yttrium atom substituted into a Zr site, thus leaving it with a *net* negative charge. $V_O^{\bullet\bullet}$ signifies a vacancy in the oxygen site that has a net double positive charge. O_O represent oxygen atoms that carry no net charge in oxygen sites. So the number of oxygen vacancies, and hence the ionic conductivity, depends on the number of Y_2O_3 molecules put into zirconia.

Calcium oxide is also a suitable additive to zirconia as a means to enhance ionic conductivity [28], e.g.,



The Ca''_{Zr} implies a net double negative charge because the calcium has a valency of 2 compared with Zr which has a valency 4. Suppose that ytterbium oxide Yb_2O_3 is substituted, then it too would follow the same reaction as in Equation 1.2.

A major application of $ZrO_2-0.05Y_2O_3$ ceramic is in oxygen detectors, to monitor the exhaust gases of internal combustion engines and use that information to control the air/fuel ratio. The device, illustrated in Figure 1.6 shows that the ionic conductor experiences different oxygen concentrations at its two exposed surfaces. The platinum catalyses the reactions



and since $O_{2, \text{air}} > O_{2, \text{exhaust}}$, oxygen ions flow through the thickness, due to the

electromotive force (E_{emf}) given by²

$$E_{\text{emf}} = \frac{RT}{4F} \ln \left\{ \frac{p_{\text{O}_2, \text{air}}}{p_{\text{O}_2, \text{exhaust}}} \right\}$$

where F is the Faraday constant.³ The measured value of E_{emf} on the voltmeter then indicates the oxygen concentration in the exhaust fumes. There are literally millions of these devices in service.

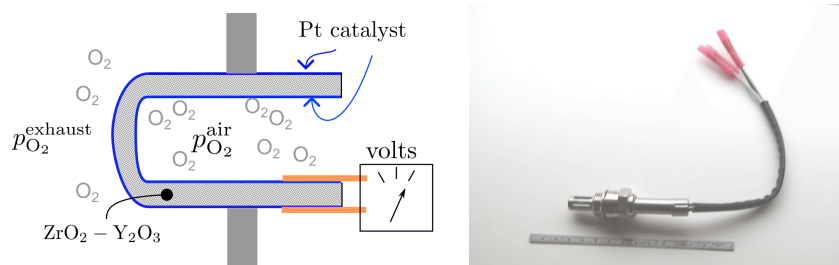


FIGURE 1.6 (a) Schematic of sensor to detect oxygen content of exhaust from an internal combustion engine. (b) An actual such sensor. Image courtesy of Advanced Ceramic Materials (<https://www.preciseceramic.com/>) via B. Cruz.

1.5 SEMICONDUCTORS: p - n JUNCTIONS

When p -type and n -type semiconductors form a junction, electrons from the n -side and holes from the p -side diffuse across the interface until the Fermi level (E_F) becomes uniform throughout the junction in thermal equilibrium Figure 1.7. This diffusion creates a region depleted of mobile charge carriers (the space-charge region) and establishes an internal electric field. Before joining, the n -type material has a higher electron concentration than the p -type material, resulting in a higher Fermi level for the n -type relative to the p -type (Figure 1.4).

When an external voltage V is applied, the system is no longer in equilibrium, and separate Fermi levels for electrons (E_{Fn}) and holes (E_{Fp}) emerge (Figure 1.8).

2. The free energy change ΔG accompanying a reaction is related to E_{emf} as $\Delta G = -NFE_{\text{emf}}$ where N is the number of electrons transferred in a reaction where both oxidation and reduction occur, i.e., a redox reaction.
3. It might be expected that an electric field would have no effect on an insulator. Faraday discovered that this is not so, by observing that a parallel plate capacitor increases its capacitance if an insulator completely fills the space in-between. These dielectrics increase capacitance by a factor ϵ_r . The unit of capacitance is therefore the Faraday, equivalent to coulombs per volt. To quote: *... a very important result ... showing for this particular piece of shell-lac a decided superiority over air in allowing or causing the act of induction ...* [p.399, 29].

During reverse bias, the external voltage increases the potential energy barrier across the depletion region. The electron Fermi level on the n -side is lowered relative to the hole Fermi level on the p -side, effectively widening the energy difference that carriers must overcome to cross the junction. This significantly inhibits current flow, resulting in very low current.

Conversely, during forward bias, the external voltage reduces the potential energy barrier. The electron Fermi level on the n -side is raised relative to the hole Fermi level on the p -side, narrowing the effective energy difference across the junction. This allows a much larger flow of majority carriers, leading to a significant electrical current.

This differential behaviour under forward and reverse bias is the fundamental principle of a diode, which permits significant current flow primarily in one direction.

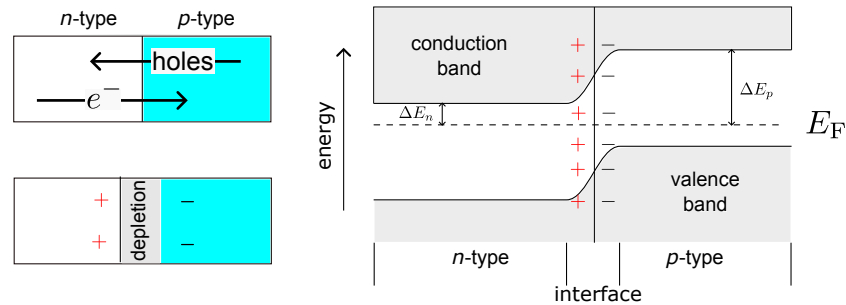
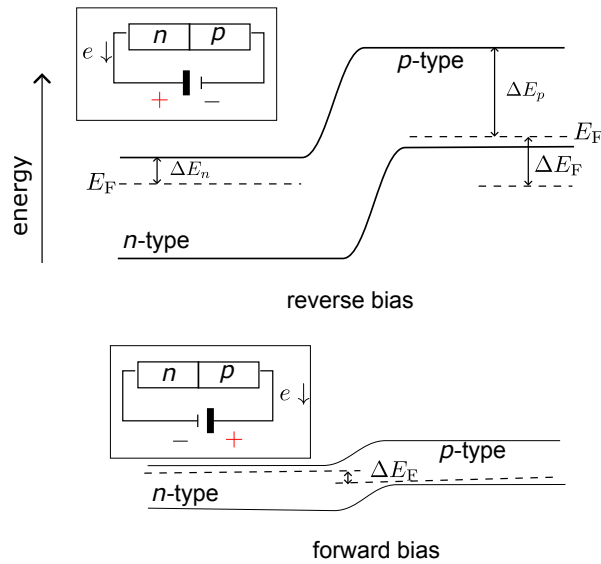
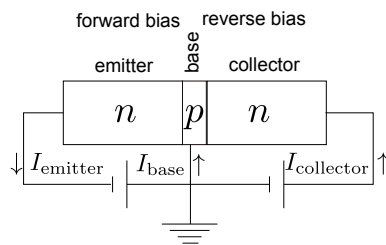


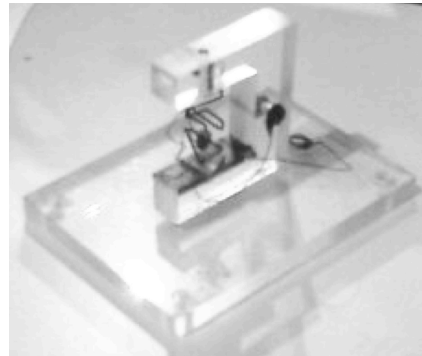
FIGURE 1.7 Band structure across a p - n semiconductor junction at equilibrium and in the absence of an applied voltage across the junction.

Transistors contain n - p - n or p - n - p ‘sandwiches’, i.e., a pair of junctions that allow the amplification of a signal or act as on-off switches for the sake of computational logic. For example, in a transistor, the layers in the n - p - n system are labelled *emitter* (10^{19}), *base* (10^{17}) and *collector* (10^{15}) respectively, where the numbers indicate the dopant concentrations (atoms cm^{-3}), Figure 1.9a. The base p -layer is relatively thin. The n - p junction is forward biased, and the p - n junction reverse biased. Electrons are the majority carriers in the emitter and are injected into the base. Due to the base being lightly doped and very thin, only a small fraction recombine with holes. A small base-current therefore replenishes the holes. Most of the electrons from the emitter flow across into the collector, constituting a large collector current, much larger than the base current; this, in effect, is amplification. To operate as a switch, the forward bias on the first n - p junction is switched off so the base current becomes zero as does the collector current.

The first such device is illustrated in Figure 1.9b.

FIGURE 1.8 Externally biased p - n junction.

(a)



(b)

FIGURE 1.9 (a) Schematic illustration of an n - p - n transistor. (b) First transistor made at the Bell Laboratories during December 1947.

1.6 VARISTORS

Some materials have an electrical resistance that varies with the applied voltage. Pure, non-stoichiometric zinc oxide typically has oxygen vacancies, making it an n -type semiconductor in which the current varies linearly with voltage. When small amounts of Bi_2O_3 or Sb_2O_3 are added during the sintering of ZnO , they form thin layers of mixed oxides at the ZnO -particle boundaries [30]. Because

this grain boundary material has defects, its Fermi level is lower than of the adjacent ZnO grains. Therefore, electrons flow into the boundary phase from the adjacent grains, leaving behind positively charged depleted regions in the vicinity. This electrostatic barrier still permits the passage of a small current. However, at large voltages in the boundary region, some of the electrons that cross the barrier have sufficient kinetic energy to induce hole formation in the depletion region. These holes are electrostatically attracted into the boundary region where they neutralise the negative charges that created the barrier in the first place, thus reducing the barrier and greatly increasing the current flow, Figure 1.10.

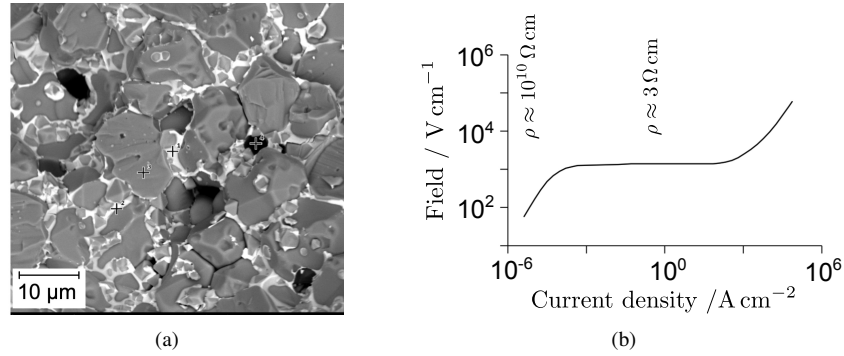


FIGURE 1.10 (a) Micrograph showing the (light contrast) layers at the ZnO particle-boundaries. Micrograph from Zhang et al. [30], reproduced under the CC BY 4.0 license, <https://creativecommons.org/licenses/by/4.0/>. Electric field versus current density plot for a ZnO based varistor. Adapted using selected data from Clarke [31].

A major application of varistors is in the suppression of transient surges in voltage which induce the material into the large current-density regime while maintaining the voltage essentially constant. This is particularly important in high-voltage power transmission systems where lightning strikes can cause significant perturbations in the steady state optimum. For that purpose, where the voltage spike can be overwhelming, multiple varistors may be wired in parallel, enabling the total current to be safely diverted by the protection device without damaging any single varistor.

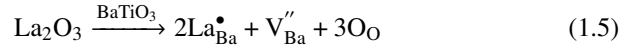
1.7 THERMISTORS

Semiconductors where the electrical resistance is sensitive to temperature, either decreasing with temperature as intrinsic semiconductors, or become more resistive as the temperature is increased. The temperature sensitivity is

$$\alpha_R = \frac{1}{\rho} \frac{d\rho}{dT}. \quad (1.4)$$

Solid solutions of mixed oxides such as $\text{Fe}_3\text{O}_4\text{-ZnCr}_2\text{O}_4$ or $\text{Fe}_3\text{O}_4\text{-MgCr}_2\text{O}_4$ become more conductive as the temperature is raised [p.160, 32]. These rely on conduction based on electron hopping between Fe^{2+} and Fe^{3+} , which becomes easier at elevated temperatures, so α_R will be negative.

Barium titanate has a tetragonal unit cell below the Curie point of 121°C , beyond which the cell becomes cubic [p.4, 6]. A small amount of lanthanum (La^{3+}) can substitute into the Ba^{2+} ; since La^{3+} has a greater valency, the system will compensate for the extra positive charge. This involves the creation of vacancies on barium sites. Using the Kröger-Vink notation,



where $2\text{La}_{\text{Ba}}^\bullet$ denotes a La^{3+} on a Ba^{2+} site with an effective charge of +1. The creation of barium vacancies compensates for these positive charges. In the polycrystalline state only, these defects can segregate to grain boundaries to present barriers to the passage of electrons, resulting in the huge increase in resistivity as the Curie temperature is exceeded, Figure 1.11. The single-crystal form does not exhibit this behaviour. The explanations here are simplified; a review by Bell et al. [33] ends by concluding that there is a need to understand the relationships between grain boundaries and functional properties.

Be that as it may, the doped, polycrystalline barium titanate is an excellent thermistor, that can be used as a current limiter should the temperature of a circuit rise uncontrollably beyond T_C due to a malfunction. And furthermore, the titanate is a much more effective thermistor than polymer variants given that it is a ceramic, making it useful for application at elevated temperatures. The resistivity can also be interpreted to manufacture temperature sensors.

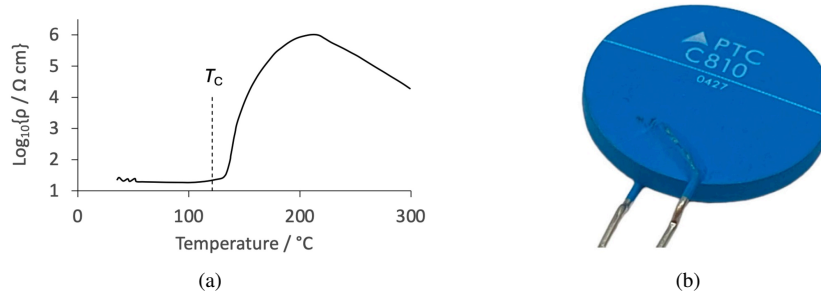


FIGURE 1.11 (a) Plot of the logarithm of resistivity ($\rho / \Omega \text{ cm}$) versus temperature, for BaTiO_3 doped with 0.5 at.% of lanthanum. Selected data from [33]. The Curie temperature plotted is for pure barium titanate. (b) Examples of a BaTiO_3 thermistor, where ‘PTC’ stands for positive temperature coefficient (α_R). Image reproduced from Safonov et al. [34] under the CC BY 4.0 license, <https://creativecommons.org/licenses/by/4.0/>. The titanate is enclosed between two metallised layers that are attached to terminals on either side.

1.8 ELECTRICAL BREAKDOWN OF INSULATORS

A dielectric material is an insulator because it does not contain loosely bound electrons but the charged ions they contain can lead to polarisation in the presence of an external electrical field. Examples include ceramics such as porcelain used to isolate 10-30 kV cables suspended between metal pylons, and polymers such as cost-effective polyvinyl chloride, polyethylene and nylon can be used to insulate wires in electrical devices, Figure 1.12a,b.

Large electrical fields can make some of these ordinarily insulating materials conductive, a phenomenon designated *electrical breakdown*. The occurrence of lightning between a cloud and the ground, or in a thundercloud, is a common example of the electrical breakdown of air under the influence of static electricity [pp.233-250, 35]. The mechanisms for such failure in the solid, liquid or gaseous states can be listed as follows:

1. A large enough field can cause the outer valence electrons to be ripped away into the conduction bands.
2. The applied field induces electrons to move, causing collisions with lattice atoms that generate additional electrons and a consequent avalanche of electrons. Obviously, the development of an avalanche requires the material to be thick enough. With this mechanism, a thin film can resist breakdown better than a thicker one.
3. Electromechanical breakdown occurs when the compressive stress caused by the attraction between oppositely charged surfaces exceeds a critical value.

The Maxwell stress σ_s that develops is

$$\sigma_s = \frac{1}{2} \epsilon_0 \epsilon_r E^2 \quad (1.6)$$

where ϵ_0 (units of $\text{C}^2 \text{N}^{-1} \text{m}^{-2}$) is the permittivity of free space and ϵ_r is the relative permittivity of the material; the electric field has units of N C^{-1} . This is a simplified equation that neglects terms dependent on the variation of ϵ_r as a function of strain [36]. If the stress is sufficiently large than the material mechanically breaks.

4. Thermal breakdown is associated with the generation of heat by the passage of electrical current, however small it may be in a dielectric. If the heat is not dissipated at the same rate that is generated, then overheating and breakdown follow.
5. If cavities or fissures exist within the dielectric material, the electrical field there can be exaggerated, leading to localised breakdown.

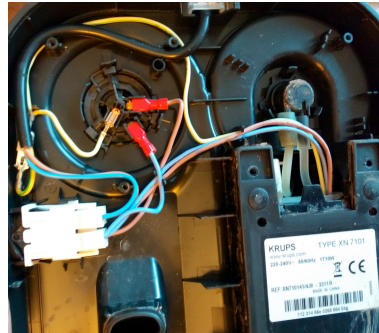
A nice image of the electrical breakdown of a polymer capacitor is shown in Figure 1.12c [37]. Some dielectric strength values are listed in Table 1.1.

TABLE 1.1 Breakdown electrical fields for a variety of insulating materials. Compilation including selected data from [38]. The value quoted for air depends on factors such as pressure, humidity, contaminants etc. The breakdown associated with lightning occurs at 1-2 orders of magnitude less than the theoretical breakdown strength of air at the appropriate altitude, because of the presence of charged ice crystals and cosmic rays that can initiate electron avalanches.

Material	Dielectric strength / kV mm^{-1}
High-density polyethylene	18.9
Flexible polyvinyl chloride	11.8-1.7
Amide polymer nylon 6/6	23.6
Mica	118
Alumina	13.4
Porcelain	35-160
Air	≈ 3
Air at 15 km height	0.4
Oil for spark machining	30-50



(a)



(b)



(c)

FIGURE 1.12 (a) Ceramic insulators that isolate high-voltage cables from electricity pylons. (b) Electrically insulated wires inside a coffee machine. The polymer insulation is flexible, which can be an advantage in such applications. (c) An 'electrical tree' resulting from the breakdown of a ferroelectric-polymer (polyvinylidene fluoride) capacitor. The polymer was blended with BiFeO_3 nanofibres. The silvery object at the centre is aluminium which alternates with the polymer to form internal electrodes after stacking. The silver paint at the edges is connected to the copper conductors used to apply voltage. As seen, the polymer has disintegrated completely. Picture courtesy of Mengfan Guo [37].

1.9 NORTH HYDE 275 kV ELECTRICITY SUBSTATION FAILURE

On the 20th of March 2025, a power failure occurred at this substation resulting in a major loss of supply to more than 70,000 domestic customers and commercial customers such as Heathrow Airport, which had to be closed down. The site contained three ‘supergrid’ transformers that reduce the voltage from 275 kV to 66 kV. Each transformer consists of an iron core with copper windings, contained in a large metal (earthed) tank filled with insulating oil. Grid transformers then connect within the distribution system to reduce the voltage to a standard domestic 230 V.

The transformer windings are energised by the high-voltage input which must be insulated from the grounded tank. This is done using a ‘bushing’ which surrounds the copper conductor usually with layers of oil-impregnated paper, separated periodically by concentric conducting foil that manages the electrical field (equalisation) and then finally, porcelain. It seems that moisture entered the bushing, causing a short circuit, with sparks igniting the oil, resulting in a fire [39].

An elevated moisture reading had been detected in 2018, but mitigation measures were not implemented [39].

Example 6: Spark machining

Spark machining, known also as an electrical discharge machining, is a precise manufacturing tool that removes material from a workpiece using controlled sparking. It is a non-contact process and yet is able to cut a sample of steel. Explain how it works.

Solution 6

During spark machining, insulating oil that is between the tool electrode and workpiece is induced to breakdown at critical values of the field caused by a pulsating DV power supply. When breakdown occurs, the dielectric fluid rapidly ionises and transforms into a plasma channel. This allows a high-energy spark to jump across the gap. The spark is extremely hot ($\approx 10^4$ °C), causing localised melting and vaporisation of the material from both the workpiece and, to a lesser extent, the tool electrode.

Example 7: Varistor heating by lightning strike

High-voltage electricity pylons are always grounded so in principle, a current due to a lightning strike can be dissipated into the earth. However, the pylon or earthing cable has a finite resistance so a huge voltage pulse can manifest as a result of the strike, which can damage insulation or cause voltages that exceed normal operation. To avoid this, a varistor assembly that short-circuits the high voltage by activating a connection to the Earth can protect against lightning, Figure 1.13.

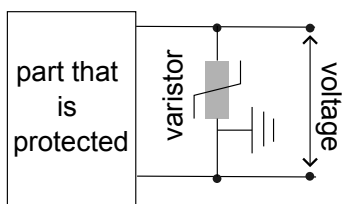


FIGURE 1.13 The varistor has a very high electrical resistance under normal operating conditions, but this decreases dramatically at high voltages, so it is able to shunt the current away to the ground from the part that needs surge protection.

Suppose that a lightning strike of duration $50\ \mu\text{s}$ triggers the varistor into its highly conductive mode that allows a current density of $10^3\ \text{A cm}^{-2}$ to flow through at almost constant voltage. Calculate the temperature rise within the varistor.

The varistor has a cross-sectional area of $10\ \text{cm}^2$ across which the current can flow, and the total mass of the varistor material is $2\ \text{kg}$. The heat capacity of the solid metal-oxide varistor is $40\ \text{J K}^{-1}\ \text{mol}^{-1}$ and it has a molar mass of $81.4\ \text{g mol}^{-1}$, and its electrical resistance is $9\ \Omega$ after breakdown into the high-current regime.

State any assumptions in your estimate.

Solution 7

A current density of $10^3\ \text{A cm}^{-2}$ can be converted to a current by multiplying with the cross-sectional area. The amount of heat generated by the current is

$$Q_{\text{heat}} = I^2 R t = (10 * 10^3)^2 \times 9 \times (50 \times 10^{-6}) = 45\ \text{kJ}. \quad (1.7a)$$

The increase in temperature can be calculated using the heat capacity and amount of varistor material, as

$$\Delta T = \frac{45000}{(40/81.4) \times 2000} = 45\ \text{K}. \quad (1.7b)$$

There important assumptions:

1. The major assumption is that the electrical properties are temperature independent. The heat capacity may also vary a little with temperature.
 2. That the process is adiabatic, i.e., no heat is dissipated into the surroundings and that the varistor material is heated uniformly.
-

Example 8: Artificial muscles

Artificial muscles that are capable of large strains when subjected to an electrical field, can be assembled using dielectric elastomers [40]. They are made by sandwiching a thin elastomer film (< 1 mm thickness) between compliant conductive electrodes. When a voltage is applied across the assembly, the accumulation of opposite charges at the electrodes cause the electrodes to mutually attract electrostatically, thus pressurising the dielectric and causing lateral expansion.

In dielectric elastomers, the electrostatic forces between the electrodes not only pull the electrodes together but also cause the elastomer film to thin. As the film thins, the electric field strength increases for a given applied voltage (since $E = V/z_t$, where z_t is thickness). At a critical voltage, the electrostatic force can no longer be balanced by the mechanical restoring force of the elastomer. The film undergoes an abrupt, localised thinning, causing a dramatic increase in the electric field, leading to electrical breakdown.

Suggest a way of ameliorating this problem.

Solution 8

Voltage pulsing is a highly effective technique for preventing or mitigating electrical breakdown in dielectric materials, especially in applications like dielectric elastomer actuators [41]. It allows operation at significantly higher peak voltages than would be possible with continuous voltage. Electrical breakdown, particularly avalanche breakdown, is not instantaneous. It's a time-dependent process that requires a certain 'formative time' for free electrons to accelerate, collide with atoms, ionise them, and build up a sufficient number of charge carriers to form a conductive channel. By applying short voltage pulses (e.g., in the μs or ns range), the voltage is applied for a duration shorter than the time required for a full electron avalanche to develop and propagate across the dielectric. Before the breakdown channel can fully form and cause catastrophic failure, the voltage is removed.

REFERENCES

1. E. Riecke: 'Zur theorie des galvanismus und der wärme (on the theory of galvanism and heat)', *Annalen der Physik*, 1898, **302**, 353–581.
2. E. Riecke: 'Ueber das verhältnis der leitfähigkeiten der metalle für wärme und für elektricität (on the relationship between the conductivities of metals for heat and electricity)', *Annalen der Physik*, 1900, **307**, 835–842.
3. P. Drude: 'Zur elektronentheorie der metalle (on the electron theory of metals)', *Annalen der Physik*, 1902, **312**, 687–692.
4. G. S. Ohm: *Die Galvanische Kette, mathematisch bearbeitet*: Berlin, Germany: Bei T. H. Riemann, 1827.
5. G. Pearson: 'The physics of electronic semiconductors', *Electrical Engineering*, 1947, **66**, 638–641.
6. H. K. D. H. Bhadeshia, and H. Yan: 'Phase transitions – an introduction with worked examples, published independently': www.phase-trans.msm.cam.ac.uk/2022/EMS523U_book.pdf, 2024.
7. D. J. Fray: 'The use of solid electrolytes in the determination of activities and the development of sensors', *Metallurgical and Materials Transactions B*, 2003, **34**, 589–594.
8. A. Moliton, and R. C. Hiorns: 'Review of electronic and optical properties of semiconducting π -conjugated polymers: applications in optoelectronics', *Polymer International*, 2004, **53**, 1397–1412.
9. M. Barsoum: *Fundamentals of ceramics*: U. K.: CRC press, 2019.
10. M. Fukuhara, C. Y. Huang, A. Bhalla, and R. Newnham: 'Grain orientation and electrical properties of $\text{Sr}_2\text{Nb}_2\text{O}_7$ ceramics', *Journal of Materials Science*, 1991, **26**, 61–66.
11. H. Ning, H. Yan, and M. Reece: 'Direct current measurements of the resistivity of strontium niobate', 2025: Private communication.
12. H. S. Shulman, M. Testorf, D. Damjanovic, and N. Setter: 'Microstructure, electrical conductivity, and piezoelectric properties of bismuth titanate', *Journal of the American Ceramic Society*, 1996, **79**, 3124–3128.
13. H. Lorentz: 'The motion of electrons in metallic bodies I', In: *KNAW (Royal Netherlands Academy of Arts and Sciences), proceedings*, vol. 7. 1905:438–453.
14. A. Sommerfeld: *Atombau und spektrallinien (Atomic structure and spectral lines)*, vol. 1: F. Vieweg & sohn akt.-ges., 1924.
15. P. Wilkes: *Solid state Theory in Metallurgy*: Cambridge, U. K.: Cambridge University Press, 1973.
16. A. R. J. P. Ubbelohde: 'Some properties of the metallic state I – metallic hydrogen and its alloys', *Proceedings of the Royal Society of London. Series A-Mathematical and Physical Sciences*, 1937, **159**, 295–306.
17. B. Miles, and W. Ramsey: 'On the internal structure of Jupiter and Saturn', *Monthly Notices of the Royal Astronomical Society*, 1952, **112**, 234–243.
18. M. D. Earle: 'The electrical conductivity of titanium dioxide', *Physical Review*, 1942, **61**, 56.
19. H. Neely, and D. Keefer: 'Resistivity studies of electron irradiated iron', *Physica Status Solidi (b)*, 1967, **24**, 217–220.
20. R. Kemp, G. A. Cottrell, H. K. D. H. Bhadeshia, G. R. Odette, T. Yamamoto, and H. Kishimoto: 'Neural-network analysis of irradiation hardening in low-activation steels', *Journal of Nuclear Materials*, 2006, **348**, 311–328.
21. G. A. Cottrell, R. Kemp, H. K. D. H. Bhadeshia, G. R. Odette, and T. Yamamoto: 'Neural network analysis of Charpy transition temperature of irradiated low-activation martensitic

24 CHAPTER 1. ELECTRICAL CONDUCTIVITY AND BREAKDOWN

- steels', *Journal of Nuclear Materials*, 2007, **367-370**, 603–609: doi:\bibinfo{doi}{doi:10.1016/j.jnucmat.2007.03.103}.
22. Y. de Carlan, M. Muruganath, T. Sourmail, and H. K. D. H. Bhadeshia: 'Design of new Fe-9CrWV reduced-activation martensitic steels for creep properties at 650 C', *Journal of Nuclear Materials*, 2004, **329-333**, 238–242.
23. J. Polák: 'Electrical resistivity of cyclically deformed copper', *Czechoslovak Journal of Physics B*, 1969, **19**, 315–322.
24. P. Duwez, F. H. Brown, and F. Odell: 'The zirconia-yttria system', *Journal of the Electrochemical Society*, 1951, **98**, 356–362.
25. J. Chevalier, L. Gremillard, A. V. Virkar, and D. R. Clarke: 'The tetragonal-monoclinic transformation in zirconia: lessons learned and future trends', *Journal of the American Ceramic Society*, 2009, **92**, 1901–1920.
26. P. Aldebert, and J.-P. Traverse: 'Structure and ionic mobility of zirconia at high temperature', *Journal of the American Ceramic Society*, 1985, **68**, 34–40.
27. F. A. Kröger, and H. J. Vink: Solid State Physics, eds F. Seitz and D. Turnbull, vol. 3, chap. Relations between the Concentrations of Imperfections in Crystalline Solids Relations between concentrations of imperfections in crystalline solids: New York, USA: Academic Press, 1956:307–435.
28. K. Kiukkola, and C. Wagner: 'Measurements on galvanic cells involving solid electrolytes', *Journal of the Electrochemical Society*, 1957, **104**, 379–387.
29. M. Faraday: Experimental researches in electricity: London: Taylor and Francis, 1839.
30. C. Zhang, H. Xing, C. Li, R. Cai, and D. Lv: 'Micro-degradation characteristics and mechanism of ZnO varistors under multi-pulse lightning strike', *Energies*, 2020, **13**, 2620.
31. D. R. Clarke: 'Varistor ceramics', *Journal of the American Ceramic Society*, 1999, **82**, 485–502.
32. A. J. Moulson, and J. M. Herbert: 'Electroceramics: materials, properties and applications': 1990.
33. J. G. Bell, T. Graule, and M. Stuer: 'Barium titanate-based thermistors: Past achievements, state of the art, and future perspectives', *Applied Physics Reviews*, 2021, **8**, 031318.
34. E. Safonov, V. Frolov, R. Zhiligitov, and Y. Petrenya: 'The specifics of PTC thermistor applications for limiting surge currents', *Energies*, 2024, **17**, 318.
35. J. M. Meek, and J. D. Craggs: Electrical breakdown of gases: Oxford, U.K.: Clarendon Press, eds N. F. Mott and E. Bullard, 1953.
36. R. Anderson: 'Mechanical stress in a dielectric solid from a uniform electric field', *Physical Review B*, 1986, **33**, 1302.
37. M. Guo: 'Electrical breakdown of a polymer capacitor': Private communication, 2025.
38. L. Berger: 'Dielectric strength of insulating materials', *Carbon*, 2006, **1**, 1–5.
39. NESO: 'North hyde review final report (<https://www.neso.energy/document/363891/download>): Tech. Rep., National Energy Systems Operator, Warwick, U.K., 2025.
40. S. Rosset, and H. R. Shea: 'Flexible and stretchable electrodes for dielectric elastomer actuators', *Applied Physics A*, 2013, **110**, 281–307.
41. T. Kobayashi, and S. K. Smoukov: 'Pulsed actuation avoids failure in dielectric elastomer artificial muscles', *International Journal of Smart and Nano Materials*, 2014, **5**, 217–226.

Chapter 2

Dielectrics

2.1 INTRODUCTION

A dielectric is an electrical insulator that possesses the crucial ability to be polarised by an external electric field. While every dielectric is inherently an insulator (meaning it does not readily conduct electricity), the specific focus for energy storage applications lies in their capacity to efficiently store electrical energy through a process known as polarisation.

During polarisation, the internal charges within the dielectric material, positive and negative, undergo a slight displacement. The positive charges shift in one direction, while the negative charges move in the opposite direction, both movements occurring parallel to the applied electric field. This subtle separation of charges gives rise to tiny electric dipoles within the material, effectively rendering one side of the material slightly positive and the other side slightly negative.

This phenomenon of polarisation forms the fundamental basis for the functioning of a capacitor as an energy storage device (Figure 2.1). The induced polarisation within the dielectric leads to an accumulation of electrical charges between two closely spaced, insulated surfaces, enabling the capacitor to store energy for later discharge.

A significant factor in the success of silicon integrated electronics is the use of SiO_2 (silica) as a dielectric, formed by oxidising the silicon substrate [1]. While silica layers can theoretically be as thin as five atomic layers, practical applications often require greater thicknesses to prevent current leakage. The primary advantage of silica is its ease of manufacturing. However, other materials with high dielectric constants (ϵ_r), such as La_2O_3 , have been explored using techniques like vapour deposition [2].

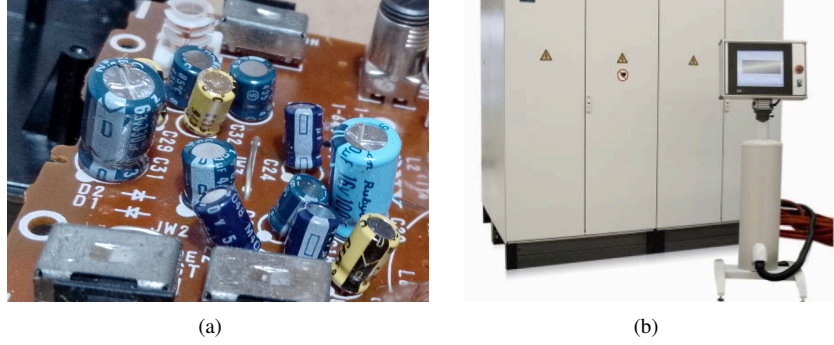


FIGURE 2.1 (a) A number of capacitors mounted on one side of a printed circuit board from a portable radio. These are made essentially by spooling polypropylene dielectric film that has been metallised on both sides with thin layers of aluminium (30 nm) which act as the electrodes, and then canning the spool. (b) Pressures for forming metals using a magnetic pulsing can reach 100 MPa. The image shows a large capacitor bank which stores energy that is discharged a pulse current 100-1000 kA to generate electromagnetic forces that can form metal into the desired shapes. Image courtesy of Stephan Kallee, PST products GmbH, Germany.

2.2 FUNDAMENTALS OF DIELECTRIC MATERIALS

The relationship $\mathcal{P} = \chi_e \epsilon_0 E$ describes the polarisation field (\mathcal{P}), where χ_e is the electrical susceptibility, a dimensionless proportionality constant.

For a flat capacitor with parallel plates of area A and a dielectric material separating them by a distance z_t , if the charge at the free surface is q , the electrical displacement \mathcal{D} is given by

$$\mathcal{D} = \frac{q}{A} \quad (2.1a)$$

where the units of \mathcal{D} are C m^{-2} , which is essentially a measure of surface charge density.

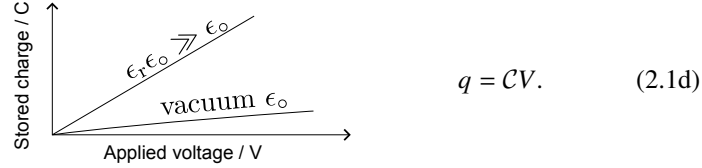
The electric displacement is also related to the field within the dielectric by:

$$\mathcal{D} = \epsilon_0 \epsilon_r E \quad (2.1b)$$

where ϵ_0 is the permittivity of free space and ϵ_r is the relative permittivity (or dielectric constant) of the dielectric material. The capacitance \mathcal{C} of this parallel-plate capacitor is given by:

$$\mathcal{C} = \epsilon_0 \epsilon_r A / z_t, \quad (2.1c)$$

with the stored charge given by:



From Equation 2.1a, the surface charge density for a vacuum capacitor is simply $\mathcal{D} = \epsilon_0 E$ but when the capacitor includes a dielectric, its polarisation must be accounted for,

$$\mathcal{D} = \epsilon_0 E + \mathcal{P} = \epsilon_0 E + \chi_e \epsilon_0 E = \epsilon_0 (1 + \chi_e) E. \quad (2.1e)$$

Since $\mathcal{D} = \epsilon_0 \epsilon_r E$, it follows that $1 + \chi_e = \epsilon_r$, and

$$\frac{d\mathcal{P}}{dE} = (\epsilon_r - 1)\epsilon_0. \quad (2.1f)$$

This derivative indicates how much the polarisation field changes for a given change in the electric field, and it is proportional directly to the ‘excess’ permittivity beyond that of free space. The relative permittivity is therefore a key material parameter that can be exploited, for example, to detect buried objects by firing radio waves into the earth and monitoring return signals that are affected by the permittivities of buried objects.

2.2.1 Polarisation

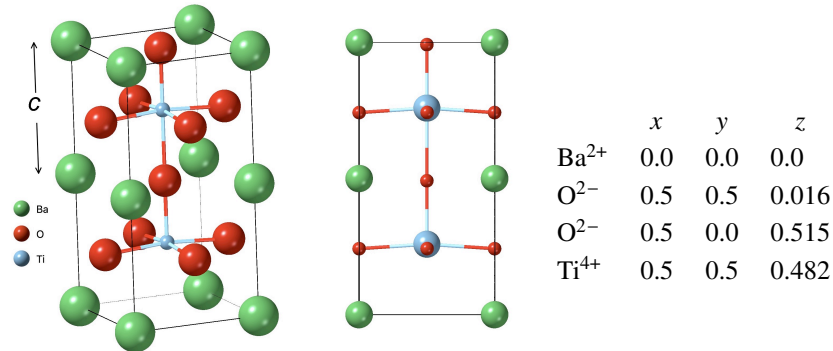
To emphasise again, when a dielectric is placed in an electrical field, the electrons and nuclei of the molecules move slightly apart as they react oppositely to the applied field. They acquire an electrical dipole moment $\mu_{\uparrow} = qz$ where $q = |\pm q|$ is the magnitude of the charge separated by a distance z . The overall polarisation field \mathcal{P} is then defined as the sum of all these individual dipole moments within a specified volume (V) of the material:

$$\mathcal{P} = \frac{\sum \mu_{\uparrow}}{V}. \quad (2.2)$$

The electric permittivity of a material is a measure of how effectively it polarises in response to an electric field. A material with a larger permittivity will exhibit a greater degree of polarisation when subjected to the same external electric field. This means its internal charges will separate more significantly, leading to a stronger induced dipole moment and thus a greater ability to store electrical energy.

Example 9: Spontaneous polarisation of tetragonal barium titanate

(a) Tetragonal barium-titanate BaTiO_3 (space group $P4mm$) has the lattice parameters $a = 0.39998 \text{ nm}$ and $c = 0.4018 \text{ nm}$ at ambient temperature. A vertical stack of two unit cells is illustrated below, together with a projection that shows better, the relative dispositions of ions along the c -axis. The table lists the fractional coordinates of the ions within a unit cell. Calculate the polarisation \mathcal{P} for a unit cell.



(b) Tetragonal lead titanate PbTiO_3 (space group $P4mm$) has the lattice parameters $a = 0.3904 \text{ nm}$ and $c = 0.4152 \text{ nm}$ at ambient temperature. In this case, both kinds of oxygen are displaced along the c -axis relative to lead at the origin, by -0.047 nm , with titanium shifted by -0.017 nm in the same direction [3]. Calculate its polarisation. On the basis of your results, comment on why lead titanate is not used in the manufacture of capacitors as is the barium variety.

Solution 9

The polarisation \mathcal{P} is strictly a vector sum of all the individual dipoles, but here the displacements of atoms relative to ideal cubic positions. Assume that the displacements are all parallel the c -axis so the summation can be scalar. Each unit cell has one titanium atom, 6 oxygen atoms with each shared between two unit cells, and 8 barium atoms with each shared between eight unit cells. Using the coordinates of atoms, the displacements of the ions relative to the centre of the c -axis are (neglect the barium ions which are symmetrically disposed about that centre, and note that the oxygen atoms at the horizontal faces are differently displaced relative to those at the vertical faces):

$$\begin{aligned}\text{Ti}^{4+} &= 0.4018 \times (0.482 - 0.5) = -0.0072 \text{ nm} \\ \text{horizontal faces } \text{O}^{2-} &= 0.4018 \times (0.016) = +0.0064 \text{ nm} \\ \text{vertical faces } \text{O}^{2-} &= 0.4018 \times (0.515 - 0.5) = +0.006 \text{ nm}\end{aligned}$$

Therefore, the net polarisation, taking account of the fact that the oxygen atoms are shared between adjacent unit cells, is

$$\begin{aligned}
 \mathcal{P} \times V_{\text{BaTiO}_3} &= (+4e) \times (-0.0072) + \\
 &\quad (-2e) \times 2 \times \frac{1}{2} \times (0.0064) + \\
 &\quad (-2e) \times 4 \times \frac{1}{2} \times (0.006) = \\
 &\quad -0.0656 \times \underbrace{(1.60217663 \times 10^{-19})}_{\text{charge on electron}} = -1.051 \times 10^{-20} \text{ C nm} \\
 &\equiv -1.051 \times 10^{-29} \text{ C m}
 \end{aligned}$$

where V_{BaTiO_3} is the volume of the unit cell. Therefore, $\mathcal{P} = -0.1636 \text{ C m}^{-2}$. The minus sign does not matter because that simply depends on the defined sense of the coordinates of the unit cell. Notice that this is the *spontaneous* polarisation (i.e., in the absence of external fields), measured as a charge per unit area on surfaces perpendicular to the polarisation. Note also the ability of a capacitor to store energy depends on \mathcal{P} via Equation 2.1e. The value of \mathcal{P} calculated here is somewhat less than the $0.13 \rightarrow 0.28 \text{ C m}^{-2}$ reported in the literature [4–6]. The reason for this large discrepancy is two-fold [7, 8]:

1. The calculation considers just the ionic polarisability, whereas electronic polarisability also contributes.
2. It turns out that the charges on the Ti, O and Ba ions are not strictly integers, but in a crystal the atoms do not feel each other's charge to the fullest extent. The effective charges are +2.063, -1.2 and -1.1 and +1.437 for the Ti, O and Ba atoms, respectively. Therefore, the ionic contribution using first principles methods turns out to be much smaller at 0.0802 C m^{-2} .

In summary, the solution here is an approximation that does not account for all items susceptible to polarisation.

In a single crystal of BaTiO_3 , the spontaneous polarisation, which is the inherent alignment of electric dipoles even in the absence of an external electric field, does not typically occur uniformly across the entire material. Instead, the crystal naturally divides itself into discrete regions known as ferroelectric *domains*. Within each domain, the dipoles are aligned in a particular direction but the polarisation direction can be reversed or oriented differently in adjacent domains. The application of a sufficiently large E would force all the dipoles to align, thus eliminating the domain structure.

For PbTiO_3 , \mathcal{P} can be calculated to be -0.8720 C m^{-2} , which is consistent with a measured value (0.78 C m^{-2}) [4]. Lead-zirconium titanate is not used in dielectric capacitors because of its low permittivity and the toxicity associated

with Pb. The BaTiO_3 is used instead, but PbTiO_3 is applied when a large piezoelectric coefficient (Chapter 4) and thermal stability due to its high Curie point are important in the choice of materials.

2.3 VARIETY OF POLARISATIONS

The fact that the measured spontaneous polarisation for barium titanate was much greater than that calculated based on integrally charged ions in the unit cell, shows that there are mechanisms beyond just the displacement of perfectly charged ions:

1. Space charge: occurs in heterogeneous materials or at interfaces (e.g., grain boundaries in polycrystalline materials, electrode-material interfaces, or impurities within the material). It involves the migration of charge carriers (ions, electrons, or vacancies) over macroscopic distances and their accumulation at these interfaces or barriers when an electric field is applied. This can be a problem in power transformers that are insulated using oil-paper (Figure 2.2), when space charge accumulates ($20\text{--}30 \text{ C m}^{-3}$), causing electric field distortion, possible partial discharge and breakdown [9, 10].

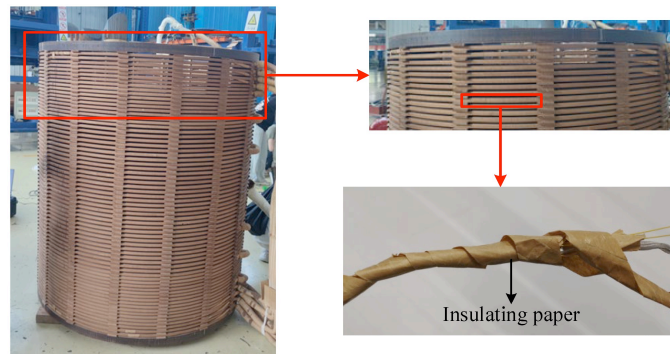


FIGURE 2.2 Oil-paper used for electrical insulation of electrical windings. Image reproduced from Yuan et al. [11] under CC BY 4.0 license <https://creativecommons.org/licenses/by/4.0/>.

2. Dipolar (orientational) polarisation occurs in materials that possess permanent electric dipole moments. These are molecules or structural units where the centres of positive and negative charge do not coincide, even in the absence of an external electric field. When an external electric field is applied, it exerts a torque on these permanent dipoles. This torque attempts to align the dipoles with the direction of the electric field (Figure 2.3a). The degree of alignment depends on the strength of the electric field and the thermal energy (temperature) that tries to randomise the dipoles. A stronger field and lower temperature lead to greater alignment.

The water molecule (H_2O) is a classic example of a polar molecule. Its bent structure means that the oxygen atom (more electronegative) attracts electrons more strongly than the hydrogen atoms, creating a partial negative charge on the oxygen and partial positive charges on the hydrogens. Since the molecule is bent, these charge centres do not coincide, resulting in a permanent electric dipole moment. This property is fundamental to the operation of a microwave oven because the oven generates an electromagnetic field that oscillates rapidly, ≈ 2.45 GHz. The water molecules (and other polar molecules) in the food attempt to reorient themselves to align with the oscillating field. This constant reorientation involves molecular friction and collisions, which dissipate energy as heat. This process, known as dielectric heating, is what cooks the food.

Crystals of ice (frozen water) therefore also are susceptible to orientational polarisation [12]. While water molecules in liquid form are relatively mobile, in the solid crystalline structure of ice, their movement is constrained. However, the permanent electric dipoles of the water molecules are still able to reorient themselves to some extent in response to an applied electric field. This reorientation, even within the rigid lattice, contributes significantly to ice's dielectric properties. In ice-crystals with a hexagonal structure, the relative permittivity has been reported to be $\epsilon_r = 96.5$, both parallel and normal to the c -axis; this remarkably high value indicates that the dipoles of water are highly responsive to an electric field. For comparison polyethylene that has $\epsilon_r \approx 2.3$. Ferroelectric domains (Chapter 4) and tiny clusters of ions in the paraelectric phase also fall in the class of orientation polarisation.

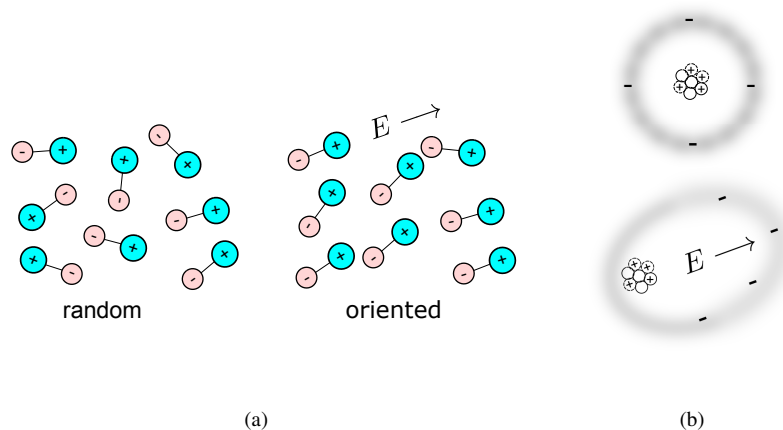


FIGURE 2.3 (a) Influence of an external electrical field E on the orientation of polar molecules, assuming that they are free to move. (b) Polarisation of an atom, with the electrical field causing the valence electron cloud to be displaced.

3. Ionic polarisation has already been discussed in the context of barium and lead titanates, p.27. Other examples include alumina, NaCl, silica.
4. Electronic polarisation arises from the distortion of the electron cloud of an atom or molecule by an external electric field. Ordinarily, in an isolated, neutral atom, the centre of the negatively charged electron cloud perfectly coincides with the positively charged nucleus, Figure 2.3b. The noble gases such as He do not polarise much. This is because they have full outer electron shells, which are very stable and tightly bound to the nucleus. The electrons are held relatively close to the nucleus, making their electron clouds difficult to distort. This results in low electronic polarisability. With its single electron, hydrogen is more susceptible to polarisation than helium. While not having a completely "full" shell, its single electron is relatively exposed compared to the tightly packed electrons in a noble gas. This makes its electron cloud more easily deformed.

The spontaneous polarisation of ferroelectrics may include contributions from ionic and electronic polarisations. As an example, the spontaneous polarisation in BaTiO_3 consists of both contributions [7], i.e., there are significant roles of charge redistribution due to both ionic displacements and shifts of electron clouds relative to their respective nuclei. The two types of polarisation are interconnected because ion displacements create strong local electric fields, which in turn induce the electronic polarisation.

2.4 CAPACITOR SUBJECTED TO ALTERNATING VOLTAGE

An alternating current (AC) periodically charges and discharges a capacitor, but its voltage lags behind the current. This is because the accumulation of charge on the capacitor plates would oppose the current, which in turn would reach zero when the former is fully charged. The current depends on the rate of change of capacitor voltage, dV/dt which becomes zero when fully charged, Figure 2.4.

It is necessary, therefore, to deal with two sets of waves, on representing the current and the other the voltage, when they are out of phase, Figure 2.4, where the voltage is 90° out of phase with the current. Trying to deal with these phase differences using only real numbers and trigonometry becomes cumbersome very quickly. Instead, complex numbers are used because they provide a framework for dealing with sinusoidal waveforms and phase relationships in electrical circuits. AC voltages and currents are typically sinusoidal and can be represented as rotating vectors in a complex plane where the real component is plotted horizontally and the imaginary one vertically.

The voltage can be written

$$V = V_o \exp\{i\phi\} \equiv V_o \cos \phi + iV_o \sin \phi \quad \text{where} \quad i = \sqrt{-1}. \quad (2.3)$$

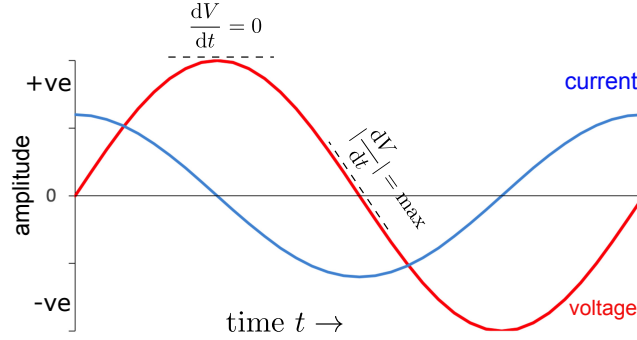


FIGURE 2.4 Current and voltage variations in a capacitor connected to an alternative current supply. The two waves are at the same frequency but the current is ahead by a quarter wavelength, i.e., by phase $\phi = 90^\circ$.

where V_0 is the amplitude and ϕ is the phase angle.

Utilising the complex plane, in Figure 2.5, (a→c) represent an ideal capacitor where there is no dissipation of energy when it is subjected to alternating stimuli, with the charge responding instantaneously to the external current, and there is no dielectric loss. On such diagrams, the vectors (phasors) are to be read anticlockwise, meaning for example that the current is ahead of the voltage, with a phase angle of 90° between I and V .

Suppose now, that there is some frequency-dependent lethargy¹ in the response of the charges, which leads to a loss current that will be in phase with the voltage, as shown in Figure 2.5d (the loss-current phasor is parallel to the voltage phasor). Such loss current dissipates energy as heat, with

$$I_{\text{loss}} = \left(\frac{1}{R} + \frac{1}{R^*} \right) V \quad (2.4)$$

where R is the ohmic resistivity as in direct current (DC) charging, whereas R^* depends on the relaxation process of dipoles when the electrical field changes. If these resistances are known then it is simple to calculate the energy loss due to joule heating ($\propto V^2$ or $\propto I^2$).

Since permittivity is the response of polarisations in a capacitor to an applied field (Equation 2.1a), then it too will have two components, one as if the dipoles within can instantaneously react to E , and the other where there is a lag in the

1. This 'lethargy' means that the various polarisation mechanisms (electronic, ionic, orientational, space charge) do not respond instantaneously or perfectly in phase with the applied alternating electric field.

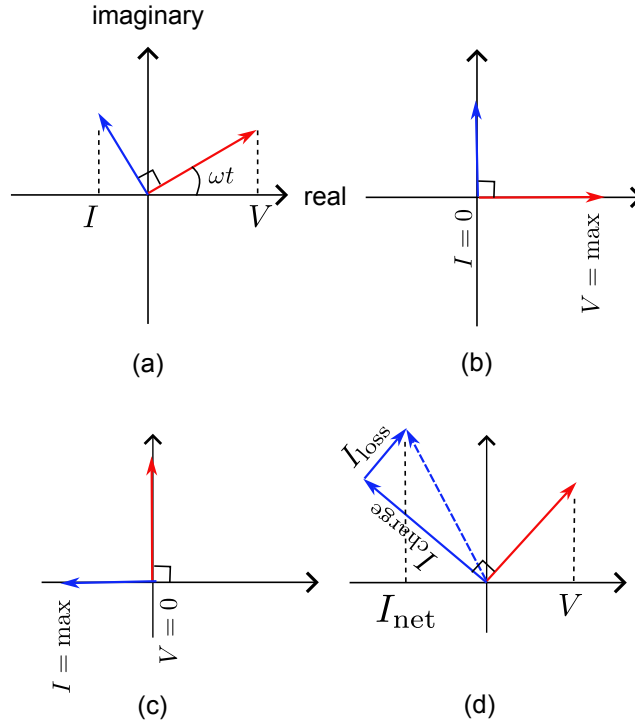


FIGURE 2.5 Polar diagrams, often referred to as ‘phasor plots’ where both amplitude and phase are easy to represent simultaneously the alternating current and voltage. (a) The product of frequency ω and time t represents a particular phase angle for the voltage, with the current being 90° ahead of that. Progress is represented by the anticlockwise rotation of the radial vectors representing current and voltage, the magnitudes of these given by the projection on to the real-number axis. (b) The case where the capacitor is charged to its maximum, so the charging current becomes zero. (c) Here the charging current is at a maximum when the capacitor is discharged. (d) There is a loss of energy in a non-ideal capacitor described in the text.

response, then the complex dielectric constant (permittivity) is:

$$\text{relative permittivity} = \epsilon'_r + i\epsilon''_r \quad \text{with } C \propto \epsilon'_r \quad \text{and} \quad R^* \propto \frac{1}{\epsilon''_r} \quad (2.5)$$

so that ϵ''_r represents the energy loss due to a variety of mechanisms of energy dissipation, such as dipoles attempting to change orientation against thermal vibrations that induce disordered orientations; there are no losses if $\epsilon''_r = 0$ and for most dielectrics, it's value is much smaller than the real part ϵ'_r which reflects the ability of the material to store electricity. It can be characterised by a relaxation time τ . When the AC frequency $\omega = \tau^{-1}$, ϵ''_r peaks to a maximum value, but at high and low frequencies, it is small. In contrast, ϵ'_r starts off at a characteristic value when ω is very small, and then decreases gradually. This is illustrated for a particular polymer in Figure 2.6.

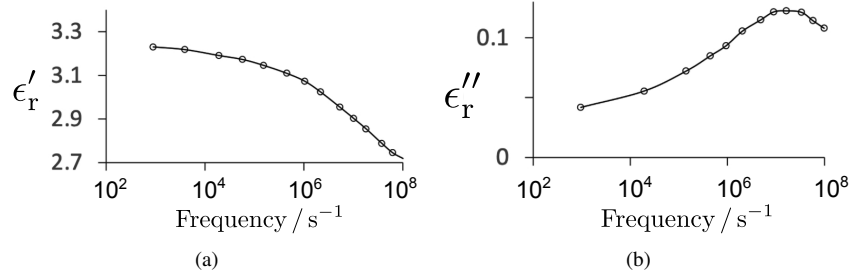


FIGURE 2.6 Measured permittivity as a function of frequency for polyvinyl chloride at 73.5°C. (a) Real. (b) imaginary. Selected data from Ishida [13].

More about dielectric loss

Energy lost as heat in a dielectric material when it is subjected to an alternating electric field is a loss that occurs because the polarisation response of the dielectric lags behind the applied field, causing energy dissipation.

For example, when the dipoles within the material do not align instantaneously with the changing electric field, leading to energy loss. A conduction loss occurs when charge carriers move in the presence of an applied electrical field causing resistive heating. The effects are frequency dependent because at low frequencies, the dipole mechanism may dominate but at higher frequencies the conduction losses become significant.

When $R = 0$ in Equation 2.4, the loss often is expressed by the ratio $\tan \delta = \epsilon''_r / \epsilon'_r$, referred to as the loss tangent. A greater $\tan \delta$ indicates greater energy loss in the dielectric material when subjected to an alternating electric field. The loss can also be affected by extrinsic factors, such as the presence of defects in the material. Impurities, grain boundaries, porosity, cracks all increase loss. Voids and gas-pockets have a lower permittivity, therefore can reduce the overall ϵ'_r , leading to an increase in $\tan \delta$, Figure 2.7.

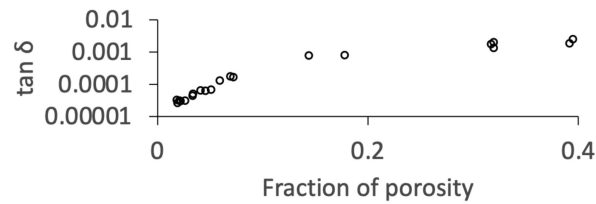


FIGURE 2.7 The loss tangent for alumina containing porosity, measured at about 9 GHz. Adapted using data from [14].

2.4.1 Very large permittivity

There exist materials such as $\text{CaCu}_3\text{Ti}_4\text{O}_{12}$ in which $\epsilon_r > 10^4$ at low frequencies. In other words, the polarisation can be huge. The oxides are usually compacted using sintering. The atomic mechanism is interesting [15] in that the grain boundaries contain a thin interface region between $\text{CaCu}_3\text{Ti}_4\text{O}_{12}$ and Cu_xO , which behaves like a metal, Figure 2.8. In materials like this, there is a sharp drop in permittivity at high frequencies. This is because the high capacitance associated with the grain boundaries relies on the movement and accumulation of charge carriers at these interfaces. The charge carriers no longer have enough time to respond and accumulate at the boundaries. The interfacial polarisation mechanism effectively ‘freezes out.’

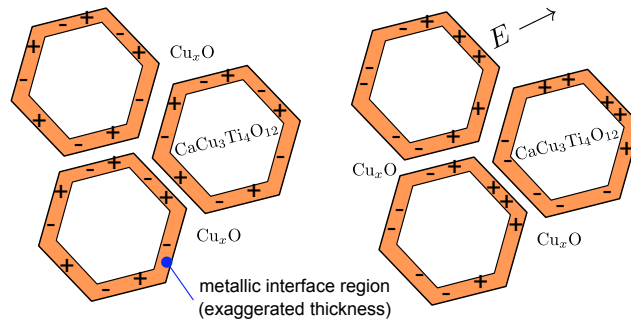


FIGURE 2.8 Diagram showing the mechanism of giant permittivity, in which the interface between the insulating oxides forms a metallic state where the ions normally are fixed but redistribute within the interface when a field is applied. Adapted from Taylor et al. [15].

2.4.2 Multilayered ceramic capacitors

The ability of a capacitor to store electricity, its capacitance, is $C = \epsilon_r \epsilon_0 A / z_t$ where A is the area and z_t the distance between the surfaces of the usually oxide dielectric with a large permittivity, such as titanium oxide ($\epsilon_r \approx 100$) or barium titanate ($\epsilon_r \approx 5000$). It follows that by stacking many of these layers with electrodes between each layer, the capacitance increases in proportion to the number of layers. Such a capacitor might have a size $5 \times 3 \times 3$ mm, containing somewhat more than 100 layers and with a capacitance of around 100 nF (Figure 2.9). When cost is an issue, the electrodes would be made from nickel or copper, though more expensive metals such as platinum may be used when the capacitor is destined for elevated temperature applications.

2.4.3 Dielectric resonator

Imagine a cavity with walls that reflect, being fed with electromagnetic waves that are reflected at its walls with negligible loss. As a result, *standing waves*

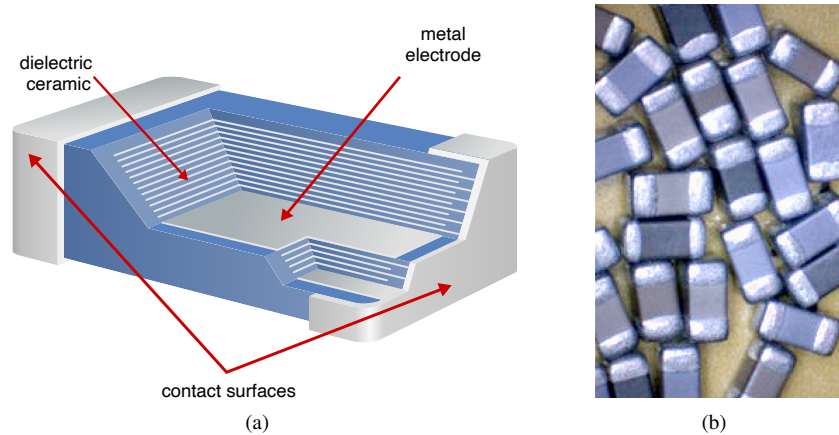


FIGURE 2.9 (a) Schematic construction of multilayered ceramic capacitor. (b) Actual multilayered capacitors. Images by Jens Both Elcap, reproduced under CC BY-SA 3.0 license.

can form by the superposition of waves of the same frequency travelling in opposite directions, oscillating with large amplitudes. Such a cavity could be made of a dielectric ceramic where the sudden change in permittivity at the cavity/dielectric walls leads to the reflection and superposition described. The interference that leads to standing waves will occur between those waves that comply with the resonance frequency of the resonator, which can in principle be controlled by manipulating the size and shape of the dielectric and its ϵ_r .

The oscillating electromagnetic field in the resonator stimulates radiation, that propagates away from the resonator which now acts like a transmitting antenna. The resonators are therefore used for wireless communications including satellite devices, and radar systems. One example is illustrated in Figure 2.10, where the co-firing means that any conductive, resistive or other support structure is fired in the kiln at the same time as the ceramic.

2.4.4 Terahertz probes

Zirconia containing a small amount of yttrium oxide has a toughness roughly $4 \text{ MPa m}^{\frac{1}{2}}$, not particularly large but sufficient to make it one of the tougher ceramics; a martensitic phase change from its tetragonal to monoclinic structures (p. 10) induced in a region where there is a stress concentration (e.g., at a crack tip) does work and therefore mitigates the surrounding stresses. Combined with its hardness, there are potential applications in dental restoration. The material does tend to degrade in a humid environment through interaction with OH^- . It is useful therefore, to be able to monitor its integrity using non-invasive techniques that avoid the ionisation of biological materials such as human tissue.

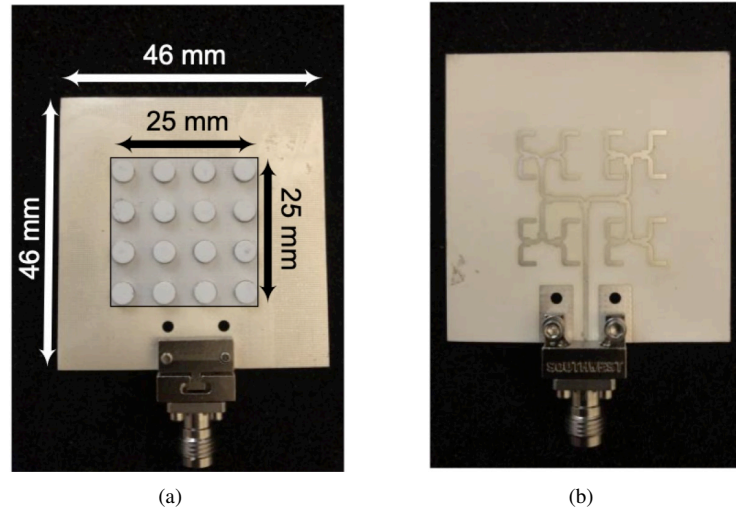


FIGURE 2.10 Low-temperature co-fired ceramic ($\epsilon_r = 5.8$) configured into a millimetre-wave dielectric resonator antenna array. (a) Top view. (b) Bottom view. Images reproduced from Niayesh and Kouki [16] under the CC BY 4.0 license (<https://creativecommons.org/licenses/by/4.0/>).

A terahertz probe that works in the frequency range $0.1 \rightarrow 10$ THz can be made using semiconductor materials [17]. The probe works by directing a short pulse of light from a laser on to a semiconductor such as GaAs (emitter). The laser thus excites electrons within the GaAs, creating electron-hole pairs. An external electrical field placed around the emitter accelerates the excited charge carrier, leading therefore, to the emission of THz waves, Figure 2.11a.

When a pulse of the THz radiation passes through the material being tested, the time delay and amplitude can be compared against a reference signal to deduce the dielectric properties of the material. This in turn enables the degradation of dental zirconia-yttria to be assessed since that sort of damage influences the dielectric properties, Figure 2.11b.

Example 10: Sintering and dielectrics

It was found that on separately sintering Al_2O_3 and TiO_2 in air, the former has a high relative density and low dielectric loss, but that when the TiO_2 exceeded a relative density of 92%, it exhibited a high dielectric loss. Why is that? [Dielectric loss refers to the energy dissipation that occurs in a dielectric material when it is subjected to an alternating electric field. This loss is primarily due to the lagging of the polarisation of the dielectric material behind the applied

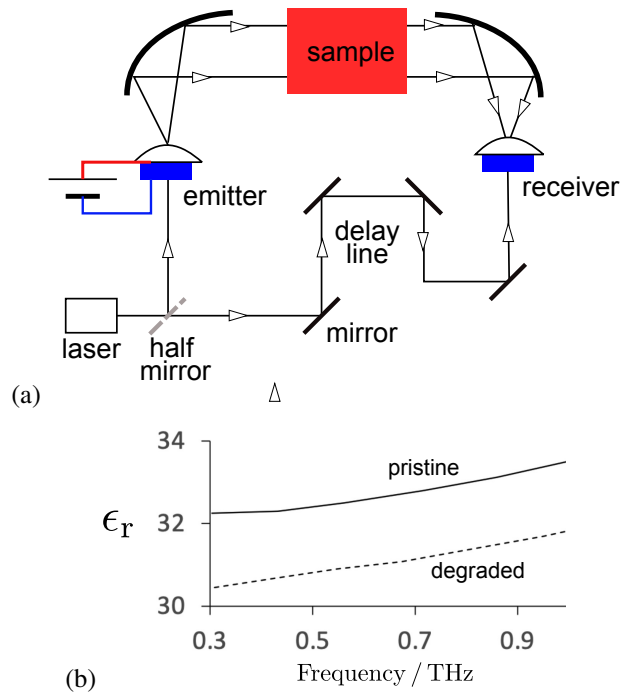


FIGURE 2.11 (a) Simplified diagram of time terahertz time domain spectrometer. (b) Change in the permittivity as a function of frequency, for both a pristine sample of yttria-stabilised tetragonal zirconia showing the decreased in ϵ_r following degradation in a humid environment. Selected data from Ahmed et al. [17].

electric field, which results in the conversion of some electrical energy into heat.]

Solution 10

The oxygen partial pressure in air decreases as the temperature is increased for the purposes of sintering. This is because the concentration per unit volume decreases when air expands, so even if the mole fraction of oxygen does not change, its concentration drops. So if the air is in contact with oxide, it becomes more favourable for the oxide to decompose and release oxygen.

In Al_2O_3 , the aluminium and oxygen atoms are strongly bonded, so during sintering it does not lose oxygen. This is not the case for TiO_2 which can better tolerate deviations from stoichiometry, so some oxygen is released to the air in the furnace at high temperatures. During cooling, kinetics limits the recovery of the oxygen concentration in the TiO_x , which in turn affects its dielectric properties.

If the TiO_x sample is sectioned, the central oxygen-depleted region exhibits a bluish tinge caused by the reduction of the oxide. The oxygen vacancies can trap charge carriers, which therefore have a reduced ability to respond to an alternating field, causing increased dielectric loss.

Example 11: Temperature coefficient of resonant frequency

Why is the temperature coefficient of the resonance frequency of a dielectric disc dependent on temperature and its thermal expansion coefficient?

Solution 11

The impedance Z of a dielectric is a measure of how it reacts (resists) to the flow of alternating current,

$$Z = \frac{1}{i\omega C} + R$$

where $C = \epsilon_0 \epsilon_r A / z_t$ is the capacitance. It follows that since the permittivity varies with temperature, and thermal expansion affects the area and thickness, the resonance frequency becomes a function of temperature.

Example 12: Strange dielectric

The dielectric property at 1kHz determined on a particular sample is found to be controlled by orientational polarisation (p. 30). Oddly, as the temperature is increased, the permittivity increases but the dielectric loss when subjected to alternating voltage decreases. Speculate on a possible mechanism that might explain this observation.

Solution 12

We have seen that permittivity defines how the polarisation responds to an external field, i.e., dP/dE . The rotation of the dipoles to comply with the field must become easier at elevated temperatures so the observed change in permittivity is expected.

The dielectric loss has two components (Equation 2.4), the direct current component, and a term due to the alternating voltage, which is proportional to $1/\epsilon_r''$. Therefore, since ϵ_r'' , the loss will decrease with increasing temperature.

Example 13: Variation in Curie point

There are Curie points of dielectrics listed below. Explain qualitatively in terms of bonds, why they vary so much between the two substances.

Substance	Chemical composition	T_C / K
Rochelle salt	$\text{KNaC}_4\text{H}_4\text{O}_6 \cdot 4\text{H}_2\text{O}$	255, 297
Lithium niobate	LiNbO_3	1415

Solution 13

The Curie point represents that beyond which dipole moments disappear because the crystal acquires a centre of symmetry, so there will be an accompanying change in bond energies. If the difference in bond energies between say the ferroelectric and paraelectric phases is taken to equal the thermal energy kT_C at the Curie point, this allows the estimation of the Curie point [18]. In the case of lithium niobate, the Nb-O bond energy changes from 502 to 366 kJ mol⁻¹ which is very large (of course, we need to sum up all bonds and their associated changes), explaining its large T_C .

In Rochelle salt, the T_C is driven by the stretching of *hydrogen bonds*, which are much weaker than the bonds in lithium niobate, hence the dramatic reduction in T_C [19].

REFERENCES

1. P. Balk: 'Dielectrics for field effect technology', *Advanced Materials*, 1995, **7**, 703–710.
2. J.-H. Jun, C.-H. Wang, D.-J. Won, and D.-J. Choi: 'Structural and electrical properties of a La_2O_3 thin film as a gate dielectric', *Journal of the Korean Physics Society*, 2002, **41**, 998–1002.
3. G. Shirane, R. Pepinsky, and B. C. Frazer: 'X-ray and neutron diffraction study of ferroelectric PbTiO_3 ', *Acta Crystallographica*, 1956, **9**, 131–140.
4. H. Basantakumar Sharma, H. Sarma, and A. Mansingh: 'Ferroelectric and dielectric properties of sol-gel processed barium titanate ceramics and thin films', *Journal of Materials Science*, 1999, **34**, 1385–1390.
5. R. Cudney, J. Fousek, M. Zgonik, P. Günter, M. Garrett, and D. Rytz: 'Photorefractive and domain gratings in barium titanate', *Applied Physics Letters*, 1993, **63**, 3399–3401.
6. V. Buscaglia, and C. A. Randall: 'Size and scaling effects in barium titanate. an overview', *Journal of the European Ceramic Society*, 2020, **40**, 3744–3758.
7. H. Chaib, L. Eng, F. Schlaphof, and T. Otto: 'Surface effect on the electrical and optical properties of barium titanate at room temperature', *Physical Review B – Condensed Matter and Materials Physics*, 2005, **71**, 085418.
8. H. Chaib: 'Spontaneous polarisation of barium titanate': Private communication to H. K. D. H. Bhadeshia, 2025.
9. M. Huang, W. You, Y. Wu, L. Zhang, Y. Li, C. Gao, and B. Qi: 'PEA-Kerr combined measurement method for space charge and electric field distribution of oil–paper composite insulation', *IEEE Transactions on Instrumentation and Measurement*, 2023, **72**, 1–12.
10. R. A. Raj: 'Space charge and its effects on oil-paper insulation in power transformers: A review', *Journal of Electrostatics*, 2023, **126**, 103861.
11. Z. Yuan, Q. Wang, Z. Ren, F. Lv, Q. Xie, J. Geng, J. Zhu, and F. Teng: 'Investigating aging characteristics of oil-immersed power transformers' insulation in electrical-thermal-mechanical combined conditions', *Polymers*, 2023, **15**, 4239.
12. E. Whalley, D. Davidson, and J. Heath: 'Dielectric properties of ice VII. Ice VIII: a new phase of ice', *The Journal of Chemical Physics*, 1966, **45**, 3976–3982.
13. Y. Ishida: 'Studies on dielectric behavior of high polymers', *Kolloid-Zeitschrift*, 1960, **168**, 29–36.
14. S. J. Penn, N. M. Alford, A. Templeton, X. Wang, M. Xu, M. Reece, and K. Schrapel: 'Effect of porosity and grain size on the microwave dielectric properties of sintered alumina', *Journal of the American Ceramic Society*, 1997, **80**, 1885–1888.
15. N. T. Taylor, F. H. Davies, S. G. Davies, C. J. Price, and S. P. Hepplestone: 'The fundamental mechanism behind colossal permittivity in oxides', *Advanced Materials*, 2019, **31**, 1904746.
16. M. Niayesh, and A. Kouki: 'LTCC-integrated dielectric resonant antenna array for 5G applications', *Sensors*, 2021, **21**, 3801.
17. S. Ahmed, M. Zhang, V. Koval, L. Zou, Z. Shen, R. Chen, B. Yang, and H. Yan: 'Terahertz probing of low-temperature degradation in zirconia bioceramics', *Journal of the American Ceramic Society*, 2022, **105**, 1106–1115.
18. X. Zhang, and D. Xue: 'Bond energy prediction of curie temperature of lithium niobate crystals', *The Journal of Physical Chemistry B*, 2007, **111**, 2587–2590.
19. A. R. J. P. Ubbelohde, and I. Woodward: 'Structure and thermal properties of crystals, VI. the role of hydrogen bonds in Rochelle salt', *Proceedings of the Royal Society of London. Series A. Mathematical and Physical Sciences*, 1946, **185**, 448–465.

Chapter 3

Ferroelectric oxides

3.1 INTRODUCTION

A dielectric material that exhibits spontaneous electric polarisation at low temperatures, even if there is no external field present at all (*cf.* BaTiO₃ in Chapter 1). Such a material is said to be *ferroelectric*.

When Joseph Valasek discovered ferroelectricity in Rochelle salt in 1920 [1, 2], ferromagnetism was already a well-established phenomenon. Ferromagnetic materials, like iron (from which ‘ferro’ is derived, meaning iron), exhibit a spontaneous magnetic polarisation (magnetisation) that can be reversed by an external magnetic field, and this reversal shows a characteristic hysteresis loop.

Valasek observed that Rochelle salt behaved in a remarkably similar way, but with electric polarisation instead of magnetic polarisation. He found that the material had a spontaneous electric polarisation (\mathcal{P}_s) that could be reversed by an applied electric field, and this relationship also exhibited a hysteresis loop (Figure 3.7c).

Therefore, because of the striking parallels in their behaviour – spontaneous ordering that can be reversed by an external field and the presence of a hysteresis loop – the term ‘ferroelectric’ was coined to highlight this analogy with ferromagnetism, even though ferroelectric materials themselves do not necessarily contain iron.¹

Ferroelectric solids have the ability to convert electrical signals into acoustic signals and *vice versa*, because the polarisation within can be periodically reoriented by an appropriately varying electric field, resulting in mechanical strains that induce acoustic waves. This electromechanical coupling is called the *piezoelectric effect* (Chapter 4). All ferroelectric materials are also piezoelectric though the opposite is not true (p. 63).

In a *linear* dielectric, $\mathcal{P} = (\epsilon_r - 1)\epsilon_0 E$ (Equation 2.1f) so the permittivity does not change with the magnitude of E . If the field is doubled, so is the polarisation. It does vary with temperature. However, for linear dielectrics, this

1. Quote from Valasek: ‘... the dielectric displacement D , electric intensity E , and polarization P ... are analogous to B , H and I in the case of magnetism. ... hysteresis in P analogous to magnetic hysteresis. This would suggest a parallelism between the behavior of Rochelle salt as a dielectric and steel, for example, as a ferromagnetic substance.’

variation is generally ‘monotonic,’ meaning it consistently increases or decreases with temperature, without sudden jumps or complex behaviour (unless there’s a phase transformation, which is a structural change in the material). For example, the permittivity of blood is described using a constant temperature coefficient (i.e., the sensitivity of ϵ_r to T) [3].

In contrast, ferroelectric materials exhibit a non-linear relationship between polarisation and electric field. Their permittivity is not constant with the magnitude of E . An example of a *nonlinear* dielectric is $\text{SrBi}_4\text{Ti}_4\text{O}_{15}$, a ferroelectric, displaying a maximum in permittivity at the Curie point beyond which it becomes paraelectric, losing its spontaneous polarisation, Figure 3.1a. The substance has an orthorhombic crystal structure though the a, b axes have similar lengths, much shorter than along c . There are some single crystal studies [4, 5] that show that the hysteresis observed below T_C is anisotropic, Figure 3.1b, becoming zero along the c -axis. This is because there is a mirror plane normal to the c -axis (Figure 3.1c). This symmetrical arrangement means that for every positive charge displacement in one direction, there’s an equal and opposite negative charge displacement, or vice-versa, effectively canceling out any net polarisation along that axis. Therefore, even below T_C , the c -axis remains non-polar, leading to zero hysteresis. Along the other two axes, charge displacement occurs under the influence of an applied field by the twisting of metal-oxygen octahedra, leading to pronounced hysteresis as the domain structure attempts to comply with the applied field.

Temperature opposes order because the entropy term in the free energy expression scales with temperature [Section 2.3, 6]. In Figure 3.1a, the increase in permittivity as the temperature approaches T_C from above is because the thermal energy is just enough to disrupt the ordering of dipoles. The effect is often described by the Curie-Weiss relationship which is a result of a mean-field theory that generally predicts second order transitions

$$\chi_e \equiv (\epsilon_r - 1) \propto \frac{1}{T - T_C} \quad \text{for} \quad T > T_C. \quad (3.1)$$

It can give a reasonable approximation for a first-order transition for temperatures well below T_C . The Curie-Weiss mean-field theory applies to both ferromagnetism and ferroelectricity, given that both have interacting dipoles.

Equation 3.1 shows that $\epsilon_r \rightarrow \infty$ at T_C because of an approximation in which the complex interactions between individual electric dipoles are simplified by replacing them with an average or ‘mean’ internal field [p.323, 7]. This internal field acts on each dipole, effectively assuming that all dipoles experience the same average influence from their neighbours. The mean-field approximation works well far from the critical point (T_C). However, close to T_C , fluctuations in polarisation become large but the theory does not account for them. The Curie-Weiss model being a mean-field theory, is conceptually best suited for single

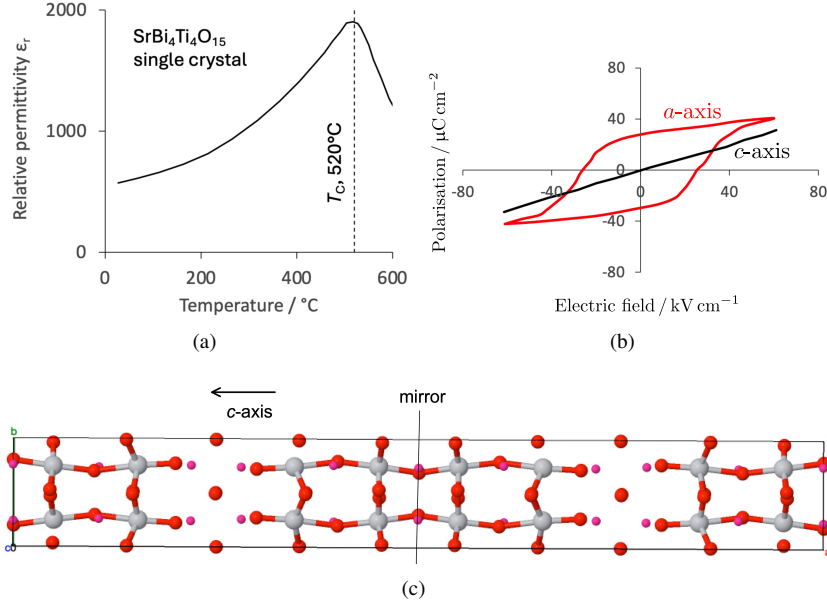


FIGURE 3.1 $\text{SrBi}_4\text{Ti}_4\text{O}_{15}$ single-crystal data. The crystal structure has an orthorhombic unit cell, with similar lattice parameters along a, b but a much longer c parameter. (a) Variation in permittivity with temperature, the permittivity peaking at the Curie point associated with the transition from ferroelectric to paraelectric behaviour. (b) Hysteresis loops measured along the a -axis and along the c -axis. The data in (a,b) represent a selection from Irie and Miyayama [4]. (c) Projection of the crystal structure on a plane normal to a .

crystals in their disordered state ($T > T_C$), where domain structures do not exist spontaneously. However, it is usefully applied to polycrystalline materials in their disordered phase as well, with deviations from ideality attributed to defects or averaging effects. The model does not apply to the multi-domain or single-domain ordered state below T_C .

3.2 DOMAIN STRUCTURES

As BaTiO_3 cools below its T_C (around 120°C), it undergoes a phase transition from cubic to tetragonal. This transition involves a slight distortion of the unit cell (p. 28), specifically an elongation along one of the original $\langle 001 \rangle_{\text{cubic}}$ directions and a contraction along the other two. This distortion breaks the centrosymmetry, leading to the off-centering of ions (specifically the Ti ion within the oxygen octahedron), which creates a spontaneous electric dipole moment along the elongated axis. This is the origin of ferroelectricity in BaTiO_3 .

Considering a single crystal of the cubic lattice, any one of the original three cubic axes could become the tetragonal c -axis following transformation. Since the

polarisation can point in either the positive or negative direction along that axis, there are 6 possible directions for the spontaneous polarisation in the tetragonal phase. The entire tetragonal crystal can adopt just one of the six polarisation directions. However, it typically doesn't do so. Instead, it spontaneously breaks up into regions called ferroelectric *domains*, with the polarisation uniform in each such domain, Figure 3.2.

When a ferroelectric material cools below its T_C , it spontaneously develops a net P_S . If the entire crystal were to polarise uniformly in one direction (single domain), surface charges would appear on the surfaces perpendicular to the polarisation direction. These would create a strong depolarising electric field E_d inside the material, acting in the opposite direction to P_S . The E_d raises the electrostatic energy of the system. By splitting into multiple domains with alternating polarisation directions (e.g., regions of $[001]$ and $[00\bar{1}]$ polarisation), E_d is significantly reduced, often becoming zero over macroscopic distances.

There is a second reason for domain formation. The ferroelectric phase transition in BaTiO_3 is a structural distortion. This distortion introduces anisotropic mechanical strain into the crystal lattice. If the crystal is constrained by surrounding material, these internal strains can lead to high elastic energy. Domains can form in such a way that the strains from adjacent domains partially cancel each other out at the domain boundaries. For example, if one domain is elongated in one direction, an adjacent domain might be elongated in a perpendicular direction, or contracted, to reduce the overall stress.

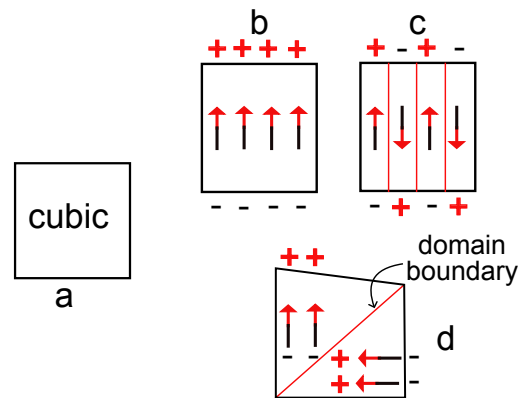
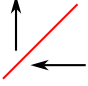



FIGURE 3.2 Schematic formation of domains in barium titanate. The cubic form (a) has no spontaneous polarisation, which develop when it transformation in the tetragonal variety (b). domain formation clearly reduces the external field (c), as do the 90° domains (d).

In tetragonal ferroelectrics, the spontaneous polarisation of adjacent domains can enclose angles of 90° or 180° , where the red lines in the diagram below indicate domain boundaries [8]:

Domain	Boundary plane, polarisation axes	Boundary thickness / nm	Boundary energy / J m^{-2}
	$(101), z, x$	$\approx 5 \rightarrow 10$	0.01
	$(100), z, -z$	$\approx 0.5 \rightarrow 2$	$0.002 \rightarrow 0.004$

When an external electric field is applied, domains whose polarisation direction is aligned with the field (or has a component aligned with it) are energetically favoured. Those whose polarisation is anti-aligned or orthogonal to the field are unfavourable. To minimise energy, the favourable domains expand by moving their domain walls, effectively switching the polarisation of the regions they encompass.

Because a domain boundary is the region across which the dipole moment changes direction. A thicker boundary (e.g., 90°) allows for a more gentle transition, making such boundaries more mobile. Dipole reversal at the 180° boundaries is relatively abrupt, with the wall thickness approaching just one unit cell [9] for perovskites like BaTiO_3 and PbTiO_3 ; such boundaries have reduced mobility. In contrast, the 90° domain walls have a width of about 21 nm [10], permitting a more gentle transition in dipole orientation across the more mobile boundary. If a material primarily contains rigid 180° domain walls that don't move easily under an applied field, the ability to reorient polarisation in response to the field (which is what permittivity measures) is limited. Conversely, a preponderance of mobile 90° domain walls that respond easily to the field leads to a higher effective permittivity.

The more mobile 90° domain-boundaries play an increasing role as the grain size of a polycrystalline sample is reduced, leading to an increase in ϵ_r , Figure 3.3a. When grains become extremely small, the energy cost of forming and maintaining domain walls (especially the more 'distorted' 90° walls) becomes prohibitive. The material might then prefer to become a single domain within each tiny grain, leading to a sharp decrease in permittivity.

A secondary effect is that when grains become very small in polycrystalline BaTiO_3 , there is a reduction in the tetragonality of the lattice, in part due to constraints from the surrounding matrix but also because the large surface-to-volume ratio can result in a change in bonding. As a consequence, the Curie temperature decreases quite dramatically, Figure 3.3b.

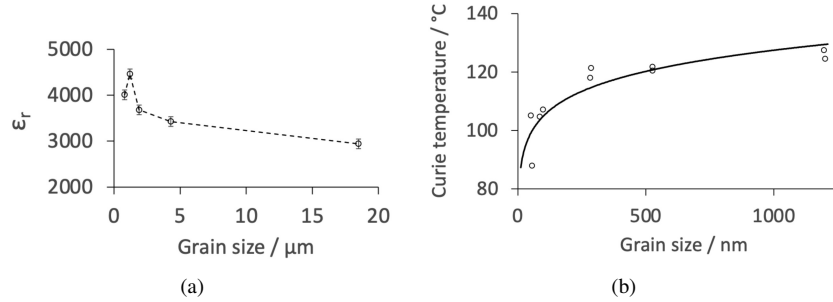


FIGURE 3.3 (a) The change in permittivity as the grain size of spark plasma sintered barium titanate. Selected data from Tan et al. [11]. (b) Dependence of the Curie temperature of polycrystalline barium titanate as a function of grain size. Selected data from Zhao et al. [12].

3.3 CHARACTERISATION

Figure 3.4 shows the domain structure of $\text{NaK}_{0.5}\text{Nb}_{0.5}\text{O}_3$ imaged using a scanning electron microscope. The contrast arises through the interaction of incident electrons with the different charge states in the individual domains, i.e., different orientations of polarisation and surface charge distribution. Domain boundaries can be regarded as interfaces so there will always be a tendency to minimise the boundary curvature.

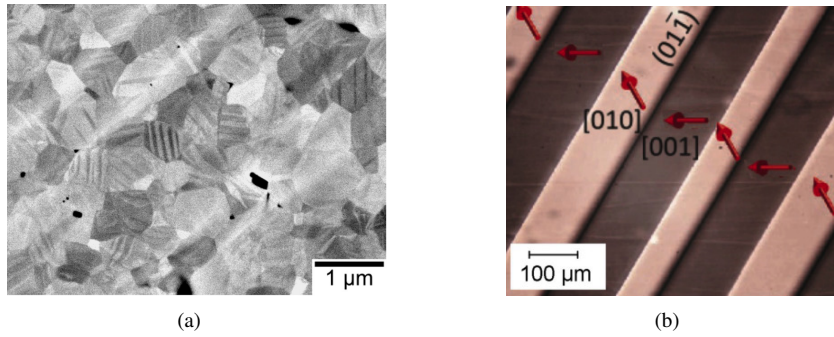


FIGURE 3.4 (a) Back-scattered scanning electron micrograph showing stripped ferroelectric-domains in $\text{NaK}_{0.5}\text{Nb}_{0.5}\text{O}_3$. Image courtesy of Haixue Yan, with details in [13]. (b) Transmission polarised-light microscopy of ferroelectric domains in BaTiO_3 . The plane of the image corresponds to $\{111\}$. The red arrows the polarisation, but have been changed from the original to reflect the correct head-to-tail sequence. Image courtesy of Bednyakov and Hlinka [14].

3.3.1 Alumina

The overwhelming interest is in the electrical properties – Figure 3.5a shows a sample of alumina, which is a linear dielectric, subjected to a voltage that varies in a triangular waveform with $V \propto \dot{V}t$ where \dot{V} is the rate of change of voltage and t is the time. Since the charge $q = CV$, where C is the capacitance, it follows that

$$\text{current } I = \frac{dq}{dt} = C \frac{dV}{dt} = C\dot{V}. \quad (3.2)$$

Since both C and \dot{V} are fixed, so is the current, which is typical of linear dielectrics. Alumina has $\epsilon_r \approx 8 \rightarrow 10$ so it has a small capacitance and large impedance, making the current extremely small.

The integration of current over time yields the charge, which over the electrode area is the ‘displacement of charge’, $\mathcal{D} = \epsilon_0 E + \mathcal{P}$ (Equation 2.1e) which approximately is equal to \mathcal{P} . For a linear dielectric, ϵ_r does not depend on $|E|$. Since the dominant contribution to current flow is permittivity, an almost rectangular I - E loops is obtained, Figure 3.5b, with an essentially linear \mathcal{D} - E loop, Figure 3.5c, with \mathcal{D} obtained by integrating the current over time.

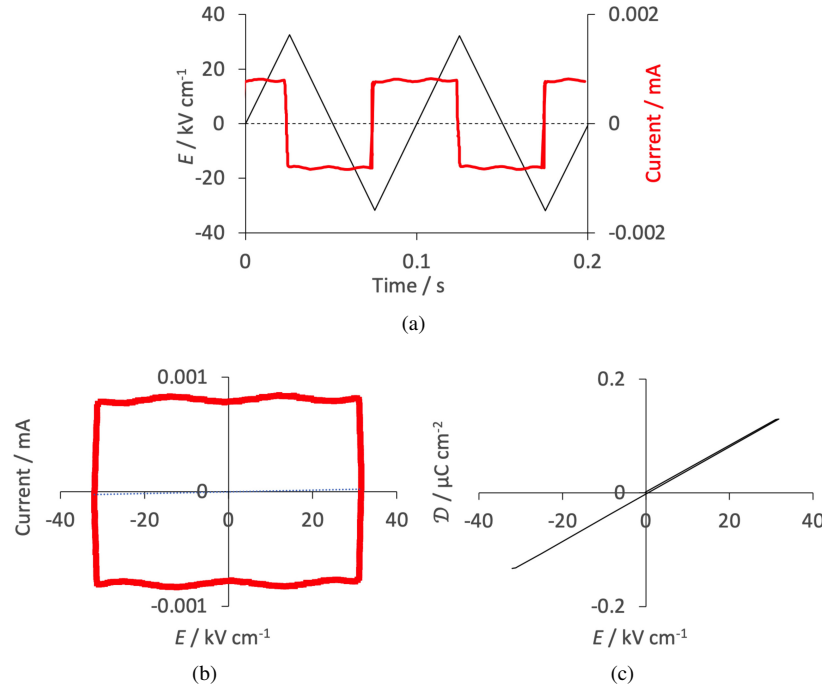


FIGURE 3.5 Alumina subjected to 10 Hz triangular-wave potential at 25 °C. Data courtesy of Haixue Yan [15].

Alumina is a good electrical insulator and is used widely as a substrate for microelectronics and power electronics because of its relatively high thermal conductivity ($\approx 30 \text{ W m}^{-1} \text{ K}^{-1}$). This can also help dissipate heat away from the source. Its thermal expansion coefficient is small (10^{-6} K^{-1}) which makes it resistant to thermal fluctuations.

3.3.2 Bismuth ferrite

Bismuth ferrite ($\text{Bi}_{0.89}\text{La}_{0.05}\text{Tb}_{0.06}\text{FeO}_3$) is ferroelectric below $T_C \approx 800^\circ\text{C}$ while at the same time antiferromagnetic (Chapter 7) below the Néel temperature of about 370°C (the magnetic properties are attributed to iron). In the circumstances illustrated in Figure 3.6, the material exhibits a linear dependence of current on voltage, i.e., Ohm's law behaviour with the current changing in proportion to the voltage. Figure 3.6c shows a maximum \mathcal{D} at $E = 0$ because the material has a high conductivity so cannot hold charge.

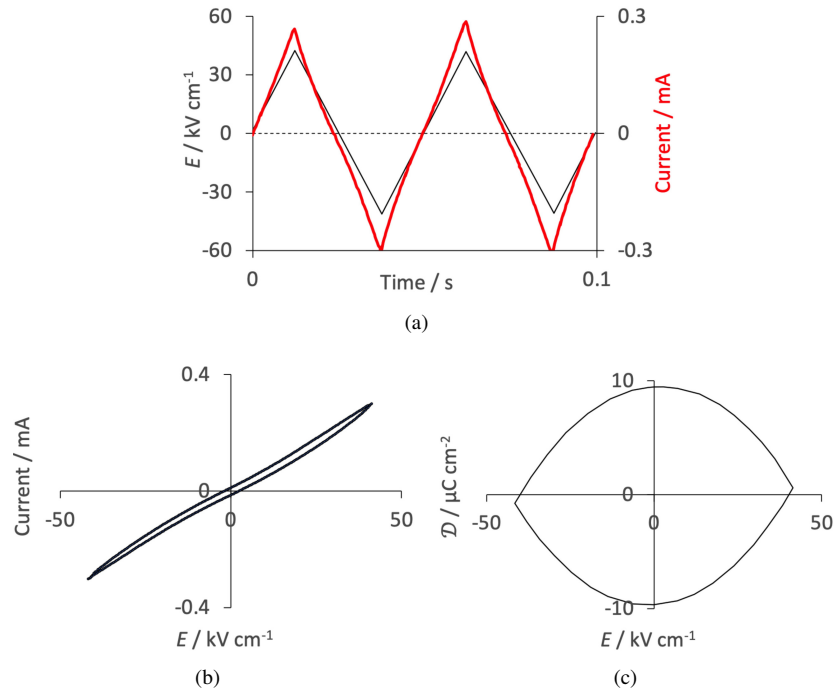


FIGURE 3.6 Polycrystalline $\text{Bi}_{0.89}\text{La}_{0.05}\text{Tb}_{0.06}\text{FeO}_3$ subjected to 20 Hz triangular-wave potential at 25°C . Data courtesy of Haixue Yan [15].

3.3.3 Sodium potassium niobate

Sodium potassium niobate $\text{Na}_{0.5}\text{K}_{0.5}\text{NbO}_3$ is a solid solution of sodium niobate (NaNbO_3) and potassium niobate (KNbO_3). Both have perovskite crystal structures. The perovskite structure (ABO_3) is common among many ferroelectric materials, where the spontaneous polarisation arises from the displacement of the B-site ion (Nb in this case) and/or the A-site ions (Na/K) from their ideal centrosymmetric positions. Its relative permittivity $\epsilon_r \approx 300$ at ambient temperature and measured at 0.1 MHz, with $T_C \approx 420^\circ\text{C}$ [16]. This is much greater than of dielectrics like alumina ($\epsilon_r \approx 8 \rightarrow 10$); the high Curie temperature indicates that it remains ferroelectric over a broad and technologically relevant temperature range. We have seen that domains can change their polarisation direction under the influence of an electrical field, by the movement of domain boundaries, which may result in the displacement of actual charge carriers (e.g., electronic defects, ionic vacancies) that are associated with the domain walls or are trapped at them. Furthermore, if charge carriers are swept along or released by the moving walls, this constitutes an actual current flow that is distinct from the simple displacement current seen in linear dielectrics. Such a change would be transient (Figure 3.7) and frequency dependent.

Lead zirconate titanate (commonly known as PZT) is arguably the most dominant and widely used piezoelectric ceramic. Its excellent electromechanical coupling properties make it highly effective in converting electrical energy to mechanical energy (actuators) and vice versa (sensors, transducers). It's the workhorse material for a vast array of applications. A major drawback is that it contains about 60 wt% of lead which can be toxic. Lead-free variants, including sodium potassium niobate, are researched and there has been some commercial progress in its exploitation. One example is a medical device, a *nebuliser* that converts liquid medication into a fine mist that can be inhaled directly into the lungs, for example, in treating the symptoms of asthma. A piezoelectric disc made of potassium sodium niobate is induced to vibrate rapidly ($\approx 120\text{ kHz}$) in response to an appropriate electric field. The vibration is transferred to a microporous diaphragm that is in contact with the liquid medication. This forces the liquid through the tiny holes in the mesh, thus creating the mist. A pioneer in this field is *Tongxiang Tsingfeng Technology Co., Ltd* [17] which markets devices made using lead-free piezoelectrics, a key product being the nebuliser.

In Figure 3.8, the piezoelectric coefficient d_{33} refers to a piezoelectric quantity relating electric charge generated to a mechanical force (p. 65), an indication of how effective a material is in converting mechanical energy into the electrical form, or *vice versa*. The subscript '33' refers to a specific crystallographic direction because it is a part of a 3×3 matrix of such coefficients, though it is the most significant (Equation 4.1 in Chapter 4).

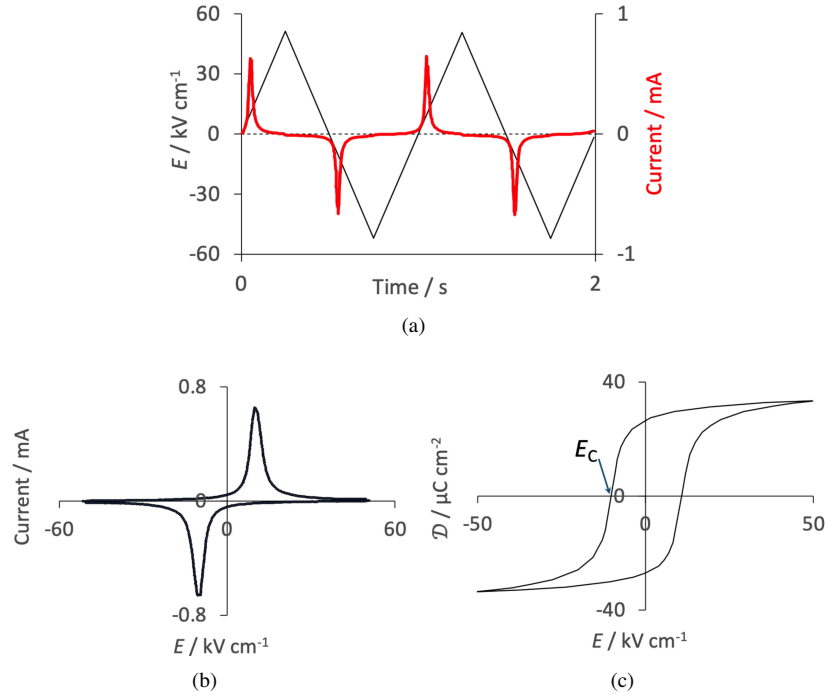


FIGURE 3.7 $\text{Na}_{0.05}\text{K}_{0.05}\text{NbO}_3$ subjected to 1 Hz triangular-wave potential at 25 °C. The arrow in (c) marks the coercive field E_c required to reach $\mathcal{D} = 0$. Data courtesy of Haixue Yan [15].

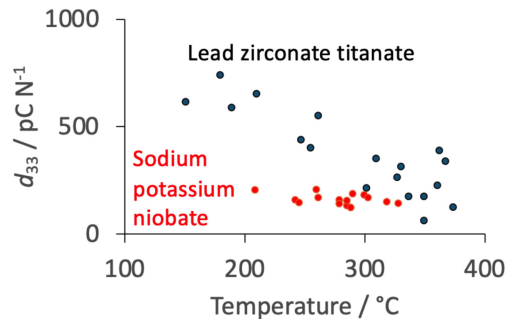


FIGURE 3.8 A comparison of the performance of lead-containing and a lead-free piezoelectric. Selected data form a compilation of published sources by Wu et al. [18].

3.4 POLING

Poling describes how a randomly oriented material is made to exhibit macroscopic piezoelectricity by aligning its domains, and introduces the concept of ‘hard’ piezoelectrics.

Changing the polarisation direction with a domain can be induced by applying an external electric field. However, the field doesn’t arbitrarily change the polarisation because the new directions must align with one of the crystallographically allowed spontaneous polarisation directions, for example the six $\langle 001 \rangle_{\text{tetragonal}}$ equivalent directions in BaTiO_3 . A polycrystalline material is composed of many tiny crystallites (grains), each with its own crystal orientation, and because the grains are likely to be randomly oriented, the net polarisation across the entire sample cancel out macroscopically, and no piezoelectricity.

In the case of LiNbO_3 , poling is used to remedy this by heating the sample to $T > T_C$ to render it paraelectric, and applying a strong DC electric field before cooling while maintaining the field. When $T < T_C$, the spontaneous polarisation forms, but now it does so preferentially aligned with the direction of the applied external field. The field can then be removed. In the case of barium titanate, the polycrystalline sample would be heated to 135°C where it has a cubic crystal structure, and then cooled under $E = 1.2 \text{ kV mm}^{-1}$ to ambient temperature and the field removed.

However, in many cases, poling is done at $T < T_C$, in other words at as high a temperature below T_C as possible. This is because the coercive field (the electric field required to switch the polarisation) decreases significantly. This means a lower electric field can be used to effectively align the domains, reducing the risk of dielectric breakdown and making the process more efficient. Higher temperatures provide more thermal energy to the dipoles within the material, making it easier for the domains to reorient and switch under the influence of the external electric field. This leads to more complete and stable poling.

The process relies on domain boundaries that do not adjust after the electrical field is removed. The so-called ‘hard’ ferroelectrics retain polarisation even when the external field is removed. Barium titanate and lead zirconate are both *hard* ferroelectrics, meaning that domain walls are pinned by defects, impurities or internal stresses. One example of a ‘soft’ ferroelectric where the polarisation after poling is less stable because of domain wall mobility, is described in the next Section.

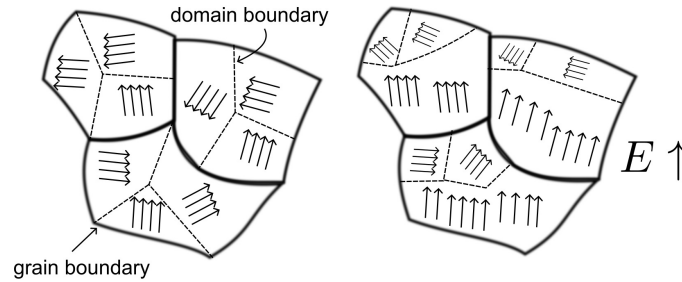


FIGURE 3.9 Polycrystalline sample showing no net polarisation because the individual grains are randomly oriented. The image on the right is after poling with the dipole directions aligned approximately to the applied DC electric field. Notice that the dipole directions after poling are identical to one of the sets before poling, since the possible orientations are governed by crystallography.

3.5 RELAXOR FERROELECTRICS

Unlike classical ferroelectrics which have a sharp, well-defined T_C where a clear phase transition occurs, relaxors show a diffuse phase transition. This means that during cooling, the change from a predominantly paraelectric (disordered) state to a ferroelectric-like (ordered) state happens gradually over a broad temperature range and is frequency-sensitive, with the permittivity going through a maximum identified as T_{\max} .

Instead of forming large, macroscopic ferroelectric domains below T_C , relaxors develop tiny polar regions which locally (few nm) where spontaneous polarisation is present due to local atomic displacements, even above the macroscopic T_{\max} .

There are small regions of ordered polarised regions that can *fluctuate* in size and orientation, Figure 3.10a. Crucially, these are not static, they ‘fluctuate’ in size and orientation. This dynamic behaviour gives relaxors their unique properties. As temperature decreases, they grow and eventually interact, leading to the macroscopic properties.

Relaxors are renowned for their incredibly high peak permittivity (Figure 3.10b) which can reach tens of thousands or even hundreds of thousands (compared to a few hundred for typical ferroelectrics) with the peak at T_{\max} . The high permittivity is attributed to the presence and dynamic behaviour of the tiny spontaneously polarised regions that are highly susceptible to an external electric field. In classical ferroelectrics, above T_C , the permittivity typically follows the Curie-Weiss law (p. 44), showing a steep decline as temperature increases, in contrast to relaxors where the decrease beyond T_{\max} much more gradually because the tiny polarised regions still exist. A temperature $T_f < T_{\max}$ is the so-called *freezing temperature* below which the field induced transition and domain switching is thermally stable and largely irreversible. The material exhibits a

stable, field-induced ferroelectric-like phase, making T_f functionally important for the stability of piezoelectric properties, similar to how T_C defines the upper limit for ferroelectric stability in classical materials.

There is so-called Burns temperature (T_B) above which the material exists in a disordered, non-polar paraelectric state,² the small polarised regions exist only below T_B .

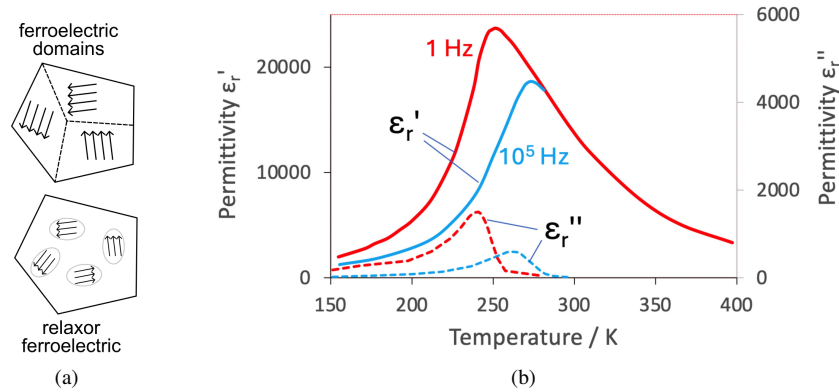


FIGURE 3.10 Schematic comparison between ferroelectric at $T < T_C$ and a relaxor ferroelectric containing small regions of polarisation. (b) Real and imaginary components of the permittivity of a relaxor ferroelectric $\text{Pb}(\text{Mg}_{\frac{1}{3}}\text{Nb}_{\frac{2}{3}})\text{O}_3$. Selected data from Bokov and Ye [19].

3.6 ANTIFERROELECTRICS

Antiferroelectrics are closely related to ferroelectrics but have a distinct spontaneous dipole arrangement and field-induced behaviour. Unlike ferroelectrics where dipoles are generally aligned in the same direction (or easily switchable to do so) to create a net polarisation, in antiferroelectrics, adjacent dipoles are aligned in an antiparallel fashion. Imagine two sub-lattices of dipoles, with the dipoles on one sub-lattice pointing in one direction and those on the other pointing in the exact opposite direction. The net spontaneous polarisation of the material is therefore zero in its ground state.

However, a sufficiently strong external electric field can overcome the internal forces that maintain the antiparallel arrangement. This leads to a field-induced phase transition where the dipoles switch to a parallel (or predominantly parallel) alignment, resulting in a net macroscopic polarisation. The material effectively becomes ferroelectric under the strong field, but it is not stable without the

2. Gerald Burns and Dacol identified the temperature below which polar nanoregions begin to form, distinct from T_C which marks the transition from the paraelectric to the ferroelectric states on cooling. The original work was based on odd behaviours in the vibrational modes of ferroelectrics.

field.

PbZrO_3 , AgNbO_3 , PbHfO_3 , NaNbO_3 are common and well-known examples of antiferroelectric perovskites. Antiferroelectric materials also lack a centre of symmetry in the unit cell. The crystal structure of both the cubic and orthorhombic (antiferroelectric) forms of lead zirconate are illustrated in Figure 3.11.

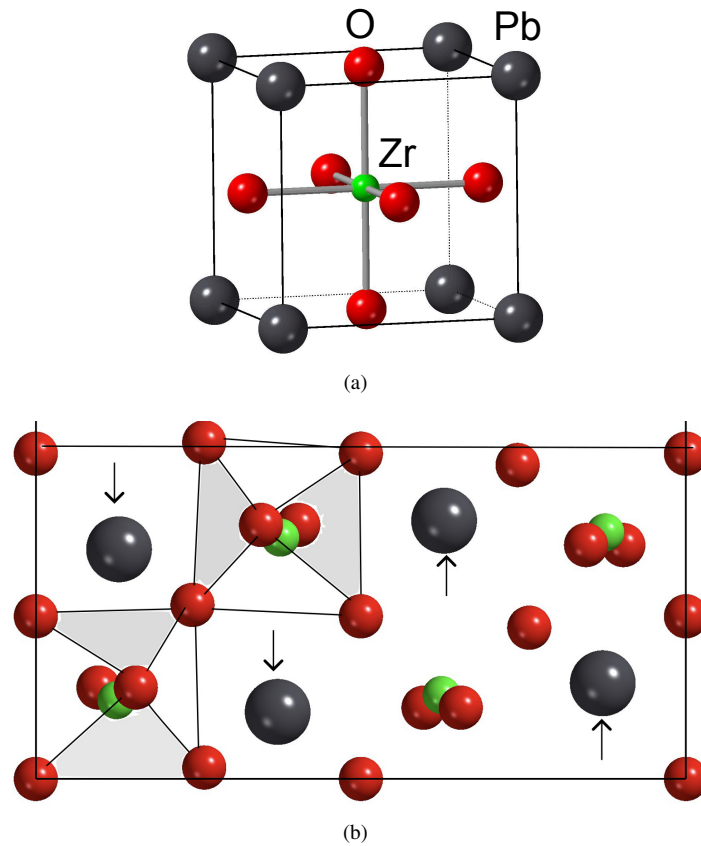


FIGURE 3.11 Lead zirconate PbZrO_3 . (a) Cubic unit cell $a = 0.5881$ nm shown in perspective. Notice the regular octahedron of oxygen atoms surrounding the zirconium atom. (b) The orthorhombic unit cell ($a = 0.5881$ nm, $b = 1.1781$ nm, $c = 0.8224$ nm) shown with the c -axis vertical to the plane of the diagram, with two of the irregular octahedra of oxygen atoms around the zirconium atoms highlighted to show the tilting of the ZrO_6 clusters. The arrows show the local polarisation due to the displacements of the lead atoms.

Lead zirconate has a permittivity $\epsilon_r \approx 200$, which makes it useful in the manufacture of capacitors that can store considerable energy. Antiferroelectric capacitors can charge and discharge rapidly, making them suitable for delivering rapid bursts

of energy. For this reason, they have apparently been used as triggers for nuclear weapons [20]. Although lead is toxic, it was stated in 2021 that there has been no commercialisation of lead-free antiferroelectric materials, because they do not seem to offer the same level of performance or stability as PbZrO_3 , and may pose manufacturing and reliability challenges.

Example 14: Permittivity as a function of temperature

Explain qualitatively why the permittivity of $\text{SrBi}_4\text{Ti}_4\text{O}_{15}$ varies with temperature as illustrated in Figure 3.1a.

Solution 14

In the absence of phase transitions, a temperature increases towards T_C , the thermal energy kT available to dipoles also increases. This helps the dipoles overcome local energy barriers that might hinder their alignment with an external electric field. With an increase in the mobility of dipoles to respond to an applied field, the permittivity increases with temperature because of increased thermal activation. They can therefore align more easily in response to the field, leading to greater polarisation, and hence permittivity. Domain walls also become more mobile for the same reason because kT helps overcome pinning points.

Above T_C , the thermal energy is sufficiently high to overcome the forces that maintain spontaneous, long-range order of electric dipoles. The material loses its ferroelectric properties and becomes centrosymmetric (in the macroscopic sense). Therefore, no remanent polarisation or hysteresis is observed.

As the Curie point T_C is exceeded, there can be no long-range alignment of dipoles. However, there may persist short-range order (tiny polar clusters) which diminishes as the temperature goes beyond T_C , leading to the peak in permittivity at 520 °C, Figure 3.1a.

Example 15: Poling conditions for ferroelectric ceramics

Why are ferroelectric ceramics poled at high-temperatures, though still below T_C ? Poling is explained on page 53.

Solution 15

Domain walls need to move to accommodate the dominance of those dipoles best aligned to the external electrical field. Since their motion is thermally activated, the domain walls are more mobile at high temperatures. Furthermore, it is easier

for dipoles to reorient at higher temperatures.

It follows that a smaller electrical field is needed to cause the alignment of dipoles across a polycrystalline material during poling at high temperatures – this has the advantage of avoiding any possibility of dielectric breakdown under the influence of the applied field.

Why below T_C ? Because above T_C , there would be no permanent domains to align. Therefore, the optimal temperature for poling is a balance: high enough to ensure good mobility, but low enough to remain in the ferroelectric phase where stable domains can be created and aligned.

In general, $\text{SrBi}_4\text{Ti}_4\text{O}_{15}$ ceramics are poled in silicon oil at 220°C , which is below T_C . Silicon oil is chemically inert and electrically insulating under poling conditions.

3.7 ELECTROCALORIC EFFECT

An adiabatic application of an electric field to a polar material causes an increase in its temperature because the dipoles align to the field, thus decreasing entropy. If the material is in contact with a heat sink, it loses the heat generated and reverts to its original temperature. The removal of the field causes that dipoles to lose alignment so the temperature of the sample drops due to the increase in entropy. There is, therefore, a capacity to cool anything in contact with it.

The coefficient of performance is as on p. 105:

$$\text{COP}_{\text{refrigeration}} = \frac{T_{\text{cold}}}{T_{\text{hot}} - T_{\text{cold}}}.$$

Example 16: Electrocaloric material selection

1. Is lead zirconate titanate (p. 77) suitable for an electrocaloric application at ambient temperature?
2. Are relaxor ferroelectrics (p. 54) applicable as ambient temperature electrocalorics?
3. The polymer polyvinylidene fluoride (p. 93) is a relaxor - are there any disadvantages in its application as an electrocaloric?

Solution 16

1. No, because its T_C is well above ambient temperature so the net polarisation is not zero. The largest electrocaloric effect occurs near its T_C because this

is where the material undergoes a phase transition with a large change in entropy. If T_c is significantly above ambient temperature, then at ambient conditions, the material is already in its ferroelectric (polarised) state.

2. Yes, because their polar switching can be induced at small electrical fields, permitting low-voltage devices. The nanoscale polar regions in relaxors can be easily aligned or disoriented by relatively weak electric fields. Because they offer high permittivity over a significant temperature range, greater deviations in temperature are tolerable in principle, though they have a low dielectric breakdown field.
3. It has a low thermal conductivity which would mean slow heating and cooling stages in Figure 3.12. It may degrade and age with time, given thermal fluctuations in the refrigeration cycle, and indeed, sunlight if exposed.

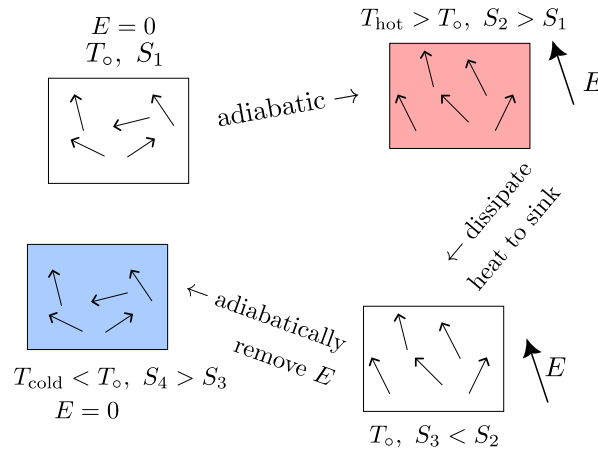


FIGURE 3.12 The dipoles initially at T_o are in random directions, but the application of an electric field causes a degree of alignment, a reduction in entropy, therefore an adiabatic increase in temperature. This heat is then allowed to dissipate into a sink which may simply be the surrounding environment, whilst still under the influence of the field. When the field is eliminated, the entropy increase due to the random alignment of dipoles, leading to cooling, i.e., refrigeration.

REFERENCES

1. J. Valasek: 'Piezo-electric and allied phenomena in Rochelle salt', *Physical Review*, 1921, **17**, 475.
2. J. Fousek: 'Joseph Valasek and the discovery of ferroelectricity', In: *Proceedings of 1994 IEEE International Symposium on Applications of Ferroelectrics*. IEEE, 1994:1–5.
3. F. Jaspard, and M. Nadi: 'Dielectric properties of blood: an investigation of temperature dependence', *Physiological measurement*, 2002, **23**, 547–554.
4. H. Irie, and M. Miyayama: 'Dielectric and ferroelectric properties of $\text{SrBi}_4\text{Ti}_4\text{O}_{15}$ single crystals', *Applied Physics Letters*, 2001, **79**, 251–253.

5. H. Irie, M. Miyayama, and T. Kudo: 'Structure dependence of ferroelectric properties of bismuth layer-structured ferroelectric single crystals', *Journal of Applied Physics*, 2001, **90**, 4089–4094.
6. H. K. D. H. Bhadeshia, and H. Yan: 'Phase transitions – an introduction with worked examples, published independently': www.phase-trans.msm.cam.ac.uk/2022/EMS523U_book.pdf, 2024.
7. C. Kittel: *Introduction to Solid State Physics*: 8th ed., New York, USA: John Wiley and Sons Inc., 2005.
8. V. Zhirnov: 'A contribution to the theory of domain walls in ferroelectrics', *Soviet Physics JETP*, 1959, **35**, 822–827.
9. J. Padilla, W. Zhong, and D. Vanderbilt: 'First-principles investigation of 180° domain walls in BaTiO₃', *Physical Review B*, 1996, **53**, R5969.
10. Q. Zhang, and W. A. Goddard: 'Charge and polarization distributions at the 90° domain wall in barium titanate ferroelectric', *Applied Physics Letters*, 2006, **89**, 182903.
11. Y. Tan, J. Zhang, Y. Wu, C. Wang, V. Koval, B. Shi, H. Ye, R. McKinnon, G. Viola, and H. Yan: 'Unfolding grain size effects in barium titanate ferroelectric ceramics', *Scientific reports*, 2015, **5**, 9953.
12. Z. Zhao, V. Buscaglia, M. Viviani, M. T. Buscaglia, L. Mitoseriu, A. Testino, M. Nygren, M. Johnsson, and P. Nanni: 'Grain-size effects on the ferroelectric behavior of dense nanocrystalline BaTiO₃ ceramics', *Physical Review B—Condensed Matter and Materials Physics*, 2004, **70**, 024107.
13. Z. Shen, D. Grüner, M. Eriksson, L. M. Belova, C.-W. Nan, and H. Yan: 'Ordered coalescence of nano-crystals in alkaline niobate ceramics with high remanent polarization', *Journal of Materiomics*, 2017, **3**, 267–272.
14. P. S. Bednyakov, and J. Hlinka: 'Charged domain walls in BaTiO₃ crystals emerging from superdomain boundaries', *Advanced Electronic Materials*, 2023, **9**, 2300005.
15. H. Yan, F. Inam, G. Viola, H. Ning, H. Zhang, Q. Jiang, T. Zeng, Z. Gao, and M. J. Reece: 'The contribution of electrical conductivity, dielectric permittivity and domain switching in ferroelectric hysteresis loops', *Journal of Advanced Dielectrics*, 2011, **1**, 107–118.
16. L. Egerton, and D. M. Dillon: 'Piezoelectric and dielectric properties of ceramics in the system potassium—sodium niobate', *Journal of the American Ceramic Society*, 1959, **42**, 438–442.
17. Anonymous: 'Tsingfeng Technology': <http://www.tsingfeng-tech.com/>, 2025.
18. J. Wu, D. Xiao, and J. Zhu: 'Potassium sodium niobate lead-free piezoelectric materials: Past, present, and future of phase boundaries', *Chemical Reviews*, 2015, **115**, 2559–2595.
19. A. Bokov, and Z.-G. Ye: 'Recent progress in relaxor ferroelectrics with perovskite structure', *Journal of Materials Science*, 2006, **41**, 31–52.
20. C. A. Randall, Z. Fan, I. Reaney, L.-Q. Chen, and S. Trolier-McKinstry: 'Antiferroelectrics: History, fundamentals, crystal chemistry, crystal structures, size effects, and applications', *Journal of the American Ceramic Society*, 2021, **104**, 3775–3810.

Chapter 4

Piezoelectrics

4.1 INTRODUCTION

The greek word $\pi\epsilon\acute{\iota}\zeta\epsilon\iota\nu$ (pronounced $\pi\acute{\epsilon}z\bar{o}$) means ‘to press or squeeze’ [1]. This etymology is the origin of the term *piezoelectric*, which describes materials that generate an electric voltage when subjected to mechanical stress, such as stretching, compression, or twisting.

While many piezoelectric materials are crystalline, such as quartz, it is notable that even amorphous thin films can exhibit this phenomenon. For instance, thin films of $\text{CaCu}_3\text{Ti}_4\text{O}_{12}$ perovskite, when sputtered onto a flexible polymer substrate, are amorphous. Despite their disordered structure, they still show piezoelectric responses. This is attributed to the presence of local dipoles associated with TiO_6 octahedra, which, despite their disorderly arrangement, contribute to the overall piezoelectric effect [2].

Figure 4.1 shows an early, ingenious application of piezoelectric quartz, and how the piezoelectric response of quartz is related to its crystal structure, which does not have a centre-of-symmetry. In a centrosymmetric crystal, the application of a force would displace positive charges in one direction and a perfectly mirrored displacement of negative charges in the opposite direction, cancelling out any net electrical dipole.

In its unstressed state, the positive and negative charge centres within each unit cell of quartz effectively overlap, resulting in no net macroscopic electrical polarisation. On the application of a stress, the SiO_4 tetrahedra are slightly deformed or twisted. This deformation causes a relative displacement of the positively charged silicon ions and the negatively charged oxygen ions within the crystal lattice. Because the structure is non-centrosymmetric, these atomic displacements are not perfectly symmetrical. The resulting separation of the centres of positive and negative charge, create tiny electric dipoles throughout the crystal.

The collective effect of these microscopic dipoles, which are now oriented in a specific direction due to the applied stress, results in a net macroscopic electrical polarisation across the crystal faces. This polarisation manifests as an accumulation of positive and negative charges on opposite surfaces of the crystal, thereby generating an electric voltage. The magnitude of the generated electrical charge (and thus voltage) is directly proportional to the amount of mechanical stress

applied. This relationship is what makes quartz useful in various sensing and energy conversion applications.

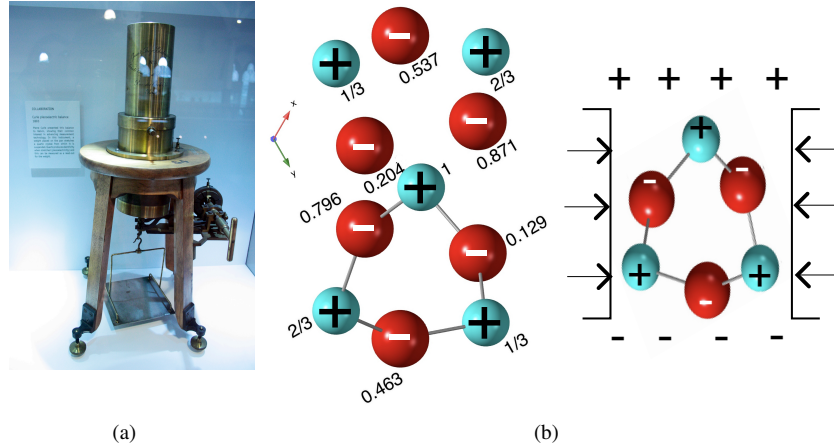


FIGURE 4.1 (a) A balance given by Pierre Curie to Lord Kelvin. The rectangular pan is suspended via a piezoelectric quartz crystal. Placing something on the pan stretches the crystal. The resulting voltage generated is a measure of the product of the mass of the object and of gravity (i.e., a force). α -quartz is non-centrosymmetric. Image by Stephen C. Dickson, reproduced under the CC BY-SA 4.0 licence, <https://creativecommons.org/licenses/by-sa/4.0/deed.en> (b) Projection along z of a α -quartz unit cell oxygen atoms coloured red; the numbers are fractional coordinates along z . The cluster of atoms on the right shows how stress induces a potential difference. Tension would have the opposite effect.

4.2 CRYSTALLOGRAPHY

As we delve into the fascinating world of piezoelectricity, it is important to reiterate the key characteristic that enables certain crystals to exhibit this property: the absence of a centre of symmetry.¹

Most crystals possess a centre of symmetry. This means that an observer positioned at the centre of the crystal who observes the atomic arrangement from any direction, say $[u_1 \ u_2 \ u_3]$, cannot distinguish it from the arrangement seen in the exactly opposite direction, $[\bar{u}_1 \ \bar{u}_2 \ \bar{u}_3]$. This is also referred to as inversion symmetry. If the crystal is inverted through this central point, the resulting atomic arrangement is indistinguishable from the original, Figure 4.2.

In crystallography, crystals are categorised into seven crystal systems based on their lattice parameters and axial relationships: triclinic, monoclinic, orthorhombic, trigonal, tetragonal, hexagonal, and cubic. Within these systems, the symmetry elements of a crystal are described by point groups, which con-

1. An introduction to crystallography *per se* is available free from [3].

sider rotations (like 2-fold, 3-fold, 4-fold and 6-fold rotation axes, where a 6-fold axis signifies a rotation of $2\pi/6$ that restores the crystal's original appearance), inversion axes (e.g., $\bar{2}$, which involves a $2\pi/2$ rotation followed by an inversion through the centre), and mirror planes (m).

There are a total of 32 crystallographic point groups. Among these, 20 represent non-centrosymmetric crystals, and it is these specific point groups that are capable of exhibiting piezoelectricity. Table 4.1 lists these non-centrosymmetric point groups.

TABLE 4.1 Point groups representing non-centrosymmetric crystals. All of these except 432 are piezoelectric but only those marked in red are ferroelectric.

Cubic	23, $\bar{4}3m$, 432	Orthorhombic	222, $mm2$
Hexagonal	6, $\bar{6}$, 622, $6mm$, $\bar{6}m2$	Monoclinic	2, m
Tetragonal	4, $\bar{4}$, 422, $4mm$, $\bar{4}2m$	Triclinic	1
Trigonal	3, $3m$, 32		

As the table shows, a point group like 432 within the cubic system is non-centrosymmetric. However, it is an exception and does not exhibit piezoelectricity. This is because its high degree of symmetry prevents a perceptible net dipole moment from forming even upon deformation.

It is further highlighted that amongst these 20 piezoelectric point groups, a subset (those marked in red in the table) also exhibit ferroelectricity, meaning they possess a spontaneous electric polarisation \mathcal{P}_s that can be reoriented by an external electric field.

In an ionic crystal without a centre of symmetry, the arrangement of positive and negative ions is such that the 'centre' of the positive charge distribution does not perfectly coincide with the 'centre' of the negative charge distribution. This inherent separation of charge leads to a permanent electrical dipole moment within the crystal. When subjected to stress, the relative positions of its constituent ions are altered, causing the magnitude or direction of the permanent electrical dipole moment to change. This in turn leads to a redistribution of surface charges on the crystal, which creates a potential difference (voltage) across its faces. This is the essence of the piezoelectric effect.

The concept extends to *pyroelectricity*. If a non-centrosymmetric ionic crystal with a permanent dipole moment experiences a uniform change in temperature, the alignment and magnitude of these inherent dipoles can be affected, thus a voltage across the material. It is important to note that while thermal expansion does occur, it is not the primary reason for the pyroelectric response. The fundamental mechanism lies in how temperature influences the atomic positions and thus the intrinsic dipole moments. To accurately characterise the pyroelectric response, the temperature change must be uniform throughout the

material to prevent the introduction of thermal strains, which could confound the measurement with a piezoelectric effect.

A *ferroelectric* material is characterised by possessing a permanent electric polarisation even in the absence of an external electric field. This means it has an intrinsic, spontaneous dipole moment that can exist stably within its structure.

In contrast, a piezoelectric material generates an electric charge in response to mechanical deformation (stress), but it does not necessarily have a permanent dipole moment in its unstressed state. A classic example is α -quartz. While each individual Si-O bond within quartz is polar, the overall tetrahedral arrangement of these bonds in the unstressed condition results in a cancellation of individual dipoles, leading to no net macroscopic dipole moment. However, when mechanical stress is applied, the symmetry is broken, leading to charge displacement and thus a temporary electrical charge, which disappears once the stress is relieved. Tourmaline is another example of a material that is piezoelectric but not ferroelectric.

Referring back to Table 4.1, all of the point groups marked in red have a unique direction, which means a vector that cannot be repeated by a symmetry operation of the point group. This is responsible for the permanent dipole in ferroelectric crystals. It follows that all ferroelectrics are inherently also piezoelectric and pyroelectric, but the reverse is not true.

The ability to reverse the polarity of a ferroelectric material by applying a sufficiently strong external electric field is a particularly valuable property. This characteristic makes ferroelectrics attractive for applications such as non-volatile memory devices, where a voltage pulse can be used to switch the material's polarisation between two stable states, representing logical '0' and '1', Figure 4.2c [4]. This provides a mechanism for retaining information even when power is removed.

The preceding discussion focused on single-crystals, but these can be expensive to manufacture. In many practical applications, polycrystalline samples, which are made by compacting powders, are a more economically viable alternative. However, in a polycrystalline material, the individual grains (crystallites) are typically oriented randomly, so the dipole moments of the individual grains tend to cancel each other out on a macroscopic scale, leading to a diminished or even absent net piezoelectric or ferroelectric response. To overcome this, poling to induce the polars to partially align (p. 53).

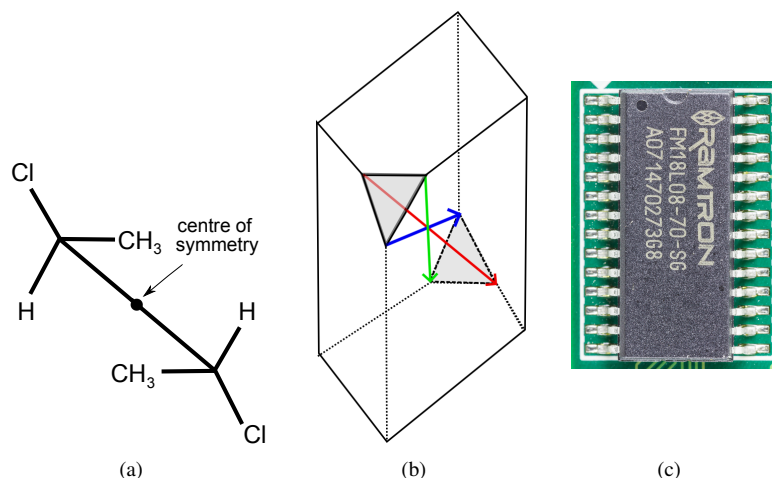


FIGURE 4.2 Illustration of centre of symmetry. (a) A molecule with the centre of symmetry identified by the dot. (b) The common point where the arrows intersect is the centre of symmetry. (c) A ferroelectric random access memory chip. Reproduced courtesy of Raimond Spekking with licence details in [5].

4.3 ANISOTROPY

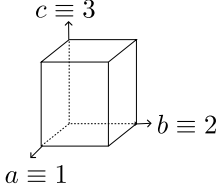
When dealing with piezoelectric materials, particularly those that are not isotropic like tetragonal crystals, it is crucial to recognise that their properties, including charge displacement and elastic strains, will vary with direction. Consequently, the charge-density displacement vector \mathcal{D} will not be uniform in all directions.

This directional dependence arises from the anisotropic nature of the crystal lattice. In anisotropic materials, the arrangement of atoms and the strength of interatomic bonds differ along various crystallographic axes. This directly influences how the material responds to applied mechanical stress and electric fields.

Specifically, in piezoelectric materials, mechanical stress induces an electric polarisation, and conversely, an applied electric field causes mechanical strain. The relationship between these quantities is described by tensors that reflect the material's symmetry. For non-isotropic crystals, these tensors have more independent components than for isotropic materials, leading to the observed directional variation.

Consider the relationship between the charge-density displacement vector \mathcal{D} and both the applied stress σ_{ij} and the external electric field E_i . The equations described below are dependent on crystal symmetry; here they are presented for an orthorhombic point group $mm2$, but can readily be adapted for tetragonal

crystals (point group $4mm$) by setting $d_{24} = d_{15}$ and $\epsilon_{r,11} = \epsilon_{r,22}$; considering the coordinate axes aligned with the unit cell (where the third axis corresponds to the c -axis), this relationship is given by:



$$\begin{aligned}
 \begin{bmatrix} \mathcal{D}_1 \\ \mathcal{D}_2 \\ \mathcal{D}_3 \end{bmatrix} &= \underbrace{\begin{pmatrix} 0 & 0 & 0 & 0 & d_{15} & 0 \\ 0 & 0 & 0 & d_{24} & 0 & 0 \\ d_{31} & d_{32} & d_{33} & 0 & 0 & 0 \end{pmatrix}}_{\text{piezoelectric coefficients}} \underbrace{\begin{bmatrix} \sigma_{11} \\ \sigma_{22} \\ \sigma_{33} \\ \sigma_{12} \\ \sigma_{23} \\ \sigma_{31} \end{bmatrix}}_{\text{stress}} \\
 &+ \underbrace{\begin{pmatrix} \epsilon_o \epsilon_{r,11} & 0 & 0 \\ 0 & \epsilon_o \epsilon_{r,22} & 0 \\ 0 & 0 & \epsilon_o \epsilon_{r,33} \end{pmatrix}}_{\text{permittivity}} \begin{bmatrix} E_1 \\ E_2 \\ E_3 \end{bmatrix} \quad (4.1)
 \end{aligned}$$

where σ_{ij} represent stress components and E_i the components of the electrical field vector. In the absence of mechanical stress (i.e., all $\sigma_{ij} = 0$), the equation simplifies, showing the material's electrical displacement purely in response to an applied electric field, which is comparable to Equation 2.1a. The piezoelectric coefficient d_{33} (which relates stress applied along the c -axis to charge displacement along the c -axis) has been found to be in the range $86 \rightarrow 177 \text{ pC N}^{-1}$ [6, 7] with d_{15} and d_{31} at 392 and -34.5 pC N^{-1} , respectively [6].

When only the stress component σ_{33} is non-zero (meaning stress is applied along the '3' direction), the piezoelectric coefficient of primary interest is d_{33} . In this specific case, the charge-density displacement components \mathcal{D}_1 and \mathcal{D}_2 are zero, implying that charge displacement primarily occurs along the '3' direction.

For applications like balances (as mentioned in Figure 4.1) that measure force along a specific axis, or actuators where mechanical motion is desired from an applied electric field, a large d_{33} is beneficial because it represents a greater charge displacement for a given stress, or a larger mechanical strain for a given electric field. To deal with the latter aspect, it is necessary to determine the strain produced as a function of stress (σ) and electrical field (E). Strain is related to stress via the compliance matrix (S_{ij}), which is the inverse of the stiffness matrix. The components of S_{ij} depend on the crystal symmetry. The form shown here suggests a material with specific crystal symmetry (e.g., tetragonal or hexagonal), as many of the off-diagonal terms are zero. This indicates that

certain stress components will only induce specific strain components:

$$\underbrace{\begin{bmatrix} \epsilon_{11} \\ \epsilon_{22} \\ \epsilon_{33} \\ \epsilon_{12} \\ \epsilon_{23} \\ \epsilon_{13} \end{bmatrix}}_{\text{strain}} = \underbrace{\begin{pmatrix} S_{11} & S_{12} & S_{13} & 0 & 0 & 0 \\ S_{12} & S_{22} & S_{23} & 0 & 0 & 0 \\ S_{31} & S_{32} & S_{33} & 0 & 0 & 0 \\ 0 & 0 & 0 & S_{44} & 0 & 0 \\ 0 & 0 & 0 & 0 & S_{55} & 0 \\ 0 & 0 & 0 & 0 & 0 & S_{66} \end{pmatrix}}_{\text{compliances}} \underbrace{\begin{bmatrix} \sigma_{11} \\ \sigma_{22} \\ \sigma_{33} \\ \sigma_{12} \\ \sigma_{23} \\ \sigma_{31} \end{bmatrix}}_{\text{stress}} + \underbrace{\begin{pmatrix} 0 & 0 & d_{31} \\ 0 & 0 & d_{32} \\ 0 & 0 & d_{33} \\ 0 & d_{24} & 0 \\ d_{15} & 0 & 0 \\ 0 & 0 & 0 \end{pmatrix}}_{\text{piezoelectric coefficients}} \underbrace{\begin{bmatrix} E_1 \\ E_2 \\ E_3 \end{bmatrix}}_{\text{electric field}}. \quad (4.2)$$

The equation shows that the total strain is a superposition of the strain caused by mechanical stress and the strain caused by the electric field. These equations are particularly valuable for designing devices that utilise:

- Single crystals where the crystallographic orientation and thus the tensorial properties are well-defined and controllable.
- Strongly crystallographically-textured polycrystalline materials that have a preferred orientation of their crystallites, allowing for a somewhat predictable anisotropic response.

Example 17: Piezoelectric response

A uniaxial compressive stress $\sigma_{33} = -1 \times 10^6$ MPa is applied along the length of a piezoelectric sample, where the length is parallel to the poling direction; all other $\sigma_{ij} = 0$. An electric ($E_3 = 1000$ V m⁻¹) field is applied along the same direction; all other $E_i = 0$. The compliance $S_{33} = 15.5 \times 10^{-12}$ m² N and $S_{13} = 5.8 \times 10^{-12}$ m² N. The piezoelectric coefficients are $d_{33} = 593 \times 10^{-12}$ m V⁻¹ [\equiv pC N⁻¹] and $d_{31} = -274 \times 10^{-12}$ m V⁻¹.

Calculate the strain ϵ_{33} .

Solution 17

Equation 4.2 simplifies to

$$\begin{aligned}
 \epsilon_{33} &= S_{33}\sigma_{33} + d_{33}E_3 \\
 \therefore \epsilon_{33} &= (16.5 \times 10^{-12} \text{ m}^2 \text{ N}^{-1}) \times (-1 \times 10^6 \text{ N m}^{-2}) \\
 &\quad + (593 \times 10^{-12} \text{ m V}^{-1}) \times (1000 \text{ V m}^{-1}) \\
 &= \underbrace{(-16.5 \times 10^{-6})}_{\text{mechanical}} + \underbrace{(0.593 \times 10^{-6})}_{\text{electrical}} \\
 \therefore \epsilon_{33} &\approx -15.9 \times 10^{-6}
 \end{aligned} \tag{4.3}$$

The negative sign indicates compression along the 3-axis. In this specific example, the compressive stress dominates the expansion induced by the electric field, leading to a net compression. If the electric field were stronger or the stress weaker, the material could expand.

4.3.1 Piezoelectric efficiency

The efficiency of a piezoelectric device in converting uniaxial mechanical stimulus into electrical energy, under the simplifying assumption of an isotropic and linear material, is dependent on:

- permittivity $\epsilon_0\epsilon_r$, which relates E and \mathcal{D} . A higher permittivity means that for a given electric field, more charge can be stored.
- The piezoelectric coefficients directly relate the applied stress (σ) to the generated charge displacement (\mathcal{D}). For uniaxial stress (σ_{33}) and an isotropic assumption, this simplifies to a single value d_* to be substituted for d_{ij} . A larger d_* implies a greater electrical output for a given mechanical input.
- Compliances that relate strain ϵ to stress.

It is assumed here, for the sake of simplicity, that the material is isotropic, linear in all respects; this allows for example, a single value d_* to be substituted for d_{ij} . and judging from Using Equations 4.1 and 4.2 permits the elementary relations

in the first lines below to be deduced by inspection:

$$\mathcal{D} = \epsilon_o \epsilon_r E \quad \sigma = \mathcal{D}/d_* \quad \epsilon = S_*(\mathcal{D}/d_*) \quad \therefore \epsilon = S_*(\epsilon_o \epsilon_r E/d_*) \quad (4.4a)$$

$$\text{based on Hooke's law,} \quad \text{mechanical energy} = \frac{1}{2} \frac{\epsilon^2}{S_*} \equiv \frac{1}{2} \frac{S_* \epsilon_o^2 \epsilon_r^2 E^2}{d_*^2} \quad (4.4b)$$

$$\text{electrical energy} = \frac{1}{2} \epsilon_o \epsilon_r E^2 \quad (4.4c)$$

$$\text{ratio mechanical/electrical} = \frac{d_*^2}{\epsilon_o \epsilon_r S_*} \quad (4.4d)$$

$$\text{by definition, efficiency} = k_e = \sqrt{\frac{d_*^2}{\epsilon_o \epsilon_r S_*}} \quad (4.4e)$$

with $0 \leq k_e \leq 1$ but in practice only 0.08 for quartz but greater than 0.9 for relaxor crystals, and these values do not change much with temperature in single crystals.

4.3.2 Measurement of efficiency

The electromechanical coupling represented by k_e can be measured using an impedance analyser. This device applies an AC voltage across a component and measures the resulting current, allowing it to calculate the impedance ($Z = V/I$) over a range of frequencies (typically Hz to MHz). A piezoelectric device (e.g., a ceramic disk, rod, or crystal) is connected to the analyser via electrodes.

The resonant frequency ν_o is the frequency at which the impedance of the piezoelectric device reaches a minimum. A minimum impedance signifies maximum energy transfer. At resonance, the mechanical vibrations in the piezoelectric material are most efficiently coupled with the electrical excitation, leading to a strong current response for a given voltage. This is analogous to a mechanical system vibrating at its natural frequency.

The anti-resonance frequency ν_a is the frequency at which the impedance of the piezoelectric device reaches a maximum. A maximum impedance signifies minimum energy transfer. At antiresonance, the electrical and mechanical aspects of the device are out of phase, hindering efficient energy conversion.

The electromechanical coupling coefficient k_e can be calculated from these two frequencies using the formula:

$$k_e = \sqrt{1 - \frac{\nu_a^2}{\nu_o^2}}, \quad (4.5)$$

a relationship based on the principle that the energy of an oscillating system is proportional to the square of the frequency. The physical dimensions of the

sample, particularly its ‘acoustic length’ (z_ℓ), the characteristic length over which the sound wave propagates), significantly affect the resonance frequencies. Thus, the frequency $\nu \propto v_{\text{sound}}/z_\ell$, where v_{sound} is the speed of sound in the material (a function of its elastic modulus) [8]. The k_e value is not a single, universal property for a material but depends on the specific mode of vibration (e.g., compression-tension, shear, radial expansion) and the orientation of the applied field/stress relative to the material’s polarisation direction.

Different modes of vibration involve different combinations of strain and stress components, and thus different piezoelectric coefficients d_{ij} and compliance constants S_{ij} become dominant. This is why different k_e values are typically quoted for a material e.g., k_{33} for longitudinal mode, k_p for planar mode, k_{15} for shear mode, Figure 4.3. The flexural (bending) mode involves a combination of different strain and stress components across the thickness and geometry of the material. It is therefore associated with an effective coupling k_{eff} based on Equation 4.5, the evaluation of which in general requires a measurement of ν_a and ν_o .

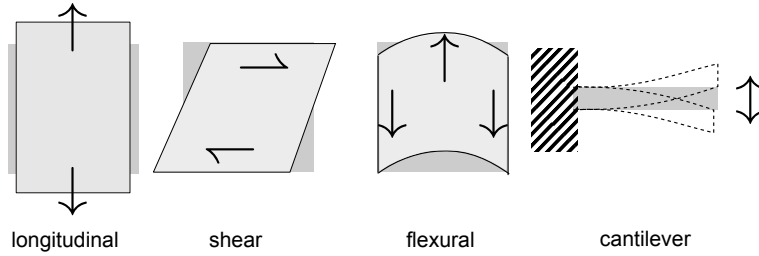


FIGURE 4.3 Some vibration modes.

4.3.3 Bank of properties

The development of materials for effective devices that are amenable to production, multi-property optimisation, rather than focusing on a single, outstanding property. This is particularly evident in the example of medical ultrasonic transducers.

A medical ultrasonic transducer is a piezoelectric device. Its primary role is to convert electrical signals into sound waves for transmitting ultrasound into the body, and convert sound waves back into electrical signals for receiving echoes to form an image. The goal is to efficiently transfer sound energy from the transducer into the biological tissue (and *vice-versa* for received echoes).

The acoustic impedance² is a product of the material's density and v_{sound} . Mismatch in acoustic impedance leads to reflections of sound waves at the interface, reducing energy transfer. A coupling gel is often used between the transducer and skin to minimise this mismatch.

The electrical impedance of the transducer (typically around $50\ \Omega$) should match the characteristic impedance of the coaxial cable connecting it to the external electronics. Mismatched electrical impedances lead to signal reflections within the cable, causing signal loss, distortion, and reduced efficiency, Figure 4.4. The standard $50\ \Omega$ impedance is common for radio frequency and pulse-generating circuits to ensure maximum power transfer and minimise reflections.

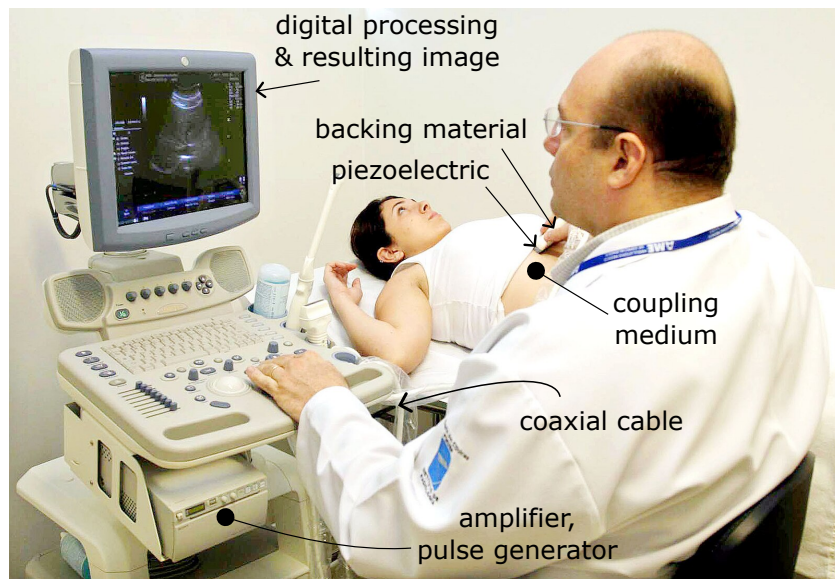


FIGURE 4.4 An ultrasound scanning system for deciphering internal biological tissue, such as during pregnancy or more generally for diagnosis. Unannotated image courtesy of [9].

2. The acoustic and electrical impedances are analogous but not identical. Both share the concept of representing the opposition to flow/transfer, but operate in different physical domains and therefore have different units. Electrical impedance (Ω) represents the opposition of current to voltage, whereas the acoustic impedance (Pa s m^{-1}) the opposition of the flow of sound waves by acoustic pressure & particle velocity.

Example 18: Medical transducer

When sound waves are transmitted across a transducer/tissue interface, the proportion reflected is given by

$$\left(\frac{Z_{\text{tissue}} - Z_{\text{transducer}}}{Z_{\text{tissue}} + Z_{\text{transducer}}} \right)^2$$

where Z represents impedance.

Explain why a simple medical transducer based on a lead zirconate titanate piezoelectric, is inefficient at coupling with human tissue, given the following properties:

	Density / kg m^{-3}	$v_{\text{sound}} / \text{m s}^{-1}$
Lead zirconate titanate	7450	4560
Human soft tissue	1050	1540

Solution 18

The impedance of each material is calculated from the product of the density and velocity, so $Z_{\text{transducer}} \approx 34 \text{ kg m}^{-2} \text{ s}^{-1}$, whereas $Z_{\text{tissue}} \approx 1.6 \text{ kg m}^{-2} \text{ s}^{-1}$. This clearly is a large mismatch, that would lead to a reflection of ≈ 0.83 of the ultrasonic waves emanating from the transducer; this is inefficient.

The use of a gel between the transducer and tissue does not significantly improve this, because the gel has an acoustic impedance that is not much different from that of tissue. There is a technology involving the addition of matching layers to the transducer, that brings its impedance closure to that of the gel or tissue [10].

4.4 TYPICAL PIEZOELECTRIC MATERIALS**4.4.1 Some non-ferroelectric piezoelectrics** *α -SiO₂ quartz*

Quartz is one of the earliest piezoelectric materials discovered and utilised. While natural quartz crystals were initially used (Figure 4.5a), industrial demand for consistent quality, purity, and larger sizes led to the widespread adoption of hydrothermally grown synthetic quartz. This process allows for precise control over crystal growth, minimising defects and optimising properties.

Quartz truly shines in the making of oscillators and resonators by converting electrical energy to mechanical vibration and *vice versa*. It forms the basis of accurate time-keeping in almost all modern watches, clocks and telephones.

Quartz possesses excellent high electrical resistivity ($> 10^{17} \Omega \text{ cm}$) at room temperature and negligible mechanical loss.

The frequency engineered into a device has a narrow bandwidth, and is insensitive to temperature under ambient conditions, but there is a transition near 300°C . It has a relatively small piezoelectric coefficient ($d_{33} \approx 2.3 \text{ pC N}^{-1}$), which is fine for high-frequency stability and precision timing (accuracy $\approx 0.4 \text{ s}$ per day) where tiny controlled vibrations are necessary, but not useful in applications requiring large displacements.

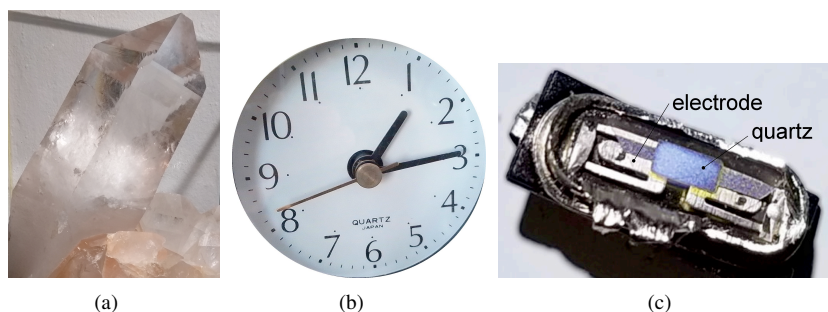
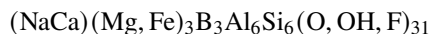


FIGURE 4.5 (a) Natural quartz crystal, almost a metre in length. (b) Clock-face inscribed 'Quartz' toward the number 6. (c) Inside a quartz oscillator. Image courtesy of Chamblis, adapted under CC BY-SA 4.0 licence <https://creativecommons.org/licenses/by-sa/4.0/deed.en>

Tourmaline

Tourmaline is essentially a borosilicate that is not a simple compound but a complex mineral with the general formula



and may include Li, Mn, Ti and Cr [11]. This multicomponent composition contributes towards its many different colours. The crystal has the point group $3m$ which from Table 4.1 would imply that it should also be ferroelectric. However, its complex and disordered structure often hinders the long-range, stable alignment of dipoles necessary for a robust, reversible spontaneous polarisation characteristic of classic ferroelectrics at ambient temperatures. This is a common situation where theoretical symmetry allows for a property, but practical material chemistry or defects can suppress or prevent its full expression. Since $3m$ is a unique polar axis (Table 4.1), tourmaline is also pyroelectric.

Tourmaline has a small $d_{33} \approx 1.8 \text{ pC N}^{-1}$ and $\epsilon_r \approx 7.5$. Since the composition is not fixed, there is a large variation in resistivity. It can be used as a pyroelectric temperature-sensor, or a piezoelectric dynamic-pressure sensor (up to about 130 MPa), for example as a blast sensor because of its rapid rise-time or even for

high-frequency pressure waves generated in plasma research. Illustrative data on this aspect are presented in Table 4.2.

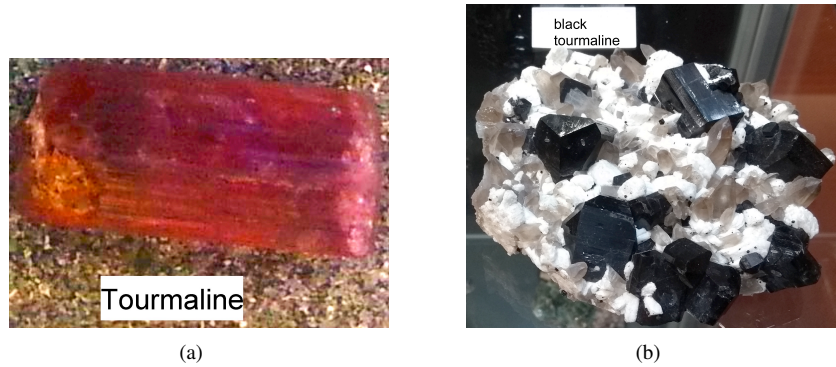


FIGURE 4.6 (a) Tourmaline, Geological Museum, Colorado School of Mines. (b) Iron-rich black tourmaline, Zürich.

TABLE 4.2 Rise time of dielectrics for potential use as practical pressure sensors [12, 13]. The ‘rise time’ which determines how effectively the sensor responds to changes in pressure.

Material	Rise time / μs	Material	Rise time / μs
Tourmaline	0.2	$\text{Pb}(\text{Zr,Ti})\text{O}_3$	65
BaTiO_3	20	LiNbO_3	7

Example 19: Rise time

Why is the rise time (Table 4.2) of tourmaline more than an order of magnitude smaller than that for LiNbO_3 ?

Solution 19

In tourmaline, acoustic waves can travel at 7.3 km s^{-1} [14] whereas the corresponding velocity in the niobate is about half that value [15]. Rise time in a piezoelectric sensor is fundamentally limited by how quickly a mechanical disturbance (like a pressure wave) can propagate through the sensing element and generate a coherent electrical signal. A faster speed of sound means that the pressure wave travels through the crystal more rapidly, allowing the entire

sensing volume to respond and generate charge in a shorter period.

Tourmaline also has a larger elastic modulus and smaller attenuation [16]. A material with a higher elastic modulus (i.e., it is stiffer) deforms less for a given stress. In dynamic sensing, this stiffness means it can respond to rapid changes in pressure with minimal ‘lag’ due to its own mechanical deformation. It resists deformation more effectively and transmits the stress-induced strain faster.

Acoustic attenuation refers to the loss of energy of the sound wave as it propagates through the material. Lower attenuation means that the mechanical stress wave maintains its amplitude and shape more effectively as it travels through the sensor. This leads to a clearer and stronger electrical signal generated, contributing to a more accurate and faster rise. If the wave is heavily attenuated, the signal might be smeared out or weakened, prolonging the apparent rise time.

Example 20: Tourmaline device

If a flat crystal of tourmaline is stressed normal to its surface, leading to the development of an excess of positive charges on one surface and negative on the other, would this surface charge vary with the thickness of the crystal? Does the potential difference vary with thickness?

Solution 20

No, the surface charge developed across a stressed crystal due to the piezoelectric effect does not depend on the thickness of the crystal, consistent with $q = d_{33} \times \text{force}$.

The piezoelectric effect generates a surface charge density on the faces perpendicular to the direction of polarisation. The brothers Jacques and Pierre Curie discovered the piezoelectric effect during 1880 [17]. It was found that the quantity of electricity developed was proportional to the pressure applied, but did not depend on the thickness of the crystal. As illustrated in Figure 4.7, the ions *between* the positively and negatively charged-surfaces neutralise so their effect is not felt at the surface, thus making the charge developed independent of the thickness.

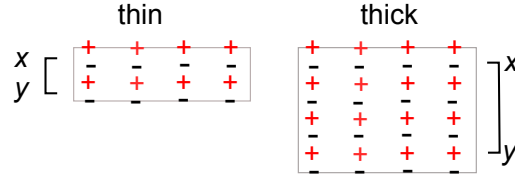


FIGURE 4.7 Why thickness does not influence the charge developed at the surfaces across a stressed piezoelectric substance. The regions marked xy contain both positive and negative charges that neutralise and hence have no effect on any long-range electrical field.

Post script: According to a German pamphlet (1707) entitled *Curious speculations in sleepless nights*, a Dutch jeweller noticed that hot tourmaline, on cooling, attracted small particles – now attributed to static electricity. From that time on, tourmaline came to be known as the electric stone or Ceylon magnet [18].

Jacques and Pierre Curie's original paper [17] begins with a paragraph on hemihedral crystals, i.e., a crystal in which only half of the possible symmetry-related faces are present in its shape, giving it an asymmetrical appearance. It then describes pyroelectricity, the development of polar electric dipole along an axis of the crystal because the temperature changes. It then reveals the discovery that when one of these crystals is compressed along the axis of the hemihedron with inclined faces, it develops electricity at the two ends of the axis.

For the second part of the question, while the *charge* developed is independent of the crystal thickness z_t , the potential difference actually does increase with thickness for a given stress, because $V = E \times z_t$ where E is the electric field strength in V m^{-1} assuming z_t is in the direction of the electric field.

Aluminium nitride

Aluminium nitride has a crystal structure with point group $6mm$, so according to Table 4.1, it could also be ferroelectric. However, its polarisation cannot be switched by an electric field lower than its large dielectric breakdown limit of $\approx 100 \text{ MV m}^{-1}$ (p. 17). In simpler terms, you would destroy the material with an electric spark before you could switch its polarisation. Therefore, in practical terms, AlN is not considered a ferroelectric material despite its point group. It behaves as a highly stable, non-switchable piezoelectric and pyroelectric.

It has an exceptionally large thermal conductivity of $\approx 200 \text{ W m}^{-1} \text{ K}^{-1}$, which makes AlN ideal for devices where efficient heat dissipation is crucial, such as high-power electronic components, light-emitting diode substrates, and power electronics packaging. It prevents localised heating that could degrade performance or lead to failure.

High-purity AlN is a wide-bandgap semiconductor and behaves as an excellent electrical insulator. Its resistivity is actually extremely high, typically in the range of $10^8 \rightarrow 10^{12} \Omega \text{ m}$ at room temperature. This high resistivity is crucial for its piezoelectric and electronic applications, as it minimises current leakage.

It can be exposed to air at 700°C without deterioration, especially in an oxidising atmosphere, which makes AlN suitable for high-temperature applications. Its small $d_{33} \approx 5.6 \text{ pC N}^{-1}$ renders it unsuitable for bulk, high-power actuators that require large displacements, but is adequate for thin-film micro-electromechanical systems and high-frequency acoustic devices.

4.5 FERROELECTRICS AS PIEZOELECTRIC MATERIALS

The ferroelectric material is $\text{PbZr}_{1-x}\text{Ti}_x\text{O}_3$ which after poling (p. 53) can be quite effectively used as in piezoelectric applications.³ It is cheap to produced, has a large piezoelectric coefficient d_{33} and remains non-centrosymmetric to a high temperature, the exact value of which depends on composition, Figure 4.8. At about $x \approx 0.52$, there is a coexistence of two different crystal structures, tetragonal and rhombohedral, Figure 4.8, associated with a particularly large d_{33} . The presence of both phases (and sometimes an intermediate monoclinic phase) creates a complex ferroelectric nano-domain structure [11, 19]. This structural instability and the energetic equivalence of multiple polarisation directions allow the domains to be very easily reoriented by the applied electric field during poling. This enhanced domain wall mobility leads to a much more complete alignment of the dipoles and, consequently, a much larger macroscopic piezoelectric response. This phenomenon is a cornerstone of high-performance piezoelectric ceramics.

Adding small amounts of donor dopants such as La^{3+} (substituting for Pb^{2+}), Nb^{5+} (substituting for Zr^{4+} or Ti^{4+}), Ba^{2+} , or Sr^{2+} (substituting for Pb^{2+}) creates the so-called soft lead-zirconate-titanate ($x \approx 0.4 \rightarrow 0.52$). These donor dopants alter the local charge balance in the lattice, primarily creating lead vacancies (A-site vacancies). The presence of these vacancies significantly increases the mobility of domain boundaries, thus reducing the coercive field (E_C) and enhancing dielectric and piezoelectric coefficients (like d_{33}). While having higher dielectric loss and a lower mechanical quality factor, these materials are well-suited for high-sensitivity, low-power applications such as microphones, accelerometers, and ultrasonic medical-imaging probes.

In contrast, the hard versions of lead titanate zirconate contain acceptor dopants (e.g., Fe^{3+} , Mn^{3+} , Cr^{3+} substituting for Zr^{4+} or Ti^{4+}). These dopants lead to the

3. Poling temperatures are in the range $25 \rightarrow 180^\circ\text{C}$, for ten minutes while under a field strength of about 3 kV mm^{-1} , resulting in d_{33} in the range $280 \rightarrow 445 \text{ pC N}^{-1}$, with the details depending on composition. This is much greater than quartz (2.3 pC N^{-1}), tourmaline (1.8 pC N^{-1}) and AlN (5.6 pC N^{-1}), explaining its widespread use in transducers and actuators.

creation of oxygen vacancies ($V_O^{\bullet\bullet}$) for charge compensation. The acceptor ions and oxygen vacancies form defect complexes that act as pinning sites for domain walls, thereby retarding domain-wall motion and increasing the coercive field. This strengthening of the material also leads to a higher mechanical quality and lower dielectric and mechanical losses, making them stable under large electric fields and mechanical stress. While their intrinsic electromechanical coupling coefficients are generally lower than soft lead zirconate titanate, their ability to operate efficiently at high power makes them particularly useful in high-power applications such as ultrasonic cleaners, high-power transducers, and resonant actuator applications. Hard lead zirconate titanate compositions are typically on the tetragonal side, with $x \approx 0.3 \rightarrow 0.4$.

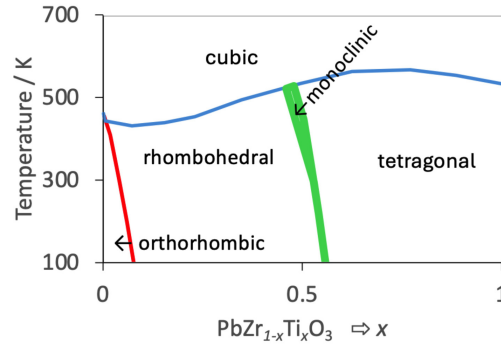


FIGURE 4.8 Phase diagram for lead zirconate titanate, adapted using data from Shi et al. [19].

4.5.1 Lead replacement

Lead is considered a toxic element so efforts are underway to find alternative piezoelectric materials, though it has to be said that the lead titanate zirconates have yet to be dislodged. This is because of their unparalleled combination of high piezoelectric coefficients d_{33} , high T_C , and excellent electromechanical coupling k . This makes it difficult to replace in many established applications where performance is paramount.

BaTiO_3 was actually the first ferroelectric ceramic discovered (in the 1940s) and is of thinking on lead-free piezoelectrics. Upon cooling below 120°C , it transforms to the tetragonal phase that is non-centrosymmetric (point group $4mm$) and ferroelectric. The polarisation direction is along the $\langle 001 \rangle_{\text{tetragonal}}$ crystal axis (Figure 4.9), with the Ti ion slightly displaced towards the corner of the oxygen octahedron.

Further cooling below $\approx 5^\circ\text{C}$ transforms the tetragonal phase into the non-centrosymmetric orthorhombic phase (point group $mm2$). The polarisation direction shifts to along $\langle 011 \rangle_{\text{orthorhombic}}$ which represents a diagonal across a face

of the octahedron.

Upon even further cooling, it transforms to the rhombohedral phase which is also non-centrosymmetric (point group $3m$). The polarisation direction shifts again, aligning along the $\langle 111 \rangle_{\text{rhombohedral}}$ (a body diagonal of the octahedron). All three allotropes are piezoelectric.

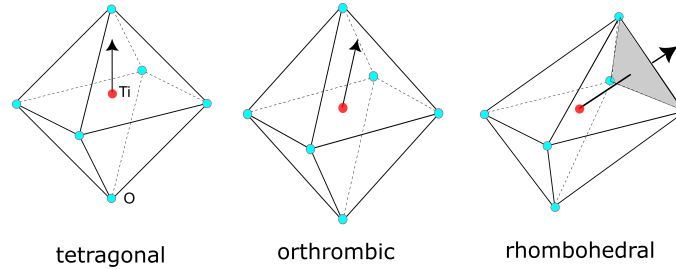


FIGURE 4.9 TiO_6 octahedra in the tetragonal, orthorhombic and rhombohedral structures of barium titanate, with the polarisation directions indicated, with polarisation directions indicated, corresponding to the $\langle 001 \rangle$, $\langle 101 \rangle$ and $\langle 111 \rangle$ directions of the cubic lattice, respectively.

We have seen (Figure 3.3) that the Curie point and permittivity are functions of the grain size in a polycrystalline sample of sintered BaTiO_3 [20]. Figure 4.10a shows that so is the piezoelectric coefficient; the observed trends are not identical for different processing conditions [20]. Figure 4.10b shows the microstructure of a sintered sample with 95.2% density. The domain size is expected to vary with the grain size, and the effect of grain size of dielectric permittivity is shown in Figure 3.3.

Barium titanate and its variants are not really poised to replace the lead-containing piezoelectrics, largely because of their relatively low values of T_C , $d_{33} \approx 191 \text{ pC N}^{-1}$ and the electrochemical coupling factor $k_e \approx 0.35$. The lead zirconate titanate can reach $d_{33} \approx 600 \text{ pC N}^{-1}$ with $T_C \approx 400^\circ\text{C}$ and a larger coupling factor $k_e \approx 0.57$ [21].

4.5.2 $\text{K}_{0.5}\text{Na}_{0.5}\text{NbO}_3$

Solid solutions of potassium and sodium niobate have optimum piezoelectric performance when mixed in about equal quantities; the crystal lattice at ambient temperature is monoclinic [22] with $d_{33} \approx 400 \text{ pC N}^{-1}$, $T_C \approx 420^\circ\text{C}$ and $\epsilon_r \approx 235$ at 35°C and 0.1 kHz [23]. It remains difficult to produce the desired microstructure and properties by synthesis and sintering, and the fact that its dielectric properties are sensitive to composition does not help. Excess sodium in precursor solutions used for depositing thin films can lead to leakage current densities that might not be acceptable [24]. There has been some commercial application of this material, p. 51.

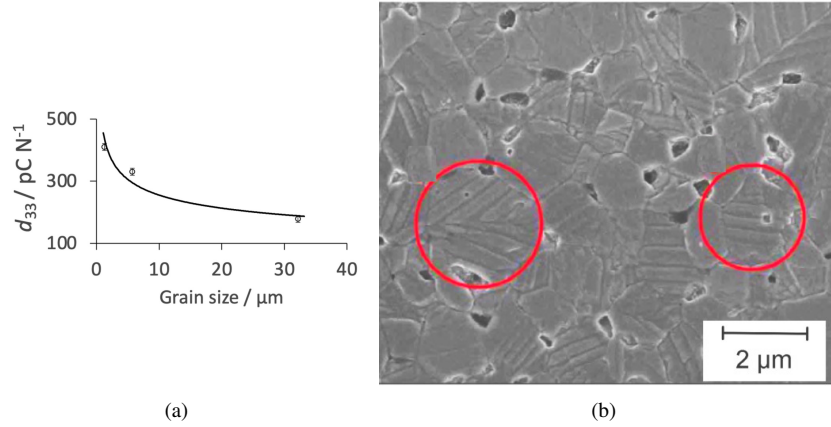


FIGURE 4.10 Conventionally sintered BaTiO_3 . (a) Dielectric coefficient as a function of the grain size. (b) Microstructure of sample conventionally sintered at 1230°C . The rings highlight domain patterns. Image courtesy of Haixue Yan.

4.5.3 $\text{Bi}_{0.5}\text{Na}_{0.5}\text{TiO}_3$

This compound has reasonable piezoelectric properties with $T_C = 320^\circ\text{C}$ and a depoling temperature near 200°C . While its room-temperature properties are generally lower than lead-based materials, $\text{Bi}_{0.5}\text{Na}_{0.5}\text{TiO}_3$ exhibits relaxor behaviour, and its piezoelectric properties, such as $d_{33} \approx 130 \text{ pC N}^{-1}$ and $k_e \approx 0.3$, can be quite significant at or near its depoling temperature [25, 26]. There are processing difficulties in making this material because its performance can be sensitive to composition and details of manufacture. Hence, a lot of speculation on potential applications, but no actual application in commercial practice.

4.5.4 Layer-structured ferroelectrics

Often referred to as Aurivillius phases after Bengt Aurivillius [27, 28], an inorganic chemist, who was the first to systematically study specific layered bismuth oxides which exhibit ferroelectricity due to their non-centrosymmetry, leading later to their ferroelectric properties. The materials exhibit especially high Curie points. Setting m to the number of perovskite octahedra within each perovskite block, the general formula can be written $(\text{Bi}_2\text{O}_2)(\text{A}_{m-1}\text{B}_m\text{O}_{3m+1})$, where ‘A’ is a large cation (like Sr, Ba, Ca, Pb, Bi, rare Earths), and ‘B’ is a smaller cation (like Ti, Ta, Nb, Fe, Cr). For some compounds with $m = 1$, such as $\text{Bi}_2\text{O}_2(\text{WO}_4)$, the perovskite block consists of a single BO_6 octahedron.

Layered-perovskites consist of alternating layers of *different* perovskite-type oxides and other oxides or compounds. Examples include:

1. The ferroelectric $\text{Bi}_4\text{Ti}_3\text{O}_{12}$ has $m = 3$, consisting of alternating $(\text{Bi}_2\text{O}_2)^{2+}$ and $(\text{Bi}_2\text{Ti}_3\text{O}_{10})^{2-}$ perovskite-like blocks. Figure 4.11a illustrates this layered structure which is orthorhombic, lacks a centre of symmetry, and exhibits ferroelectricity. It has a Curie point of 923 K in thin-film form [29].

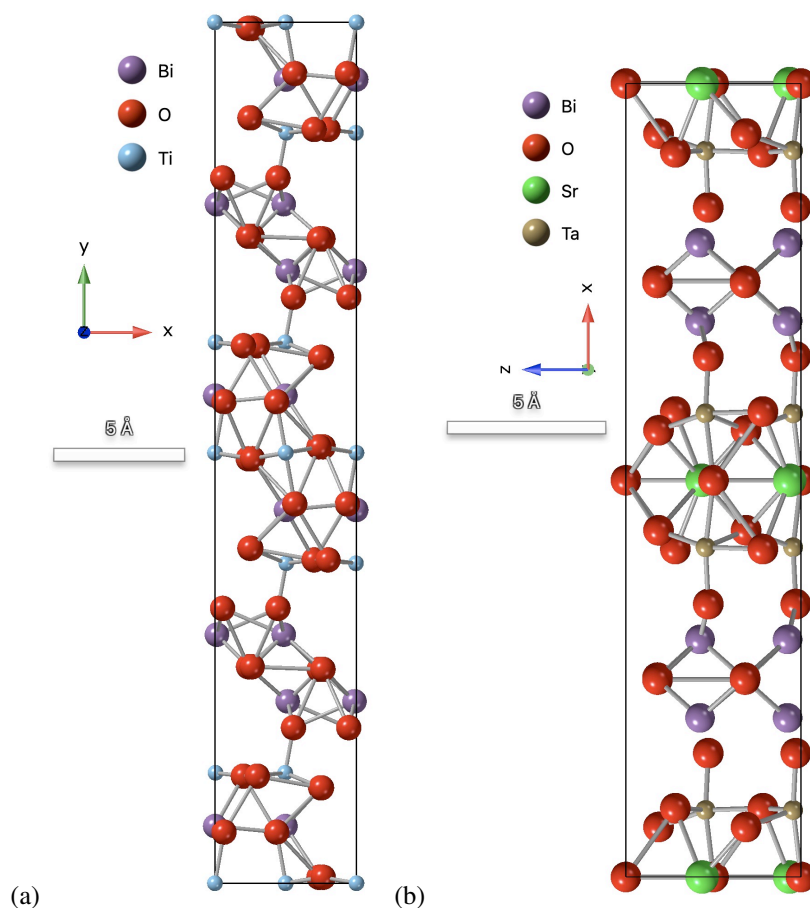


FIGURE 4.11 (a) Crystal structure of $\text{Bi}_4\text{Ti}_3\text{O}_{12}$. (b) Crystal structure of $\text{SrBi}_2\text{Ta}_2\text{O}_9$.

2. $\text{SrBi}_2\text{Ta}_2\text{O}_9$ has alternating layers of oxides as shown in Figure 4.11b. It has $m = 2$, consists of alternating $(\text{Bi}_2\text{O}_2)^{2+}$ and $(\text{SrTa}_2\text{O}_7)^{2-}$ perovskite-like blocks. Figure 4.11b illustrates this layered structure that has $T_C \approx 590$ K.
3. The $\text{Nd}_2\text{Ti}_2\text{O}_7$ ferroelectric ceramic has $T_C = 1755$ K, making it thermally stable for elevated temperature applications. where no other ferroelectric or piezoelectric material could survive, such as sensors in extreme environments

(e.g., jet engines, nuclear reactors, drilling equipment). However, it is **not** an Aurivillius phase. Its structure can be represented by the formula $A_2B_2O_7$ (where 'A' is a rare-earth element and 'B' is Ti, Nb, or Ta). Specifically, in $Nd_2Ti_2O_7$, the structure consists of perovskite-like slabs of TiO_6 octahedra and Nd^{3+} ions. These slabs are stacked along a particular crystallographic direction and are separated by 'oxygen-rich gaps' or just by the arrangement of the A-site cations, rather than distinct Bi_2O_2 layers.

4.6 FIELD-INDUCED EFFECTS IN FERROELECTRICS

Beyond the fundamental piezoelectric effect and polarisation switching, ferroelectrics exhibit several other field-induced phenomena. Polarisation switching is when the spontaneous polarisation direction can be reversed by an external electric field exceeding the coercive field E_c , which is the magnitude of the electric field that must be applied in the opposite direction to the initial polarisation to reduce the net polarisation to zero (Figure 4.14). The dielectric response may become non-linear so ϵ_r is no longer a constant (*ceteris paribus*) because of domain wall motion. A sufficiently strong electric field can induce a structural phase transition in a ferroelectric material, even change to a paraelectric state if the field is applied close to the Curie point.

Piezoelectric strain ϵ is proportional to the electric field E in non-centrosymmetric crystals. This is because the applied electric field interacts with the dipole moments within the material, which tend to align with the field, causing macroscopic strain.

Electrostriction is a phenomenon observed in all dielectric materials, distinguishing it from piezoelectricity which requires non-centrosymmetric crystal structures. This universal property of dielectrics involves the induction of mechanical strain (ϵ) when an electric field (E) is applied. As noted by Devonshire [30], this strain is proportional directly to the square of the electric field, meaning $\epsilon \propto E^2$, Figure 4.12. Consequently, the strain is always positive, regardless of the direction or sign of the applied electric field. The constant of proportionality relating the strain to the square of the electric field is referred to as the electrostrictive coefficient.

Example 21: $Pb(Zr_xTi_{1-x})O_3$ polarisation versus electric field

A polycrystalline sample of ferroelectric lead zirconate titanate is subjected to the unidirectional electrical-field illustrated in Figure 4.13. Sketch and explain the corresponding polarisation-versus-field plot.

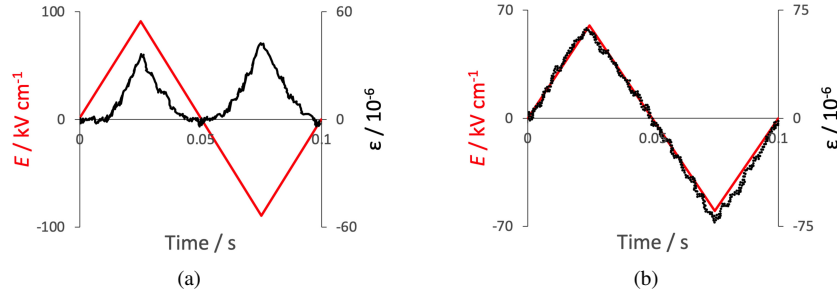


FIGURE 4.12 (a) Electrostriction in $\text{BaBi}_2\text{Nb}_2\text{O}_9$. Note the nonlinear variation in strain with the magnitude of the field. (b) Combined electrostrictive and a much larger piezoelectric strain in LiNbO_3 . In this case the strain varies almost linearly with $|E|$. Images adapted from [31].

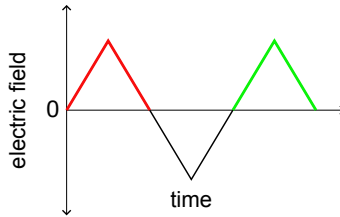


FIGURE 4.13 Variation of applied electric-field with time.

Solution 21

Figure 4.14 shows that as the field is increased from zero to its maximum positive value ($1 \rightarrow 2$), dipoles tend to conform with the applied field, leading to the growth of those domains that best comply with the direction of the field. As the field is reduced towards zero ($2 \rightarrow 3$), the dipoles do not switch back immediately because of the difficulty in reorientation that leads to the hysteresis loop. The field has to be reversed ($3 \rightarrow 4$) to $-E_c$ to achieve that, with the orientations of some of the dipoles rotated through 180° . As the field becomes even more negative ($4 \rightarrow 5$), dipole switching (opposite to '2') occurs with domain growth, with the orientations preserved ($5 \rightarrow 6$) until the field $+E_c$ is reached ($6 \rightarrow 7$).

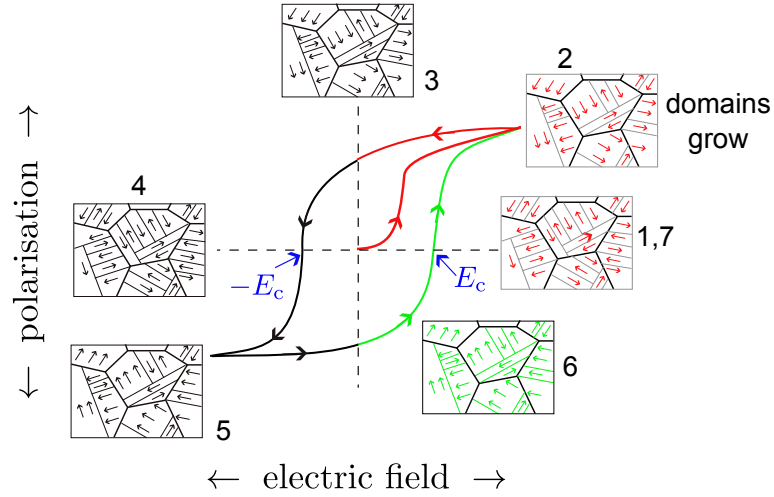


FIGURE 4.14 Schematic illustration of the polarisation response of lead zirconate titanate to applied electric field. The heavy black lines represent grain boundaries whereas the light lines are domain boundaries. The colours correspond to the cycles in Figure 4.13.

Example 22: $\text{Pb}(\text{Zr}_x\text{Ti}_{1-x})\text{O}_3$ strain versus electric field

A polycrystalline sample of ferroelectric lead zirconate titanate is subjected to the unidirectional electrical-field illustrated in Figure 4.13. Sketch and explain the corresponding strain-versus-field plot.

Solution 22

The strains are a combination of piezoelectric, electrostatic and domain switching effects. The second cycle induces domain reversal, as does the third cycle.

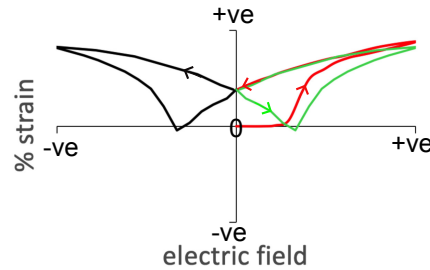


FIGURE 4.15 Schematic illustration of the strain response of lead zirconate titanate to applied electric field of sufficient strength to cause domain switching. The colours correspond to the cycles in Figure 4.13.

REFERENCES

1. Anonymous: ‘Oxford english dictionary’: <https://doi.org/10.1093/OED/1013965084>, 2024.
2. J. Han, S. H. Park, Y. S. Jung, and Y. S. Cho: ‘High-performance piezoelectric energy harvesting in amorphous perovskite thin films deposited directly on a plastic substrate’, *Nature communications*, 2024, **15**, 4129.
3. H. K. D. H. Bhadeshia: *Geometry of Crystals, Polycrystals, and Phase Transformations*: Florida, USA: CRC Press, ISBN 9781138070783, freely downloadable from www.phase-trans.msm.cam.ac.uk, 2017.
4. D. A. Buck: ‘Ferroelectrics for digital information storage and switching (report R-212)’: Master’s thesis, Massachusetts Institute of Technology, 1952.
5. ‘Raimond Spekking / CC BY-SA 4.0 (via Wikimedia Commons) (<https://commons.wikimedia.org/wiki/File:Medical-Econet-PalmCare-CPU—Ramtron-FM18L08-70-SG-5631.jpg>), <https://creativecommons.org/licenses/by-sa/legalcode>’: 2025.
6. D. Berlincourt, and H. Jaffe: ‘Elastic and piezoelectric coefficients of single-crystal barium titanate’, *Physical Review*, 1958, **111**, 143.
7. S.-E. Park, S. Wada, L. Cross, and T. R. Shrout: ‘Crystallographically engineered BaTiO₃ single crystals for high-performance piezoelectrics’, *Journal of Applied Physics*, 1999, **86**, 2746–2750.
8. M. G. Cain, and M. Stewart: ‘Piezoelectric resonance’: Tech. Rep. Measurement and good practice guide 33, ISSN 1368-6550, National Physical Laboratory, London, U.K., 2001.
9. Leval: ‘Aparelho de ultrassom’: Wikimedia.org, public domain, 2008.
10. M. R. Draheim, and W. Cao: ‘Finite element and experimental study of impedance matching layer optimization’, In: *Medical Imaging 1997: Ultrasonic Transducer Engineering*, vol. 3037. California, USA: SPIE, 1997:135–139.
11. S. Zhang, and F. Yu: ‘Piezoelectric materials for high temperature sensors’, *Journal of the American Ceramic Society*, 2011, **94**, 3153–3170.
12. C. Deng, Y. Zhang, D. Yang, H. Zhang, and M. Zhu: ‘Recent progress on barium titanate-based ferroelectrics for sensor applications’, *Advanced Sensor Research*, 2024, **3**, 2300168.
13. K. Sanchez, B. Achour, A. Coustou, A. Lecestre, S. Charlot, M. Lavayssière, A. Lefrançois, H. Aubert, and P. Pons: ‘Transient response of miniature piezoresistive pressure sensor dedicated to blast wave monitoring’, *Sensors*, 2022, **22**, 9571.
14. M. Lewis, and E. Patterson: ‘Microwave ultrasonic attenuation in topaz, beryl, and tourmaline’, *Journal of Applied Physics*, 1973, **44**, 10–13.
15. A. De Bernabe, C. Prieto, and A. De Andres: ‘Effect of stoichiometry on the dynamic mechanical properties of LiNbO₃’, *Journal of Applied Physics*, 1996, **79**, 143–148.
16. C. Shekhar Pandey, and J. Schreuer: ‘Elastic and piezoelectric constants of tourmaline single crystals at non-ambient temperatures determined by resonant ultrasound spectroscopy’, *Journal of Applied Physics*, 2012, **111**, 013516.
17. J. Curie, and P. Curie: ‘Développement par compression de l’électricité polaire dans les cristaux hémihédres à faces inclinées (development, via compression, of electric polarization in hemihedral crystals with inclined faces)’, *Bulletin de la Société minéralogique de France*, 1880, **3**, 90–93.
18. J. Thomson: ‘Piezo-electricity and its applications’, *Engineering*, 1919, **107**, 543–544.
19. Y. Shi, R. He, B. Zhang, and Z. Zhong: ‘Revisiting the phase diagram and piezoelectricity of lead zirconate titanate from first principles’, *Physical Review B*, 2024, **109**, 174104.
20. Y. Tan, J. Zhang, Y. Wu, C. Wang, V. Koval, B. Shi, H. Ye, R. McKinnon, G. Viola, and H. Yan: ‘Unfolding grain size effects in barium titanate ferroelectric ceramics’, *Scientific reports*, 2015,

- 5, 9953.
21. D. Guo, L. Li, C. Nan, J. Xia, and Z. Gui: 'Modeling and analysis of the electrical properties of PZT through neural networks', *Journal of the European Ceramic Society*, 2003, **23**, 2177–2181.
22. J. Tellier, B. Malic, B. Dkhil, D. Jenko, J. Cilensek, and M. Kosec: 'Crystal structure and phase transitions of sodium potassium niobate perovskites', *Solid State Sciences*, 2009, **11**, 320–324.
23. K. Singh, V. Lingwal, S. Bhatt, N. Panwar, and B. Semwal: 'Dielectric properties of potassium sodium niobate mixed system', *Materials research bulletin*, 2001, **36**, 2365–2374.
24. C. Ahn, S. Lee, H. Lee, A. Ullah, J. Bae, E. Jeong, J. Choi, B. Park, and I. Kim: 'The effect of K and Na excess on the ferroelectric and piezoelectric properties of $\text{K}_{0.5}\text{Na}_{0.5}\text{NbO}_3$ thin films', *Journal of Physics D: Applied Physics*, 2009, **42**, 215304.
25. K. Belgacem, C. Stanciu, S. Perju, and M. Cernea: 'Role of the dopants in improving the piezoelectric properties of $\text{Bi}_{0.5}\text{Na}_{0.5}\text{TiO}_3$ ', *Journal of Electronic Materials*, 2023, **52**, 4455–4474.
26. S. Supriya: 'A review on lead-free $\text{Bi}_{0.5}\text{Na}_{0.5}\text{TiO}_3$ based ceramics and films: dielectric, piezoelectric, ferroelectric and energy storage performance', *Journal of Inorganic and Organometallic Polymers and Materials*, 2022, **32**, 3659–3676.
27. B. Aurivillius: 'Mixed bismuth oxides with layer lattices I,II. the structure type of $\text{CaNb}_2\text{Bi}_2\text{O}_9$ ', *Arkiv kemi*, 1949, **1**, 463–480, 499–412.
28. B. Aurivillius: 'Mixed bismuth oxides with layer lattices III. structure of $\text{BaBi}_4\text{T}_4\text{O}_{15}$ ', *Arkiv kemi*, 1950, **2**, 519–527.
29. A. Agasiev, M. Mamedov, and M. Muradov: 'Electrical conductivity and dielectric properties of $\text{Bi}_4\text{Ti}_3\text{O}_{12}$ ', *Journal de Physique III*, 1996, **6**, 853–861.
30. A. F. Devonshire: 'XCVI. theory of barium titanate: Part I', *The London, Edinburgh, and Dublin Philosophical Magazine and Journal of Science*, 1949, **40**, 1040–1063.
31. G. Viola, T. Saunders, X. Wei, K. Chong, H. Luo, M. Reece, and H. Yan: 'Contribution of piezoelectric effect, electrostriction and ferroelectric/ferroelastic switching to strain-electric field response of dielectrics', *Journal of Advanced Dielectrics*, 2013, **3**, 1350007.

Chapter 5

Organic materials

5.1 INTRODUCTION

Both polymer-based dielectrics and molecular ferroelectrics offer advantages as organic materials. While polypropylene, a thermoplastic polymer, achieves a high molecular weight of 10^5 g mol^{-1} due to its long chains of linked C_3H_6 monomers, molecular ferroelectrics like 2-Amino-5-nitropyridine $\text{C}_5\text{H}_5\text{N}_3\text{O}_2$ are composed of unlinked, low-molecular-weight molecules, with the latter having a molecular weight of $139.11 \text{ g mol}^{-1}$. These organic materials share several desirable characteristics, including the ability to be synthesised at low temperatures, inherent flexibility, low density, and potential biocompatibility.

Biaxial polypropylene thin films are made by stretching along orthogonal directions parallel to the plane of the sheet. This orients the molecules within, leading to a reduction in free volume which influences their dielectric properties. They have a small loss tangent $\tan \delta \approx 0.0002$ up to $\approx 85^\circ\text{C}$, have an electrical breakdown field in excess of 600 MV m^{-1} , but a low relative permittivity ($\epsilon_r \approx 2.25$) meaning a limited capacity to stored energy of $\approx 1 \rightarrow 2 \text{ J cm}^{-3}$ [1]. The relationship between permittivity and stored energy per unit volume J_V for linear dielectrics can be derived beginning with Equation 2.1a whereby

$$\begin{aligned}\mathcal{D} &= \epsilon_o \epsilon_r E \\ J_V &= \frac{1}{2V} \int_V E \mathcal{D} dV \\ &\equiv \frac{1}{2} \epsilon_o \epsilon_r E^2\end{aligned}$$

In spite of the small energy density, metallised oriented-polypropylene is used to make capacitors (Figure 5.1) because of the low energy loss during repeated charging and discharging. The material possesses very high dielectric strength (p. 18), meaning that it can withstand a large electric field before breakdown. This allows for the use of very thin films, maximising capacitance for a given volume.

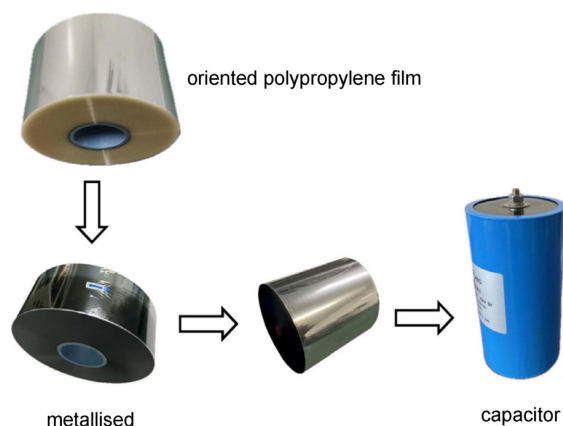


FIGURE 5.1 Steps in the making of a capacitor based on oriented polypropylene. Image reproduced with altered annotation, from [2] under the CC BY 4.0 license, <https://creativecommons.org/licenses/by/4.0/>.

5.2 POLARISATION MECHANISMS IN POLYMERS

The basic mechanisms of polarisation in dielectrics have already been described in Section 2.3. Issues that are specific to polymers are discussed here.

1. Electronic polarisation in polymers occurs when an external electrical field causes temporary dipoles to develop as the electron clouds of molecules are shifted. This effect can occur in a polymer that is ordinarily not polar. For example, the covalent bonds between carbon and hydrogen in polyethylene are displaced relative to the positive nuclei when an electrical field is applied. The resonant frequencies associated with electronic polarisation $\omega > 10^{15} \text{ s}^{-1}$ so it does not contribute to losses due to devices such as capacitors subjected to oscillating electrical fields.
2. In polymers, atomic polarisation involves the relative displacement of entire atoms amongst group of atoms (ions) within the polymer backbone or side groups. The mechanism is therefore slower than electronic polarisation with resonant frequencies in the range $10^{11} \rightarrow 10^{14} \text{ s}^{-1}$.
3. Polypropylene does not contain permanent dipoles. If polymers have ionic groups, they respond to an applied electric field. Polyacrylic acid contains carboxylic acid groups ($-\text{COOH}$) that can ionise into COO^- in the presence of moisture, making it susceptible to ionic polarisation. Ionic migration involving the physical transport of ions within the polymer is a slow process (seconds \rightarrow hours) and is fundamental to the operation of supercapacitors (Figure 5.2), which have two electrodes in an electrolyte. An applied voltage causes ions to migrate towards the electrodes, causing an accumulation of charge at the electrode-electrolyte interface, to form an inner layer of strongly

adsorbed ions and a more diffuse outer layer of ions. It is this ‘separation’ of charge that constitutes ionic polarisation, with capacitance increasing when the double layer thickness (typically $< \text{nm}$) is reduced; the thickness is much smaller than in conventional capacitors where a solid dielectric separates the charges.

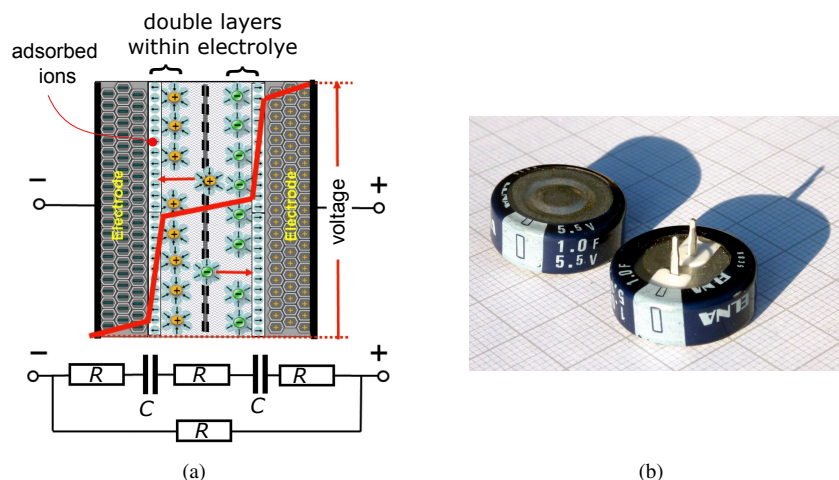


FIGURE 5.2 (a) Schematic illustration of a supercapacitor, showing the electrical double-layers, the two capacitances within, corresponding to the pair of double layers. (b) Lithium ion supercapacitors. Images reproduced in modified form, under the CC0 1.0 Universal public domain license.

4. Polyvinyl chloride molecules have permanent dipoles due to polar chlorine atoms, which can align with an applied electrical field leading to orientation polarisation. Nylon (polyamide) also contains polar $-\text{CONH}-$ groups that contribute to orientation polarisation.
5. Space-charge polarisation is particularly relevant for polymers that have been modified to include additives, fillers or plasticisers because these lead to a heterogeneous structure. Polyvinyl chloride with ionic additives can react to an applied electric field by the accumulation of charges at interfaces. Some 228 different substances can be added to enhance heat stability, flexibility, antistatic properties, flame retardants etc. [3].
6. Polymers are sometimes blended, e.g., polyethylene and polypropylene. The interface's nature depends on processing conditions, sometimes leading to dispersed phases, such as droplets of one polymer within the other. The resulting interfaces can accumulate charges when exposed to electrical fields, leading to interfacial polarisation. Composite polymers where the constituents remain distinct, are another example where interfacial polarisation plays a role. Examples include glass-reinforced plastics or polymers reinforced with fine particles of silica.

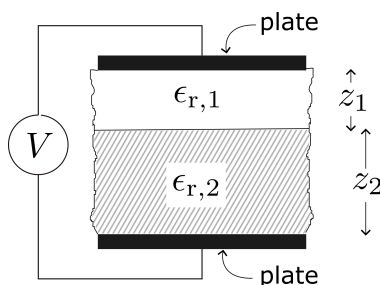
7. In some polymers, the application of a electric field can cause the shape (conformation) of molecular chains to alter, influencing polarisation. The magnitude of the effect depends on chain mobility, which would be much more limited in crystalline polymers. Therefore, such polarisation is relevant in flexible or rubbery polymers such as the elastomer styrene-butadiene rubber.

5.3 POLYMER COMPOSITE DIELECTRICS

Imagine mixing small, highly conductive metal spheres into a rubber matrix to make the rubber itself more conductive; here, it's about making the polymer more polarisable or charge-storing. This is attempted by introducing inorganic particles that intrinsically possess a much higher dielectric constant (e.g., titanates like BaTiO_3 often have ϵ_r in the hundreds to thousands) into a polymer matrix, although any improvement is rather small in general [4].

A uniform dispersion of particles is desirable, sometimes difficult to achieve when there are Van der Waals interactions that cause aggregation. If the particles form a network, conduction along the particle/matrix interfaces can lead to dielectric losses and reduce the threshold for electrical breakdown.

A simplified treatment of the non-uniform electric field within a two-phase material is in terms of a two-layered composite in which the interface has no role in this context [5], as follows, assuming that the electric field is normal to the plates:



The alteration of charge density on the *plates* that connect the composite to the voltage, the electric displacement field (\mathcal{D}) must be constant throughout the composite, i.e., $\mathcal{D}_1 = \mathcal{D}_2$. Since $\mathcal{D} = \epsilon_o \epsilon_r E$ the ratio of the respective electrical fields is proportional to

$$\frac{E_1}{E_2} = \frac{\epsilon_{r,1}}{\epsilon_{r,2}} \quad (5.1a)$$

$$\text{and } V = E_1 z_1 + E_2 z_2 \quad (5.1b)$$

In other words, the material with the lower permittivity will experience a higher electric field, and *vice versa*. Using these equations, isolating the electrical fields, noting that $z_1 + z_2 = z$ and that $E = V/z$ gives

$$E_1 = \frac{V}{\epsilon_{r,1}} \left(\frac{z_1}{\epsilon_{r,1}} + \frac{z_2}{\epsilon_{r,2}} \right)^{-1} \equiv \frac{V}{z_1 + z_2 \left(\frac{\epsilon_{r,1}}{\epsilon_{r,2}} \right)} \equiv \frac{E}{V_V \left(1 - \frac{\epsilon_{r,1}}{\epsilon_{r,2}} \right) + \frac{\epsilon_{r,1}}{\epsilon_{r,2}}} \quad (5.1c)$$

where $V_V = z_1/z$ is the volume fraction of phase 1. In a similar manner,

$$E_2 = \frac{E}{V_V \left(\frac{\epsilon_{r,2}}{\epsilon_{r,1}} - 1 \right) + 1} \quad (5.1d)$$

If phase 1 is identified with the polymer and phase 2 with the added particles, then the nominal field in the latter is less than that in the polymer, and *vice versa*. This means that even if the particles themselves can withstand high fields, the polymer matrix, which forms the continuous phase, is subjected to localised field enhancements. This can cause the polymer to break down at overall applied voltages much lower than its intrinsic breakdown strength, effectively reducing the overall dielectric strength of the composite.

Composites can consist of alternating layers of different polymers, rather than of particles dispersed in a matrix, with the aim of increasing the dielectric constant, the energy density J_V and reducing loss in capacitor applications. Such composites are easy to manufacture by co-extrusion of two different polymers [6].

Example 23: Electrical fields in polymer composite

This example applies the derived equations for electric field distribution in a two-layered composite to highlighting implications for their electrical behaviour. Polyvinylidene fluoride has molecular chains with polar groups $-\text{CF}_2$ and $-\text{CH}_2$, which renders it piezoelectric. A layered composite of polycarbonate and the polyvinylidene fluoride is created with equal thicknesses of each polymer. Given that $\epsilon_{r,\text{carbonate}} = 3$ and $\epsilon_{r,\text{fluoride}} = 12$, calculate the fields within each polymer when the externally applied field $E = 200 \text{ MV m}^{-1}$.

Solution 23

Since this is a 50-50 composite, $V_V = 0.5$, so using Equations 5.1c and 5.1d gives

$$E_{\text{carbonate}} = \frac{200}{0.5(1 - \frac{3}{12}) + \frac{3}{12}} = 320 \text{ MV m}^{-1}$$

$$E_{\text{fluoride}} = \frac{200}{0.5(\frac{12}{3} - 1) + 1} = 80 \text{ MV m}^{-1}.$$

There is, therefore, a much reduced field in the polyvinylidene fluoride which is not sufficient to cause dipole switching in thin layers of the polymer, its ferroelectric behaviour effectively ‘suppressed’ due to the shunting of the electric field into the lower permittivity polycarbonate. Thus, the hysteresis in the \mathcal{D} versus E plot, associated with such switching, is absent in the composite state [6]. The main contribution to the hysteresis is the field-induced movement of ions within the fluoride, which is easier across short distances. This means that the hysteresis decreases with the layer thicknesses are reduced, Figure 5.3.

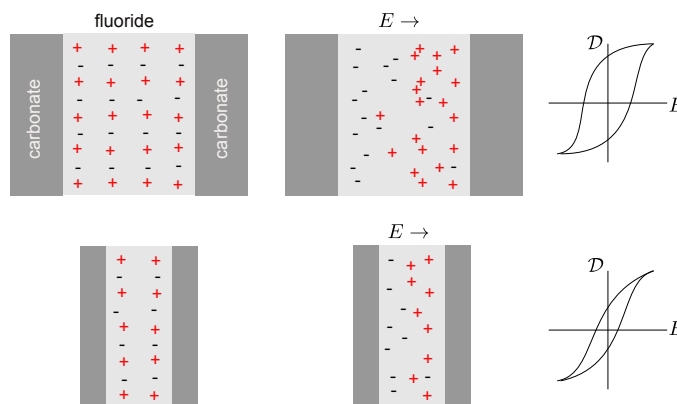


FIGURE 5.3 Schematic diagram illustrating the effect of the thickness of layers in polymer composite consisting of a 50/50 mixture of polyvinylidene fluoride and polycarbonate. The ions have less steric hinderance when displaced by electrical field applied normal to the layers. Adapted from [6].

This example vividly illustrates a critical aspect of dielectric composite design: simply adding a high-permittivity material does not guarantee enhanced performance, particularly for ferroelectric applications. The internal electric field distribution can profoundly alter the behaviour of the constituent materials, potentially preventing them from exhibiting their desired properties and impacting the overall electrical characteristics of the composite.

5.4 DIELECTRIC POLYMERS: ORIENTATIONAL POLARISATION

Ordinary dielectrics that are not polar, either because of the existence of a centre of symmetry or the absence of polar groups, are said to be *linear* because $\mathcal{D} \propto E$. Polyethylene does not contain permanent dipoles and the molecule has symmetry, so the primary polarisation mechanism is electronic, Figure 5.4a.

A polymer that contains a small fraction of isolated islands of randomly oriented polar groups that interact weakly with the matrix so that their dipoles rotate almost independently, or one that is in its paraelectric state, will at low E behave almost linearly in its \mathcal{D} - E response, but non-linearity manifests when the dipole response saturates at a large enough electric field strength, Figure 5.4b. Examples include polyethylene oxide that has been doped with lithium salts, and polyamide-6 containing certain additives. Note that there is no hysteresis because of the absence of spontaneous polarisation.

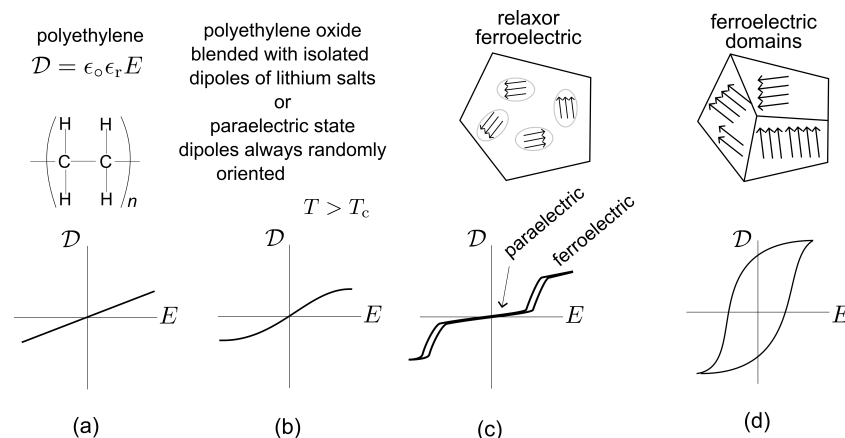


FIGURE 5.4 Charge displacement \mathcal{D} as a function of an applied electric field, for a variety of dielectric polymers.

Relaxors (page 54) can exhibit a 'double' hysteresis loop, Figure 5.4c, initially almost a linear response, followed by the alignment of dipole domains with respect to the applied field. The hysteresis during the reversal of the field is due to the fact that the domains do not switch instantaneously during field reversal. The hysteresis loop may become single if the dipole orientation changes even at small electrical fields. Polyvinylidene fluoride and its copolymers are common ferroelectric relaxor polymers that contain separated domains of electrical dipoles. There are small regions where the dipoles are locally ordered but no long-range ferroelectric order.

A crystalline polymer with long-range ferroelectric order consists fully of domains and exhibits the classical \mathcal{D} - E response as illustrated in Figure 5.4d. Domains that comply with the external fields grow at the expense of those that do not, and the process essentially reverses when the direction of the field is reversed. Crystalline polyvinylidene fluoride has a polar unit cell in which the direction of polarisation can be changed by the application of an electrical field [7]. The crystal structure of greatest interest in the present context is the β form with an orthorhombic unit cell with a macroscopic polar dipole moment that renders it ferroelectric, Figure 5.5.

The three further allotropes of crystalline polyvinylidene fluoride are α which is non-polar because of the way in which the pair of *trans-gauche* polymer chains in the unit cell with their dipole moments pointing in opposite directions. The γ and δ varieties have a net polar dipole but much weaker than that of β because of differences in chain conformations [7]. Since α is the most stable phase on cooling from the melt to ambient temperature, the formation of β instead is induced by crystallisation under high pressure; it is the favoured phase under 100 \rightarrow 300 MPa of uniaxial compression of films [8], because it has a 15% greater density than α .

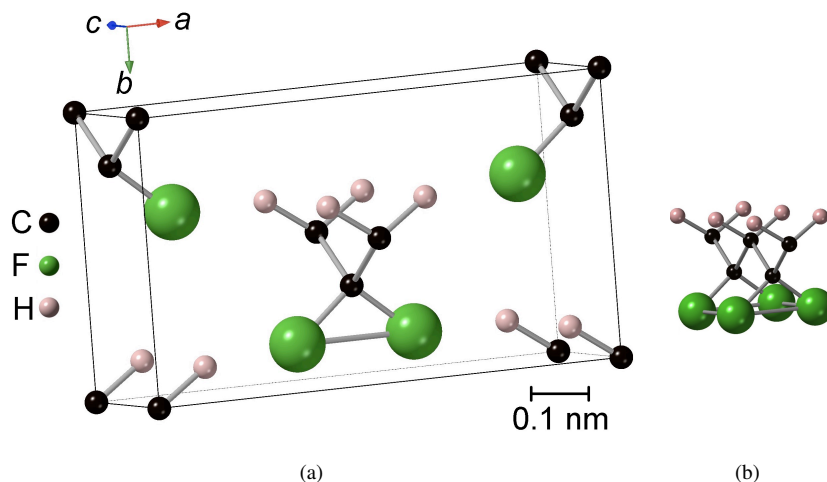


FIGURE 5.5 (a) The β orthorhombic form of polyvinylidene fluoride $(-\text{CH}_2\text{CF}_2)_n$. The molecule is in a *trans*-conformation which renders the largest dipole moment, and the dipole moments of the two molecules in the unit cell are oriented parallel to the b -axis. [9]. The dipoles can be flipped through 180° by an electrical field, i.e., the material is ferroelectric [7]. (b) Polymer chain along c -axis, showing zig-zag of carbon-atom chain.

5.5 MOLECULAR FERROELECTRICS

The first ferroelectric, Rochelle salt (page 43), was discovered in 1920 [10], a discovery marked the beginning of the field of ferroelectricity. It exhibits ferroelectricity in the temperature range $-18 \rightarrow 24^\circ\text{C}$. Inorganic oxides like BaTiO_3 , PbZrO_3 and $\text{PbZr}_x\text{Ti}_{1-x}\text{O}_3$ became highly successful in various applications due to their robust ferroelectric properties. Molecular ferroelectrics are composed of chemical compounds of low molecular weight when compared against polymers. The molecules have spontaneous polarisation that can be reversed by the application of an external electric field.

One example is a particular non-centrosymmetric bromide crystal ($\text{C}_6\text{H}_{14}\text{BrN}$); its spontaneous polarisation comes from the bromine anion and the organic cation. This indicates that the charge separation and resulting dipole moments originate from the specific arrangement and inherent polarity of the ionic constituents within the crystal lattice. It has $T_c = 426\text{ K}$, which exceeds that barium titanate. Other properties such as spontaneous polarisation, dielectric constant and dielectric loss also compare well against BaTiO_3 [11].

The case for molecular ferroelectrics remains weak, there have been no applications to date. This is largely because established ferroelectric oxides are easy to manufacture and design into components. The molecular ferroelectrics are studied mostly in thin film form – they *may* have uses in the manufacture of flexible devices, but nothing has emerged to date.

Example 24: Design of wearable ferroelectric device

What engineering and material parameters would you need to consider in creating a wearable, long-lasting, monitoring device based on molecular ferroelectrics, for use by humans or animals?

Solution 24

1. A device such as this must be small, and have a sufficient area to respond to signals such as the pressure pulses due to heartbeat. The ferroelectric is therefore best applied as a thin film onto a substrate that is biocompatible and itself is flexible (such as a plastic).
2. It could in principle be manufactured using ink-jet printing of the ferroelectric on to the substrate. This would be a cheap and effective method since the areas to be printed are not large, nor is it necessary to print more than one layer. It is likely therefore that the ferroelectric would not be single-crystalline. So it may be necessary to apply poling – with a bit of imagination, it may be feasible to apply a suitable field that creates a poled structure during

deposition (?).

3. Bear in mind that designing a sensor is not sufficient, it would require connections, which in turn would need to feed into an interpretation device that is powered. The obvious way is to couple with a watch or mobile telephone, but this clearly is not reasonable when dealing with animals. Some sort of wireless communication could in principle be implemented.
4. Flexibility creates additional problems. In general, even thin films can fail by fatigue when subjected to alternating stresses. This would need to be investigated depending on the ferroelectric selected.
5. Is the sensor likely to suffer sensitivity or steady deterioration through contact with inevitable bodily fluids?
6. What is the level of contact necessary between the film and body to ensure accurate biometric sensing? Does the curvature of the body reduce the effective contact area? Is it possible to design a sensor based on ferroelectrics that does not require direct contact?
7. What material parameters determine flexibility and what engineering parameters do so?

Bear in mind that this is not a comprehensive list!

5.6 CONDUCTING POLYMERS

Consider graphene, the structure of which is illustrated in Figure 8.2. Each carbon atom in graphene is sp^2 hybridised, meaning that one $2s$ orbital mixes with two $2p$ orbitals ($2p_x$ and $2p_y$) to form three sp^2 hybrid orbitals that lie in the plane of the graphene sheet and form strong covalent bonds with their neighbours. Each carbon atom still has one unhybridised p_z orbital lying normal to the plane of the graphene. So these p_z orbitals overlap sideways, forming delocalised π -bonds across the entire graphene lattice, free to move, resulting in outstanding in-plane electrical conductivity.

Unlike graphene, polyacetylene $(-\text{CH}=\text{CH}-\text{CH}=\text{CH}-)_n$ consists of ‘one-dimensional’ long chains of alternating single and double C–C bonds; this *conjugation* of bonds means that every other carbon atom has an unhybridised p_z orbital (the one that forms the π -bond). In a typical single bond, electrons are localised between two atoms (σ -bonds). In a double bond, there’s one σ -bond and one π -bond. So although there are delocalised π -bonds they only allow conduction along the chain.

Also important is that pure graphene has a band structure in which the valence and conduction bands touch at specific points, allowing electrons to move essentially like massless particles, exhibiting very high mobility. On the other hand, polyacetylene is an intrinsic semiconductor. This means electrons need a certain amount of energy to jump from the valence band to the conduction band,

limiting its intrinsic conductivity. Therefore, the conductivity can be tuned using dopants. The larger band gap (relative to graphene) in polyacetylene is because only every other carbon atom has an unhybridised π -bond. With bond alternation, the periodic potential experienced by the electrons changes resulting in the opening up a gap at the Fermi level.

Some representative values of the electrical conductivities of polymers are presented in Table 5.1.

TABLE 5.1 Some typical electrical conductivities of polymers. The values are dependent on synthesis method, purity, degree of polymerisation, type and concentration of dopant, morphology, and processing conditions of the polymer.

	Electrical conductivity / S m^{-1}
cis-polyacetylene	10^{-7}
Doped polyacetylene	$10^4 \rightarrow 10^7$
Polypyrrole	10^8
Poly(3,4-ethylenedioxythiophene)	10^{-3}
Graphene (single layer)	$\approx 8 \times 10^7$

5.7 ORGANIC LIGHT-EMITTING DIODE

An organic light-emitting diode is a solid-state lighting device that uses carbon-based materials to emit light when an electric current is passed through them. It typically consists of a stack of thin layers of organic material sandwiched between two electrodes:

1. A glass substrate for mechanical support (a flexible device might have a flexible plastic substrate).
2. A transparent conductive layer (e.g., indium tin oxide, p. 134) that injects holes into the organic layers.
3. A series of distinct organic layers, the constitution of which can be found elsewhere [12]: one that facilitates hole injection from the anode, another that transports holes to the emissive layer (where the material is excited to emit photons), an electron transport layer to take electrons towards the emissive layer, and a layer that facilitates electron injection from the cathode. The cathode itself is a metal such as aluminium which injects electrons into the organic layers.

The application of a voltage leads to holes and electrons migrating into the emissive layer, recombining in the emissive layer to form an excited, unstable state called an exciton, which then releases excess energy in the form of a visible

light photon. The colour can be engineered by manipulating band gaps.

Example 25: Organic light emitting diode

An experimental organic light-emitting diode has the following characteristics during continuous operation:

Active emissive area	25 mm ²	Operating voltage	4.0 V
Operating current	20 mA	Luminance	1500 cd m ⁻²
Peak emission wavelength	530 nm		

Calculate (a) the electric power consumption; (b) the current efficiency which is a measure of how much light (in candelas) is produced per unit of current injected into the device. It's often expressed in cd A⁻¹; (c) the luminous flux, which is the total amount of visible light emitted by the source, measured in lumens. It can be calculated from luminance and the active area; (d) the power efficiency, a measure of how efficiently the electrical power input is converted into visible light output, expressed in lumens W⁻¹.

Solution 25

- (a) The power consumed is

$$I \times V = (20 \times 10^{-3}) \times 4 = 0.08 \text{ W}.$$

- (b) The current efficiency is

$$\frac{\text{luminance} \times \text{active area}}{\text{operating current}} = \frac{1500 \times (25 \times 10^{-6})}{20 \times 10^{-3}} = 1.875 \text{ cd A}^{-1}.$$

- (c) The luminous flux is the product of the luminance, active area and π assuming a flat display and that the surface appears constant regardless of the angle of view:

$$1500 \times (25 \times 10^{-6}) \times \pi = 0.1178 \text{ lumens}.$$

- (d) The power efficiency is the ratio of luminous flux to the power consumption:

$$\frac{\text{luminous flux}}{\text{electrical power consumption}} = \frac{0.1178}{0.08} = 1.4725 \text{ lumens W}^{-1}.$$

This is two orders of magnitude smaller than in routine inorganic light-emitting diodes and an order of magnitude less than an incandescent bulb.

REFERENCES

1. T. M. Chung: 'Functionalization of polypropylene with high dielectric properties: applications in electric energy storage', *Green and sustainable chemistry*, 2012, **2**, 29–37.
2. X. Sun, Y. Qiao, Y. Li, C. Cao, and S. Feng: 'Insulation resistance characteristics of dry DC link capacitors in the presence of high temperatures and operating voltages', *Energies*, 2024, **17**, 1147.
3. E. Bird, M. Griffiths, E. Holden, D. Pacifici, E. Pemberton, K. Schofield, and E. Tarring: 'Polyvinyl chloride (PVC) additives: a scoping review': Tech. Rep., Environment Agency, UK Government, Bristol, UK, 2024.
4. L. Zhu: 'Exploring strategies for high dielectric constant and low loss polymer dielectrics', *The Journal of Physical Chemistry Letters*, 2014, **5**, 3677–3687.
5. J. Kuffel, and P. Kuffel: *High voltage engineering fundamentals*: Oxford, U. K.: Elsevier, 2000.
6. M. Mackey, D. E. Schuele, L. Zhu, L. Flandin, M. A. Wolak, J. S. Shirk, A. Hiltner, and E. Baer: 'Reduction of dielectric hysteresis in multilayered films via nanoconfinement', *Macromolecules*, 2012, **45**, 1954–1962.
7. R. G. Kepler, and R. Anderson: 'Ferroelectric polymers', *Advances in physics*, 1992, **41**, 1–57.
8. N. Meng, X. Ren, G. Santagiuliana, L. Ventura, H. Zhang, J. Wu, H. Yan, M. J. Reece, and E. Bilotti: 'Ultrahigh β -phase content poly (vinylidene fluoride) with relaxor-like ferroelectricity for high energy density capacitors', *Nature communications*, 2019, **10**, 4535.
9. R. Hasegawa, Y. Takahashi, Y. Chatani, and H. Tadokoro: 'Crystal structures of three crystalline forms of poly (vinylidene fluoride)', *Polymer Journal*, 1972, **3**, 600–610.
10. J. Valasek: 'Piezo-electric and allied phenomena in Rochelle salt', *Physical Review*, 1921, **17**, 475.
11. D.-W. Fu, H.-L. Cai, Y. Liu, Q. Ye, W. Zhang, Y. Zhang, X.-Y. Chen, G. Giovannetti, M. Capone, J. Li, and R.-G. Xiong: 'Diisopropylammonium bromide is a high-temperature molecular ferroelectric crystal', *Science*, 2013, **339**, 425–428.
12. B. Geffroy, P. Le Roy, and C. Prat: 'Organic light-emitting diode (OLED) technology: materials, devices and display technologies', *Polymer international*, 2006, **55**, 572–582.

Chapter 6

Thermoelectrics

6.1 SEEBECK EFFECT

Thomas Johann Seebeck, in his investigations, identified a crucial condition for the manifestation of magnetism in metallic circuits: a temperature difference at the points of contact between the constituent elements. This observation laid the groundwork for what is now known as the Seebeck effect.

The Seebeck effect describes the phenomenon where a temperature difference applied across a junction of two dissimilar metals, such as bismuth and antimony, generates an electric current. This current, in turn, can deflect a magnetic needle.

The underlying mechanism involves the charge carriers within the material. On the hotter side of the junction, these charge carriers gain thermal energy. This increased energy causes them to migrate towards the colder side of the material. This movement of charge carriers establishes a voltage difference that runs parallel to the applied temperature gradient. Consequently, electricity is generated directly within the solid-state device due to this thermoelectric phenomenon.

The relationship between the induced voltage and the temperature gradient in a thermoelectric material is quantified by the Seebeck coefficient, S_e :

$$S_e = -\Delta V / \Delta T \quad (6.1)$$

where the negative sign indicates that the direction of the induced voltage is opposite to that of the temperature gradient. A large value of this coefficient increases the utility of the thermoelectric material. But a good thermoelectric device must also have a low thermal conductivity if the temperature gradient is to be maintained.

For a thermoelectric material to be practically useful, it needs a high Seebeck coefficient, as this leads to a larger generated voltage for a given temperature difference. However, achieving high thermoelectric performance also requires a low thermal conductivity. If a material has high thermal conductivity, heat will quickly flow from the hot side to the cold side, diminishing the temperature gradient that drives the Seebeck effect. This makes it difficult to maintain the necessary temperature difference for efficient electricity generation.

Therefore, good thermoelectric materials are characterised by a combination of high electrical conductivity (to allow current flow) and a large Seebeck coefficient (to generate voltage), along with low thermal conductivity (to maintain the temperature gradient). This often presents a challenge in material design, as the properties related to charge carrier transport (electrical conductivity and Seebeck coefficient) are typically linked, and efforts to improve one can negatively impact the other, or increase thermal conductivity.

One remarkable application of thermoelectric materials is found in the power sources of the Voyager deep space missions. Launched in 1977, these probes are currently in interstellar space and continue their epic journeys, powered by these advanced systems.

The core of the Voyager battery utilises the heat generated by the radioactive decay of plutonium-238 oxide. This heat is then converted into a few hundred Watts of electricity by a thermoelectric couple made from a doped silicon-germanium (SiGe) alloy (approximately 78 at.% Si). The choice of SiGe is strategic due to its ability to withstand both shock and extremely high temperatures, with the hot junction operating at 1273 K and the cold junction at 573 K.

To create the thermoelectric couple, the SiGe alloy is specifically doped. One SiGe element is doped with boron, resulting in a *p*-type thermoelectric material, while another is doped with phosphorus, making it an *n*-type material. This combination of *p*-type and *n*-type thermoelectric elements is essential for efficient conversion of heat into electrical energy.

A Seebeck coefficient can be defined even for a single material, with a positive value when the charge carriers are holes (*p*-type) and negative when the carriers are electrons (*n*-type). For example, $S_e^{\text{pure Si}} \approx 440 \mu\text{V K}^{-1}$, and $S_e^{\text{pure Ge}} \approx 330 \mu\text{V K}^{-1}$, but the numbers depend on purity, whether single-crystal or polycrystal etc. [1]. It follows that in a couple consisting of single-phase materials α and β , $\Delta S_e = S_e^\alpha - S_e^\beta = -\Delta V / \Delta T$.

This relationship highlights how a larger difference in Seebeck coefficients between the two materials in a couple leads to a greater induced voltage for a given temperature difference, which is crucial for efficient thermoelectric power generation.

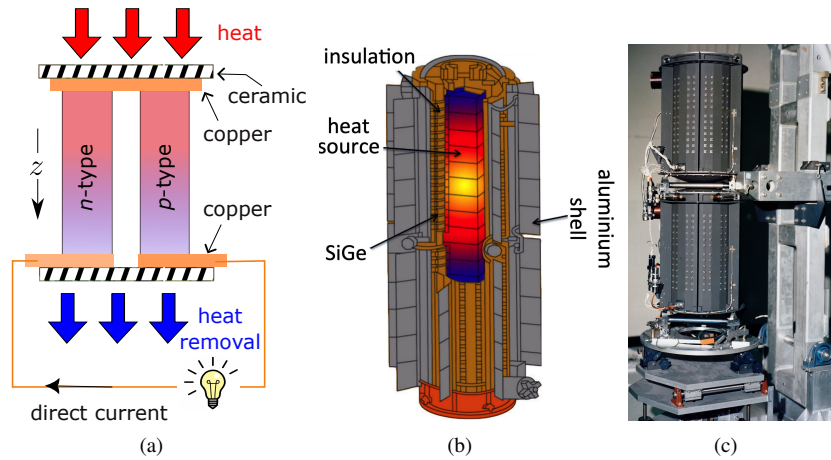


FIGURE 6.1 (a) Schematic of thermoelectric battery. z is simply the distance coordinate pointing downwards, parallel to the electron flow in the n -type and antiparallel to the hole flow in the p -type semiconductor. (b) Design of a thermoelectric battery for very long-range spacecraft, where the heat is generated using a radioactive source and the resulting temperature gradient induces a potential difference across the SiGe to provide electricity. Image courtesy of Parker Betty, adapted under the CC-BY-SA-4.0 licence <https://creativecommons.org/licenses/by-sa/4.0/deed.en> (c) Real battery, courtesy of NASA/JPL-Caltech.

Example 26: Sign of Seebeck coefficient

The n -type $\text{Si}_{0.8}\text{Ge}_{0.2}$ semiconductor that is doped with phosphorus has a Seebeck coefficient of $-109 \mu\text{V K}^{-1}$ whereas the p -type version has $S_e = 113 \mu\text{V K}^{-1}$ [2]. By considering the flow of electrons in the n -type and the flow of holes in the p -type, explain the opposite signs of S_e in these two semiconductors.

Solution 26

Referring to Figure 6.1, note the direction of the coordinate z .

In n -type $\text{Si}_{0.8}\text{Ge}_{0.2}$ doped with phosphorus, the primary charge carriers are electrons. When a temperature gradient is applied (e.g., one end is hot and the other is cold), the electrons at the hotter end gain more kinetic energy, and as a result, tend to diffuse from the hot region to the cold region to equalise their energy distribution. This movement of negative charge towards the colder end effectively creates a build-up of negative charge at the cold end and a deficiency of negative charge at the hot end. Since voltage is defined as the potential difference from a higher potential to a lower potential, if the cold end becomes

more negative relative to the hot end, then the induced voltage direction is such that the potential at the hot end is higher than the cold end. There is a decrease in both voltage and temperature so both ΔV and ΔT are positive; bearing in mind that $S_e = -\Delta V/\Delta T$, S_e will be negative. The observed Seebeck coefficient of $-109 \mu\text{V K}^{-1}$ for the n -type $\text{Si}_{0.8}\text{Ge}_{0.2}$ confirms this.

In p -type $\text{Si}_{0.8}\text{Ge}_{0.2}$ doped with boron, the primary charge carriers are holes. When a temperature gradient is applied, the holes at the hotter end have higher energy so they diffuse towards the cold region. The resulting accumulation of positive charge there makes $\Delta V < 0$ but ΔT still is positive, making S_e positive. The observed Seebeck coefficient of $113 \mu\text{V K}^{-1}$ for the p -type $\text{Si}_{0.8}\text{Ge}_{0.2}$ confirms this.

Example 27: Broken thermocouple

A thermocouple consists of copper and nickel wires welded together; the copper wire fractures close to the original junction. Is it appropriate to implement a repair by soldering the broken bits together?

Solution 27

No, it is not appropriate to repair a thermocouple by simply soldering the broken copper and nickel wires together at the original junction point.

A thermocouple works on the principle of the Seebeck effect, where a voltage is generated due to a temperature difference across a junction of two dissimilar metals. Soldering introduces a third, different metal (the solder itself) at the critical sensing junction. Solder is typically an alloy of tin, lead, silver, or other metals.

Each new junction (copper-solder and solder-nickel) will generate its own thermoelectric voltage. These additional voltages will contribute to or subtract from the intended voltage generated by the copper-nickel junction. The result is an inaccurate temperature reading. The thermocouple will no longer provide a true measurement of the temperature at the point you are trying to sense. The calibration will be completely off.

A proper repair would involve the spot welding of the broken copper wires.

Example 28: Criteria for thermoelectric performance assessment

What are the material parameters that you would use to select the best thermoelectric material out of the many available?

Solution 28

To select the best thermoelectric material, the primary material parameter is the dimensionless thermoelectric figure of merit, ZT . This single parameter encapsulates the essential properties that determine a material's efficiency in converting heat into electrical energy (or vice-versa for cooling applications). The merit is defined at

$$ZT = \frac{\sigma S_e^2}{\kappa} \times T. \quad (6.2)$$

Maximising $|S_e|$ means that a greater voltage would be generated per degree of temperature difference, leading to a higher power output.

1. The larger the thermoelectric effect, i.e., greater $|S_e|$ would naturally be desirable. The energy generated is, however, proportional to S_e^2 . This is because in Ohm's law, $V = IR$ and power $= IV = V^2/R$, hence the use of S_e^2 .
2. The thermal conductivity κ should be minimised so that viable temperature gradients can persist.
3. The electrical conductivity σ should be maximised to avoid resistive losses.

The best thermoelectric material available today has $ZT = 1$, whereas a value of 3 is required to construct the equivalent of a kitchen refrigerator that has no moving parts. Thermoelectrics are not, therefore, competitive in the refrigerator market but in the context of routine use, they have niche applications, for example as picnic coolers that can be powered in a car [3].

To practically select the *best* thermoelectric material from many available, especially beyond the idealised $ZT = 1$ scenario, several other material parameters and practical considerations are crucial.

Thermoelectric devices experience thermal cycling, so the material must be mechanically robust to withstand strain without fractures. Its ductility affects both processing and reliability. It should be stable in the operating environment, perhaps requiring oxidation and corrosion resistance. Ease of manufacture is vital in the particular form required (e.g., thin films or powders). It must also be compatible with electrodes, substrates and encapsulation materials with respect to thermal expansion, chemical reactivity and electrical contact resistance.

Example 29: Efficiency of a refrigerator

The efficiency of a refrigerator is determined by the ratio of the heat removed from the cold reservoir and the work input required to remove that heat, which leads to the definition of the coefficient of performance (COP) as [3]

$$\text{COP} = \frac{T_{\text{cold}}\zeta - T_{\text{hot}}}{\Delta T(\zeta + 1)} \quad (6.3)$$

$$\text{with } \zeta = \sqrt{1 + \mathcal{Z}\bar{T}}, \quad \Delta T = T_{\text{hot}} - T_{\text{cold}}, \quad \bar{T} = \frac{T_{\text{hot}} + T_{\text{cold}}}{2}$$

What is the temperature to which a single-junction thermoelectric with $\mathcal{Z}\bar{T} = 1$ cool down to if operating in an ambient environment ($T_{\text{hot}} = 300 \text{ K}$) and with $\text{COP} = 0.3$?

Imagine a scenario where $\mathcal{Z}\bar{T} \rightarrow \infty$. What would happen to COP?

Solution 29

As a first step, program Equation 6.3 into a spreadsheet or equivalent, and show that the numbers fit when $T_{\text{cold}} = 241.9 \text{ K}$. This is the ideal calculation. But there are practical factors that may increase this temperature, for example, contamination and condensation on the cold surface.

If $\mathcal{Z}\bar{T} \rightarrow \infty$, so does ζ , hence,

$$\text{COP}_{\text{refrigeration}} = \frac{T_{\text{cold}} \times \infty - T_{\text{hot}}}{\Delta T \times \infty} \equiv \frac{T_{\text{cold}}}{\Delta T} \equiv \frac{T_{\text{cold}}}{T_{\text{hot}} - T_{\text{cold}}}$$

so COP approaches the Carnot limit for a refrigerator. For example, if $\mathcal{Z}\bar{T} = 10^9$, $\text{COP} = 4.16$, a value that does not change with two significant figures after the decimal if $\mathcal{Z}\bar{T} = 10^{20}$. This demonstrates that as the thermoelectric figure of merit becomes arbitrarily large, the performance of the device approaches the ideal thermodynamic limit, where internal irreversibilities due to finite electrical and thermal conductivities become negligible.

Note that in contrast, the ratio of the heat delivered to a hot reservoir to the work input has the Carnot efficiency

$$\text{COP}_{\text{heat pump}} = \frac{T_{\text{hot}}}{T_{\text{hot}} - T_{\text{cold}}}.$$

6.2 CONFLICTING THERMOELECTRIC REQUIREMENTS

The figure of merit focuses minds on the optimisation of thermoelectric properties, but maximising $\mathcal{Z}T$ involves conflicting parameters. The materials should

contain only one kind of charge carrier because if both electrons and holes move towards the cold end, their respective Seebeck voltages cancel. Low carrier-concentration (n) insulators and semiconductors have large Seebeck coefficient because from theory, $S_e \propto n^{-2/3}$ [4], but compromise electrical conductivity (Equation 1.1b). Good thermoelectric semiconductors usually have a carrier concentration of $10^{19} \rightarrow 10^{21} \text{ cm}^{-3}$; the quantity $S_e \sigma$ maximises at larger carrier-concentrations though $Z\bar{T}$ does not because both σ and κ increase.

Thermal conductivity in this context comes from electrons/holes that transport heat and phonons (quantised vibrations of atoms in crystal). The electronic contribution to thermal conductivity is related directly to n , leading to the behaviour illustrated schematically in Figure 6.2.

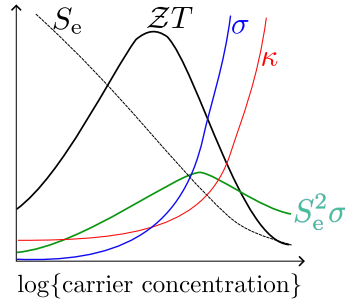


FIGURE 6.2 How the figure of merit goes through a maximum as a function of carrier concentration. Schematic adaptation from [4].

6.3 PELTIER EFFECT

The idea that a conductor is heated by the passage of an electrical current was known in the early 19th century, for example the investigations of Volta and Ampère, and later established by Joule; at a large enough current, the conductor may fuse or vaporise. The belief therefore, was that current *always* led to heat dissipation. Jean Charles Athanase Peltier, however, questioned this universality. He was aware of work by Davy and Becquerel that hinted at more complex thermal-electrical interactions. To investigate, he used minute currents to minimise Joule heating, which scales with $I^2 \mathcal{R}$ and a variety of materials, notably bismuth joined with copper electrodes. Unexpectedly, he observed that the current through the bismuth-copper junction did not flow in the direction he initially expected. He soon found that at the junctions between bismuth and copper, one junction would become hotter and the other colder than the centre of the bismuth bar. Crucially, this effect reversed when the direction of the current was reversed [5]. This was a direct contradiction to simple Joule heating, which is always dissipative regardless of current direction.

He had discovered what we now refer to as the *Peltier effect*, where a temperature difference is created at the junction of two dissimilar materials when an electric current flows through them, causing one side to heat up and the other to cool down. The amount of heat absorbed or released is directly proportional to the electric current, the proportionality constant being the Peltier coefficient.

Figure 6.3 illustrates the effect. When electrons move from a material where they have a higher average energy (higher Fermi level or conduction band energy) to a material where they have a lower average energy, they release the excess energy. This energy release manifests as heat at the junction. Conversely, when electrons move from a lower energy level to a higher energy level, they absorb energy from the surroundings, leading to cooling at the junction.¹ The same principle applies if the charge carriers are holes (positive charges), but the direction of energy change would be opposite for the same conventional current direction.

One application is in small-scale refrigeration where quiet operation, no moving parts, and precise temperature control are desired, Figure 6.3b.

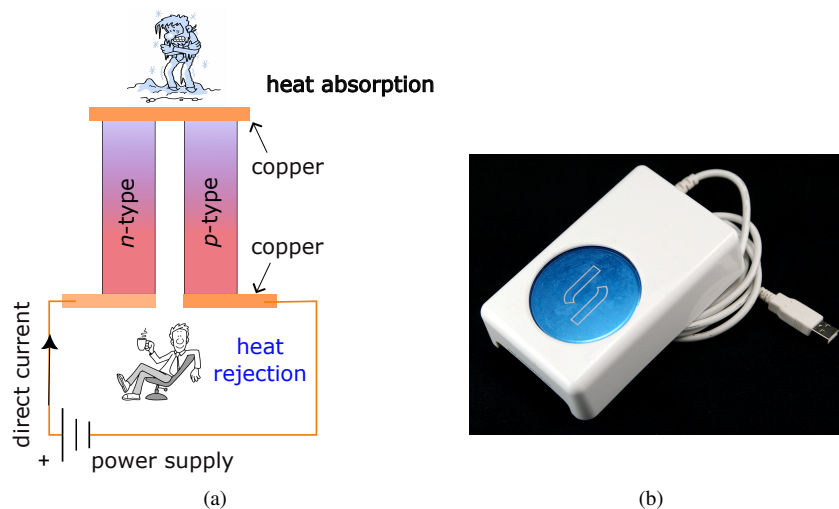


FIGURE 6.3 (a) Schematic illustration of a device based on the Peltier effect. (b) A beverage cooler. Although the thermoelectric used is not known, it is likely to be Bi_2Te_3 which works well around ambient temperatures. It may be alloyed with Sb_2Te_3 to further reduce its thermal conductivity. Reproduced courtesy of Hustvedt, under CC BY-SA 3.0, <https://commons.wikimedia.org/w/index.php?curid=11084988>

1. Analogy: Think of it like a waterfall. If electrons ‘fall’ from a higher energy level to a lower one, they release potential energy as kinetic energy or heat. If they are ‘pumped’ uphill to a higher energy level, they absorb energy from the surroundings.

6.4 PHONON-GLASS ELECTRON-CRYSTAL

The terminology used here is a little clumsy, though the meaning implies that the ideal thermoelectric material should act like a ‘phonon glass’ (poor thermal conductor) and an ‘electron crystal’ (good electrical conductor). Thermal conductivity is reduced if phonons, which are quantised vibrations that carry heat, are scattered effectively. Good electrical conductivity requires minimal scattering of charge carriers. This means having a relatively ordered crystalline structure for efficient charge transport. These two goals are often in conflict. Materials that are good at scattering phonons (e.g., disordered, amorphous materials) also tend to scatter electrons, reducing electrical conductivity. The aim therefore, is to find materials that decouple these properties.

Lead telluride (PbTe) is effective at scattering phonons due to strong anharmonic interactions between its atoms. Anharmonicity means that the restoring forces between atoms are not simply proportional to their displacement, leading to more complex and effective phonon scattering. This strong phonon scattering results in a very low thermal conductivity for PbTe, around $\kappa \approx 2 \text{ W m}^{-1} \text{ K}^{-1}$ [6]. To put this in perspective, it’s only about four times greater than polyethylene, a well-known thermal insulator. This low κ is crucial for maintaining a high temperature gradient and thus high efficiency. PbTe also exhibits good electronic conductivity, typically $300 \rightarrow 5000 \text{ S cm}^{-1}$, and a high Seebeck coefficient (typically $\pm 300 \mu\text{V K}^{-1}$), both of which are tuneable by controlling the carrier concentration (doping). The combination of low thermal conductivity and good electronic properties leads to a high $ZT = 1.4$ [7], larger than previously following a reassessment of transport properties [4].

Thermoelectric generators made from materials like PbTe are ideal for recovering waste heat, such as that generated by automobile exhaust systems. While these systems have been successfully demonstrated in real cars, their widespread implementation has not yet occurred, but barriers may include high material costs, long-term stability, and the toxicity of lead.

Other thermoelectric tellurides which are not considered to be phonon glasses because of less pronounced anharmonicity, include Bi_2Te_3 , Sb_2Te_3 , GeTe , $(\text{Sb}_{0.8}\text{Bi}_{0.2})_2\text{Te}_3$ and SnTe . All of these exhibit reasonable $ZT \approx 1$ over particular temperature ranges. Bi_2Te_3 is appropriate for ambient temperature applications whereas PbTe works well at higher temperatures.

REFERENCES

1. W. Fulkerson, J. Moore, R. Williams, R. Graves, and D. McElroy: 'Thermal conductivity, electrical resistivity, and seebeck coefficient of silicon from 100 to 1300 k', *Physical Review*, 1968, **167**, 765–782.
2. C. B. Vining, W. Laskow, J. O. Hanson, R. R. Van der Beck, and P. D. Gorsuch: 'Thermoelectric properties of pressure-sintered $\text{Si}_{0.8}\text{Ge}_{0.2}$ thermoelectric alloys', *Journal of Applied Physics*, 1991, **69**, 4333–4340.
3. G. Mahan: 'Good thermoelectrics', *Solid State Physics*, 1998, **51**, 81–157.
4. G. J. Snyder, and E. S. Toberer: 'Complex thermoelectric materials', *Nature materials*, 2008, **7**, 105–114.
5. J. C. A. Peltier: 'Nouvelles expériences sur la calorité des courans électriques (new experiments on the heat effects of electric currents)', *Annales de chimie et de physique*, 1834, **56**, 371–386.
6. D. Guo, H. Zhang, Z. Xu, C. Li, K. Li, B. Shao, D. Chen, Y. Ma, and J. Sun: 'The room-temperature thermoelectric property of PbTe enhanced by mean-free-path filtering', *Journal of Alloys and Compounds*, 2022, **893**, 162296.
7. A. D. LaLonde, Y. Pei, and G. J. Snyder: 'Reevaluation of $\text{PbTe}_{1-x}\text{I}_x$ as high performance *n*-type thermoelectric material', *Energy & Environmental Science*, 2011, **4**, 2090–2096.

Chapter 7

Optical and magnetic materials

7.1 OPTICAL MATERIALS

Electromagnetic radiation (Figure 7.1) travels through a vacuum at a speed

$$c = 299,792,458 \text{ m s}^{-1} = [\epsilon_o \mu_o]^{-\frac{1}{2}}, \quad (7.1)$$

where μ_o is the magnetic permeability of free space. The radiation is characterised by oscillating electric and magnetic fields that are mutually perpendicular, and to the travel direction of the wave. When electromagnetic radiation enters a material, it interacts with charge carriers within the material, leading to a change in its velocity; the polarisation mechanisms have been discussed in Chapter 2. The speed of light in a material is given by

$$v = [\epsilon_o \epsilon_r \mu_o \mu_r]^{-\frac{1}{2}} \quad (7.2)$$

where μ_r is the relative magnetic permeability and $\epsilon_o \epsilon_r$ is the permittivity of the material concerned. The sum of transmitted, refracted, absorbed, and reflected intensities of light equals the original intensity of the incident light.

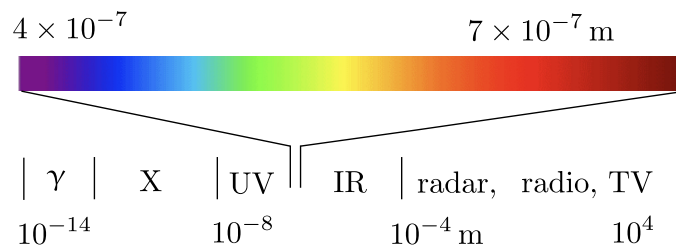


FIGURE 7.1 The electromagnetic spectrum is a continuous range of all known electromagnetic radiations, ordered by their frequency or wavelength. A part of the electromagnetic spectrum is indicated here with wavelengths marked. Radio waves have the longest wavelengths, used in broadcasting, wireless communication and radar. Gamma rays (γ) have the shortest wavelengths and highest energies, produced in nuclear reactions and by radioactive decay. They are highly ionising and used in medical treatments (e.g., radiotherapy for cancer) and sterilisation. X-rays (X) were so called by Conrad Röntgen because of they were a mystery at the time of their discovery. Ultraviolet (UV) radiation causes sunburn and infrared represents thermal radiation, used for example in night vision devices.

Example 30: Opacity

A semiconductor has its band gap $E_g = 1.1$ eV. Show that the material is opaque to visible light.

Solution 30

To understand why a semiconductor with the stated band gap is opaque to visible light, it is necessary to compare the energy of visible light photons with the semiconductor's band gap energy.

Visible light spans a wavelength range from approximately $0.4\ \mu\text{m}$ (blue/violet) to $0.7\ \mu\text{m}$ (red). the energy ΔE of photons corresponding to these wavelengths can be calculated using the following equation:

$$\Delta E = h\nu \equiv \frac{hc}{\lambda}$$

where h is Planck's constant, ν is the frequency and λ is the wavelength. The range of ΔE corresponding to the wavelength range of visible light, is therefore $1.8 \rightarrow 3.1$ eV. This is sufficient to excite electronic transitions in the semiconductor which has $E_g = 1.1$ eV, making it opaque.

If the band gap were larger than the highest energy photon in the visible spectrum (i.e., $E_g > 3.1$ eV), then visible light photons would not have enough energy to excite electrons across the band gap, and the material would be transparent to visible light. However, even in such transparent materials, defects, impurities, interfaces, or porosity can lead to selective absorption of certain wavelengths, causing the material to appear coloured.

In conclusion, because all photons in the visible light spectrum possess energy greater than the semiconductor's band gap, they are absorbed by the material to promote electrons to the conduction band. This absorption process prevents the light from passing through, making the semiconductor opaque to visible light.

7.2 METALS

Metals have partially filled electron bands (Figure 1.4) so there always are available unoccupied energy levels close to the occupied ones. Incident photons of light (across a wide spectrum including visible, IR, and UV) can easily excite electrons from occupied states to these immediately available unoccupied states within the same band. This absorption of photons occurs readily.

The absorption of light in metals is efficient and rapid. The intensity of incident light decreases to $1/e$ of its original value within a depth of only a few tens of

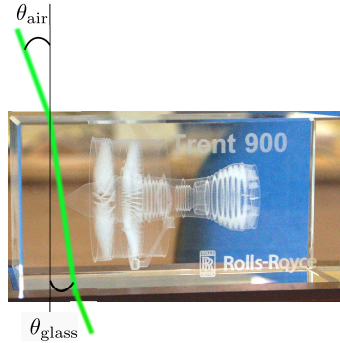
nanometers. This strong absorption contributes significantly to their opacity. While most metals appear silvery-grey, gold and copper are notable exceptions with distinct colours. This coloration arises because their d -electrons can absorb specific wavelengths of visible light: gold absorbs blue and violet light so the reflected light has the complementary colours yellow/gold. Copper absorbs blue and green, leaving the reflected light reddish-orange.

Metals possess a high density of free electrons. These free electrons are mobile and efficiently re-emit the absorbed energy of incident photons as reflected light. This strong re-emission is the reason why metals can function as mirrors.

Visible light photons are perfectly matched for electronic excitations within the bands, leading to opacity and reflection. X-rays and γ -rays, with their much higher energies, bypass these lower-energy electronic transitions and interact via more energetic processes, allowing for deeper penetration. When these high-energy radiations do interact with metals, the absorption occurs through scattering by free electrons, by a photoelectric effect in which an electron is ejected from the atom, and by interacting with atomic nuclei to create matter-antimatter pairs (electron-positron pairs).

7.3 DIELECTRICS

Silica glass is a dielectric, an electrical insulator. It is able to reflect light, the amount depending on the relative refractive indices of glass and air. When a plane wave is incident at an angle θ_{air} to the interface between the air and glass, it will adopt a different angle θ_{glass} during its travel through the glass,



$$\underbrace{n_{\text{air}} \sin \theta_{\text{air}} = n_{\text{glass}} \sin \theta_{\text{glass}}}_{\text{Snell's law}} \quad (7.3)$$

where n here represents the refractive index of the medium identified by the subscript, representing the ratio of the speed of light in a vacuum to that in the medium ($n = c/v$).¹ The fraction of light that is reflected when $\theta_{\text{air}} = 0$, is $[(n_{\text{air}} - n_{\text{glass}})/(n_{\text{air}} + n_{\text{glass}})]^2$ [p.429, 2], which with $n_{\text{air}} \approx 1$ and $n_{\text{glass}} \approx 1.5$, only 4% of the light would be reflected, the rest being transmitted.

1. After Willebrord Snellius (1580-1626), a Dutch mathematician, published posthumously [1].

Using Equations 7.1, 7.2 and the definition of the refractive index (c/v) when the permittivity is from electron polarisation, is given by

$$n = \frac{c}{v} = \frac{(\epsilon_0 \epsilon_r \mu_0 \mu_r)^{\frac{1}{2}}}{(\epsilon_0 \mu_0)^{\frac{1}{2}}} = (\epsilon_r \mu_r)^{\frac{1}{2}} \quad \text{so if } \mu_r \approx 1, \quad \text{then } n = \sqrt{\epsilon_r} \quad (7.4)$$

giving a direct relationship between the refractive index and relative permittivity of the dielectric; for such materials, it often is reasonable to assume that the relative magnetic permittivity of a dielectric is almost unity.

This relationship highlights that the optical properties (refractive index) of a non-magnetic dielectric material are linked directly to its electrical properties (relative permittivity), a crucial concept in understanding the interaction of light with materials in fields like optics, materials science, and electrical engineering.

Translucency is the property of a material that allows light to pass through it but scatters some of that light. This scattering prevents a clear, distinct image of an object from being seen through the material. The translucency of a smooth-surfaced dielectric depends on its structure-dependent scattering and absorption. Yttria containing zirconia (p. 2) has applications as dental prostheses, where colour and translucency are controlled for aesthetic reasons. The grain size of the zirconia is the controlling factor in determining its translucency, because boundaries scatter visible light, so smaller grain sizes enhance translucency [3]. But the size should not be smaller than the wavelength of the light because scattering is then limited. A completely transparent prosthetic might be unpleasant to look at because it would not appear like a natural tooth.

Example 31: Absorption as a function of thickness

A sapphire plate of thickness z_t has a beam of light incident along the normal to its largest surface, with intensity I_o . Assuming that none of the light is reflected, derive an equation relating the transmitted intensity to the thickness.

Solution 31

The decrease in light intensity (dI) as it travels through a small element of thickness (dz) within the material is proportional to the current intensity (I) and the thickness element itself. This relationship is expressed as:

$$dI = -b_1 I dz \quad (7.5a)$$

where b_1 is an empirical ‘absorption coefficient’, the magnitude of which depends on how strongly the material absorbs light. This coefficient is a function of the

wavelength of the light, but typically has a value $4.7 \times 10^{-3} \text{ mm}^{-1}$ for $\lambda = 400 \text{ nm}$ at ambient temperature [4]. The negative sign indicates that the intensity is decreasing. To find the total transmitted intensity through the entire thickness z_t , it is necessary to integrate this differential equation from its initial value I_o at $z = 0$ to its final transmitted value I at $z = z_t$:

$$\int_{I=I_o}^I \frac{dI}{I} = \int_{z=0}^{z_t} -b_1 dz \quad \text{so that} \quad I = I_o \exp\{-b_1 z_t\}. \quad (7.5b)$$

Other factors that influence the absorption coefficient for visible light include:

1. Chemical composition, because the electronic structure determines how the material interacts with light. For example, organic dyes have large absorption coefficients for particular wavelengths, making them coloured. It is the molecular structure and concentration of the dye, and the solvent in which it is dissolved that influence the absorption process. For example, the absorption coefficient of strawberry dye dissolve in ethanol can be $\approx 2 \text{ km}^{-1}$ for $\lambda = 400 \text{ nm}$ [5].
2. The temperature influences the absorption coefficient via the vibrational and electronic states of the material.
3. Whether a material is crystalline, amorphous, solid, liquid or gas influences b_1 because the scattering centres will naturally differ. Pure, amorphous polymers such as polymethyl methacrylate and polycarbonate are essentially transparent because of the absence of interfaces, but any additives can reduce transparency by invoking absorption mechanisms.
4. Impurities, the size and shape of inclusions and features of the microstructure have an effect of absorption.
5. The refractive index of the material has a role, for example when voids in ceramics are of a size greater than the wavelength of light. If n is anisotropic, then a polycrystalline ceramic can appear translucent when both reflection and refraction occur at grain boundaries because of the difference in n associated with the change in crystallographic orientation across the boundary.
6. Polymers are often a mixture of crystalline and amorphous arrangements of long molecules, in which case there will exist differences in n at interfaces between these phases.

7.4 LINEAR OPTICS

Electromagnetic waves such as light consist of oscillating electric and magnetic fields. In linear optics, the response of the material to the electric field is linear (Equation 2.1a) with the electric displacement $\mathcal{D} = \epsilon_o \epsilon_r E$; in the present context, the relative permittivity ϵ_r is that at the appropriate optical wavelength. Such a linear material would have a constant refractive index (Equation 7.4) for a given

λ , making it more predictable in assessing the propagation of light through the material. Polymethyl methacrylate and alumina are examples of linear optical materials.

Objects absorb heat from sunlight during the day time, and lose heat by radiating infrared waves ($\lambda = 8 \rightarrow 15 \mu\text{m}$) into the much colder space above. This is why humans feel hot on a cloudless sunny day when the heat absorbed is greater than that radiated, but cold at night when radiation wins the heat balance.

A coating of a material which might help cool a building or vehicle during the day time should therefore have a high ability to reflect sunlight ($\lambda = 0.3 \rightarrow 2.5 \mu\text{m}$) with the capability to radiate heat away in the long wavelength infrared range. This latter characteristic is described in terms of an emissivity which is 1 for a perfect black body. Un-poled and unstressed polyvinylidene fluoride (Figure 5.5) exhibits linear optics, does not degrade in ultraviolet light due to its strong C-F bonds, and as a co-polymer with polytetrafluoroethylene reflects at least 96% of sunlight at a thickness of $300 \mu\text{m}$ and its emissivity is 0.97 [6]; cooling of $3 \rightarrow 6^\circ\text{C}$ below ambient has been achieved using this composite, the lower value corresponding to conditions where the atmosphere is humid.

7.5 ANISOTROPY OF REFRACTIVE INDEX

Some crystals exhibit different optical properties depending on the direction of light. One way to visualise this is to construct a three dimensional ellipsoid, the axes of which are parallel to the basis vectors of the unit cell. The lengths of its semi-axes correspond to the principal refractive indices (Figure 7.2a).

When incident light enters an anisotropic material, its electric field vector interacts differently with the atomic structure depending on its orientation relative to the crystal axes. This results in the light being resolved into two mutually perpendicular polarisation components, which experience different refractive indices and therefore travel at different speed through the material. This is illustrated in Figure 7.2b, which show the two components with refraction indices n_o and n_e , where conventionally, the subscripts stand for ordinary and extraordinary rays, respectively. Crystals where the beam splits into two orthogonally polarised rays in this manner are said to exhibit *birefringence*, Figure 7.2c.

Crystals with cubic lattices are optically isotropic with just one refractive index, irrespective of the direction of the incident beam. Those with a single 3, 4 or 6-fold axis of symmetry have one circular section on the ellipsoid that is parallel to the equatorial x - y plane because $n_x = n_y \neq n_z$. The normal along z is known as the optic axis; light parallel to that would not split (no birefringence), as if the crystal is isotropic. Since there is one optic axis, the single 3, 4, 6 rotation symmetries are said to be uniaxial. But monoclinic and triclinic crystals would have all three principal refractive indices different, so there would be two circular sections of the ellipsoid, two optic axes normal to those sections, and

are therefore said to be biaxial.

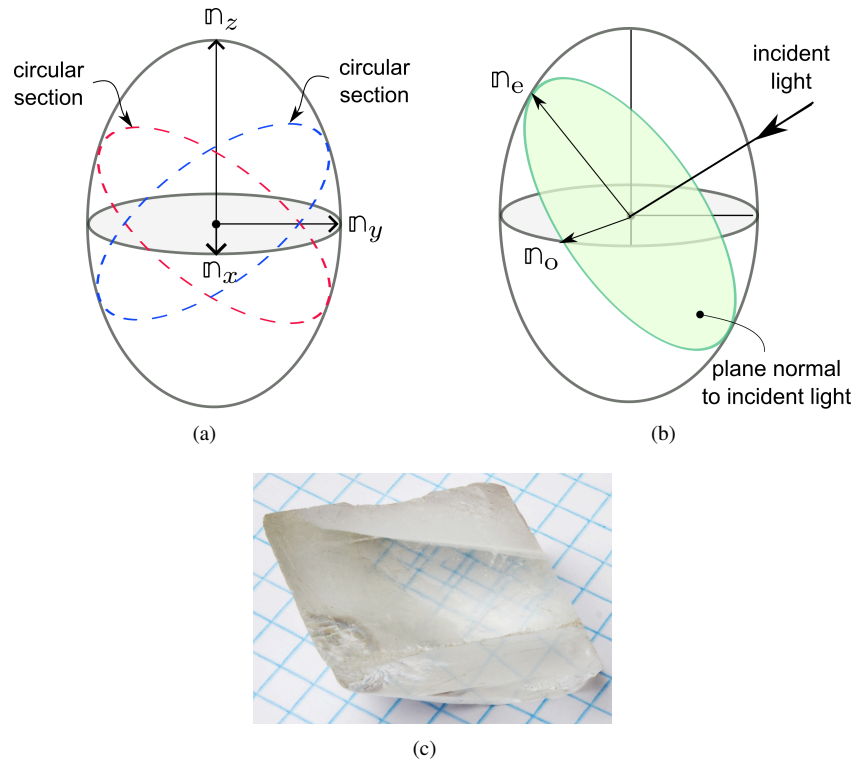


FIGURE 7.2 (a) A three-dimensional general ellipsoid representing a crystalline material with three different refractive indices along the basis vectors of the unit cell, which are parallel to the coordinate frame x , y , z . With such an ellipse, it is possible to find two circular cross-sections. The two circles would merge into one if $n_x = n_y$ and the ellipsoid would have rotational symmetry about the z -axis. (b) A beam of light from an arbitrary direction, would split into an ordinary and extraordinary ray. (c) A calcite crystal (trigonal crystal class) showing how the square pattern splits into two images. Reproduced under the CC-BY-SA 3.0 licence <https://en.wikipedia.org/wiki/>, from work by 'APN MJM'.

Some screens use liquid crystals, which are birefringent materials whose molecular orientation can be controlled by electric fields. This allows the manipulation of light transmission and the creation of images [p.96, 7]. Birefringent films are incorporated into security holograms, such as those in banknotes. Hidden patterns become visible when viewed using polarised light.

7.6 NON-LINEAR OPTICS

A dielectric material has charged particles that are firmly bound so alternating electric field such as that associated with a light wave, induces transient os-

cillatory motions with corresponding polarisation. The linear dependence of displacement \mathcal{D} on E implicit in Equation 2.1a, is an approximation that is valid for ‘small’ fields. The polarisation response of the material need not be linear with field when the displacement is large.² This is expressed by representing the displacement \mathcal{D} as a polynomial with higher order terms:

$$\mathcal{D} = \epsilon_o \epsilon_r E + \underbrace{b_2 E^2}_{\text{second order}} \dots \quad (7.6a)$$

where b_2 is the second-order non-linear susceptibility of the material. As a consequence, the permittivity (and hence its refractive index n) ceases to be constant

$$\Delta n = \frac{d\mathcal{D}}{dE} = \epsilon_o \epsilon_r + \underbrace{2b_2 E}_{\text{Pockels effect}} + \dots \quad (7.6b)$$

The dielectric lithium niobate (p. 40) has a linear electro-optic response so its refractive index is directly proportional to the applied electric field. Friedrich Pockels [10, 11] discovered this effect in non-centrosymmetric crystals, a phenomenon important in understanding how electrical fields influence the propagation of light. The effect describes how \mathcal{D} of the material responds quadratically to the electric field, while the refractive index change is linear with the applied DC electric field. Its origin is a nonlinear response of the material’s electrons to the total electric field which including that of light.

In 1875, the Reverend John Kerr who started off in theology but diverted into mathematics [12], discovered that any material including liquids and centrosymmetric dielectrics, exhibits weak birefringence the strength of which is proportional to the square of the electric field [13–15]. The origin of the effect is the electric field of light interacting with the polar molecules or electron-clouds of non-polar atoms in the material. If Equation 7.6a is expanded with an additional third order term,

$$\mathcal{D} = \epsilon_o \epsilon_r E + b_2 E^2 + \underbrace{b_3 E^3}_{\text{third order}} \dots \quad (7.6c)$$

where b_3 is known as the Kerr constant. It follows that

$$\Delta n = \frac{d\mathcal{D}}{dE} = \epsilon_o \epsilon_r + 2b_2 E + \underbrace{3b_3 E^2}_{\text{Kerr effect}} \dots \quad (7.6d)$$

2. Similarly, Hooke’s law (stress \propto strain) fails at very large stresses where the elastic response becomes non-linear before the onset of plasticity [8, 9].

Example 32: Convergent lens

Explain how an ordinary convergent lens made of glass works. Hence explain how the Kerr effect can be used to focus a laser beam that has a Gaussian distribution of intensity about its centre.

Solution 32

Glass has a bigger refractive index than air. From Equation 7.3 and referring to Figure 7.3, the light when it enters the lens bends towards the normal to the surface at its entry point. When it exits, it bends away from the normal. This leads to a focusing action.

The Kerr lens relies on the fact that the refractive index is bigger when the intensity of light is greater. With a Gaussian distribution, the intensity will be greater at the central cross-section of the beam. Light at the centre therefore moves slower than at the peripheries. So the wavefronts of light become more convexly curved; the wavefront in a material with uniform n would be flat. The curvature steers light rays towards the centre of the beam, which is the basis of the Kerr lens. This is a self-induced lens, there is no physical lens.

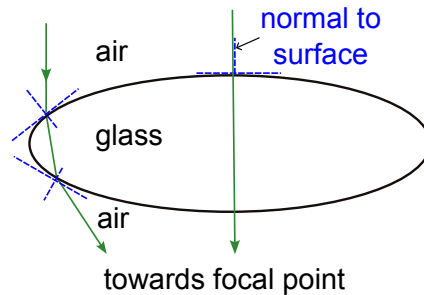


FIGURE 7.3 The ray paths across a convex lens.

Example 33: Optical switch

How would you design an electro-optic switch based on the Pockles effect? A switch such as this would only permit the passage of light through the device when an electrical field is applied. It can be used, for example, for controlling short-duration laser pulses used in the precise machining of materials and laser surgery.

Solution 33

The Pockels effect describes a phenomenon where the refractive index of certain transparent, non-centrosymmetric crystals changes in direct proportion to an applied electric field. The induced change in refractive index is anisotropic, meaning it varies with direction. This anisotropy makes the crystal birefringent (having two different refractive indices for different polarisations of light) when an electric field is applied. In essence, the effect allows an electric field to control the polarisation state of light passing through a crystal, which can then be used in conjunction with polarisers to create an optical switch.

In Figure 7.4a, incident light passes through a polariser, which only allows the vertically polarised light to continue on to the crystal. The crystal is transparent but has a uniform refractive index so the plane of polarisation of the light is unchanged. It then reaches the crossed polariser (90° to the input polariser), which does not allow the passage of vertically polarised light. This is the ‘off’ state of the switch.

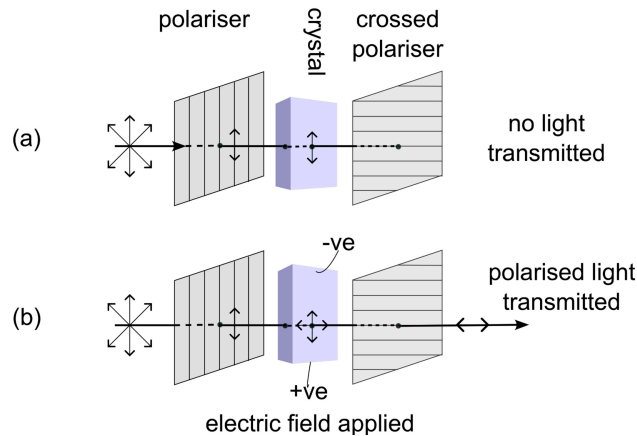


FIGURE 7.4 An illustration of the operation of an electro-optic switch. There are crossed polars at either end with an electro-optic crystal in the middle, oriented such that the light is not parallel to an optic axis when the crystal becomes birefringent under the application of an electric field. The double-headed arrows indicate the polarisation directions.

When an electric field is applied to the crystal, Figure 7.4b, the light that enters the crystal splits into an ordinary and extraordinary beam, with mutually perpendicular planes of polarisation. The ordinary beam will be vertically polarised, unchanged after its emergence from the polariser. On leaving the crystal, the horizontally polarised extraordinary beam can pass through the crossed polariser. This is the ‘on’ position of the switch.

Note that the crystal must be oriented such that the incident light is not par-

allel to an optic axis. Suitable crystals include lithium niobate, potassium dihydrogen phosphate, because these have high electro-optic coefficients ($2b_2$ in Equation 7.6a) and are transparent to the desired optical wavelength. The electro-optic coefficient for lithium niobate is about $30 \rightarrow 32 \text{ pm V}^{-1}$ and that for potassium dihydrogen phosphate, $\approx 10.5 \text{ pm V}^{-1}$.

One effect has not been considered here, is that as the ordinary and extraordinary rays travel through the crystal at different speeds, a phase difference accumulates between them. When the two orthogonally polarised components emerge from the crystal, they recombine. The resulting polarisation state depends on the initial polarisation state and, critically, on this accumulated phase difference. If the phase difference is exactly half a wavelength, when the two orthogonal components emerge from the birefringent crystal, their resultant electric field vector will oscillate in a plane that is rotated by 90° relative to the original incident polarisation. For example, if the input was vertically polarised and the crystal's axes were at $\pm 45^\circ$, the output will be horizontally polarised.

7.7 TYPES OF MAGNETISM

The vast majority of a material's magnetic properties originate from its electrons, though there are much weaker magnetic moments associated with atomic nuclei. The origin of the properties described here is in the magnetic moments associated with electrons, primarily those associated with the spin of the unpaired electrons in atomic orbitals. The electron can be imagined to be a charge rotating about an axis; a current loop such as this generates a magnetic field and thus has an associated orbital magnetic moment.³ The alignment of the spins of electrons on the arrays of atoms in a material can sometimes lead to a reduction in energy, the so-called exchange interaction, with consequent changes in the macroscopic magnetic properties. When the spins are all identically oriented, the material is said to be ferromagnetic. When neighbouring spins of equivalent magnitude point in opposite directions, the material is said to be antiferromagnetic.

Magnetic ordering has a profound influence on phase stability; for example, iron would not exist in the crystal structure that is most widely used, were it not for ferromagnetism.

The spin of an electron is characterised by a spin quantum number s , which has values of $\pm \frac{1}{2}$. The unit magnetic moment is the Bohr magneton, $\mu_B = e\hbar/2m_e$, where \hbar is the reduced Planck constant and m_e is the rest-mass of an electron. Because the spin can be in one of two senses, the magnetic dipole of the electron

3. This picture is convenient but inaccurate because in a classical calculation, the velocity at which the electron would have to spin to produce the observed magnetic moment would be greater than that of light. The term 'spin' really refers to a quantised rotation that has no counterpart in classical mechanics.

either supports, or opposes an applied magnetic field. A magnetic field of strength H_{mag} (amperes per metre) may lead to an induced magnetic dipole moment per unit volume, M . The magnetic susceptibility of the material is then given by M/H_{mag} . The susceptibility is negative if the induced moment opposes the applied field.

A free electron will tend to align itself to the applied magnetic field, but in metals the vast majority of electrons are in states where the opposite spin state is already occupied. The Pauli exclusion principle permits only two electrons with opposite spins, per state. If all the electrons are spin-paired in this way, then the atom has no net magnetic moment and the material can only be *diamagnetic*.

7.7.1 Diamagnetism

Diamagnetism is a weak, temperature-independent negative susceptibility which causes the material to be repelled by a magnetic field. Any substance can be diamagnetic. As discovered by Landau, an electron gas⁴ such as that associated with metallic bonding, will exhibit diamagnetism in a magnetic field, the electrons move within the metal in spirals, but in a quantised manner, about the field direction. This induced current results in a magnetic moment which, according to Lenz's law, opposes the applied field. Lenz's law states that when the flux through an electrical circuit is changed, an induced current is set up in a direction that opposes the change in flux. The real scenario may be more complex in a metal because the electron gas moves under the influence of the periodic potential associated with the ion cores within the crystal structure.

Lithium-ion batteries typically utilise a lithium phosphate anode and a graphite cathode. During discharge, lithium ions move towards the graphite cathode, where they intercalate between the basal planes of the graphite flakes rather than depositing as lithium metal. This intercalation process, where ions enter the graphite through its edges, is a safe operational mechanism. To enhance the speed of this intercalation and improve charge/discharge performance, efforts are made to optimise the alignment of graphite flakes. One promising technique involves orienting the basal planes of the graphite flakes perpendicular to the copper current collector [16]. This alignment allows lithium ions to enter the graphite more directly, avoiding a tortuous path.

A method to achieve this desired alignment is to apply a magnetic field while a suspension of graphite is drying on the copper substrate. Graphite exhibits strong anisotropic diamagnetism, meaning its magnetic susceptibility varies significantly with direction. This property causes the graphite flakes to rotate and align optimally in response to the magnetic field, leading to improved lithium ion transport and, consequently, better battery performance.

4. An *electron gas* refers to delocalised electrons within the substance, not bound by individual atoms but free to move throughout the structure.

Example 34: Graphite & magnetic field

Does graphite react to an externally applied magnetic field? How could this be exploited in the design of lithium-ion batteries?

Solution 34

Graphite reacts to an applied magnetic field primarily because it is a diamagnetic material, and specifically, it exhibits unusually strong diamagnetism compared to most other common diamagnetic substances. The diamagnetic response of graphite is highly anisotropic. It's much stronger when the magnetic field is perpendicular to the layers than when it's parallel to them. This is because the delocalised electrons are largely confined within their layers.

Lithium-ion batteries: in conventional graphite anodes, the graphite flakes are often randomly oriented. Lithium ions primarily intercalate (insert) and de-intercalate (extract) along the edges of the graphene layers (the 'a-b' plane); transport normal to the basal plane of graphite (along the 'c' axis) is much slower. Random orientation leads to tortuous and inefficient pathways for lithium ion diffusion, especially during fast charging/discharging.

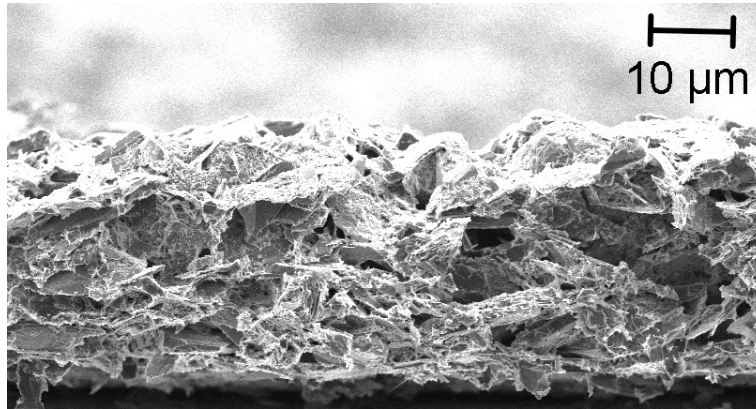
By applying a static magnetic field during the slurry casting or drying process of graphite electrode manufacture, it becomes possible to align the graphite flakes [16]. The goal would be to orient the basal planes of the graphite particles (where lithium ion transport is fastest) predominantly perpendicular to the current collector and parallel to the main direction of lithium ion flow during charge/discharge.

Figure 7.5a shows experiments in which a flake graphite slurry layer on a copper substrate was first dried in the absence of an imposed magnetic field, illustrating graphite flakes randomly oriented. Lithium ions would have to navigate their way into the edges of these flakes in order to intercalate; such a path would be tortuous and inefficient. This limits the kinetics (speed) of the battery's charge/discharge cycles.

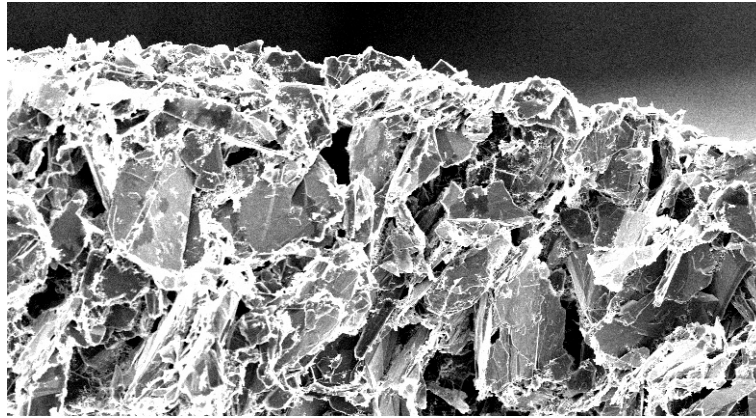
When dried under the influence of a 3 Tesla magnetic field, the flakes tend to align with their basal planes normal to the surface of the electrode, thus providing an easy pathway for the lithium ions to engage between the (0001) planes of the graphite. Detailed electrochemical experiments demonstrated an improvement in the charge/discharge rates.

Due to graphite's strong anisotropic diamagnetism, the flakes will tend to align themselves in a way that minimises their potential energy in the magnetic field. Specifically, the flakes will orient their basal planes (the flat, wide surfaces of the graphene layers) to be normal (perpendicular) to the applied magnetic field direction. This is the mechanism of alignment.

In essence, by leveraging the diamagnetic anisotropy of graphite, engineers can fabricate battery anodes with highly ordered graphite structures, thereby dramatically improving the efficiency of lithium ion transport and enabling faster and more effective battery operation.



(a)



(b)

FIGURE 7.5 Experiment in which flake graphite slurry was allowed to dry on a copper substrate. (a) No magnetic field applied during the drying process. (b) Drying under the influence of a 3 T magnetic field. Images courtesy of Nihal Abu, Shahad Alfadhli and Salvatore Grasso of Queen Mary University of London.

7.7.2 Paramagnetism

The cause of paramagnetism is the presence of unpaired electrons in the atoms, ions, or molecules of the material. Each unpaired electron has a permanent magnetic dipole moment (primarily due to its spin). Unlike diamagnetism, paramagnetism involves a magnetic moment that is proportional to the applied magnetic field. In a paramagnetic material, the spins associated with each atom are aligned at random except when the distribution is biased by an applied magnetic field. The effect is to cause the energies of those electrons more parallel to the applied field to decrease relative to those that oppose the field (Figure 7.6). To achieve a uniform Fermi potential, some of the electrons transfer from states with spins anti-parallel to the applied field, to those where the spin is parallel. This leaves a net imbalance in the spins. The resultant magnetisation depends on the excess number of spins. The effect is much smaller than if all electrons were able to change their spins to lie parallel with the field, but this is not permitted by the Pauli exclusion principle. Paramagnetism is therefore a weak effect which reinforces the applied field.

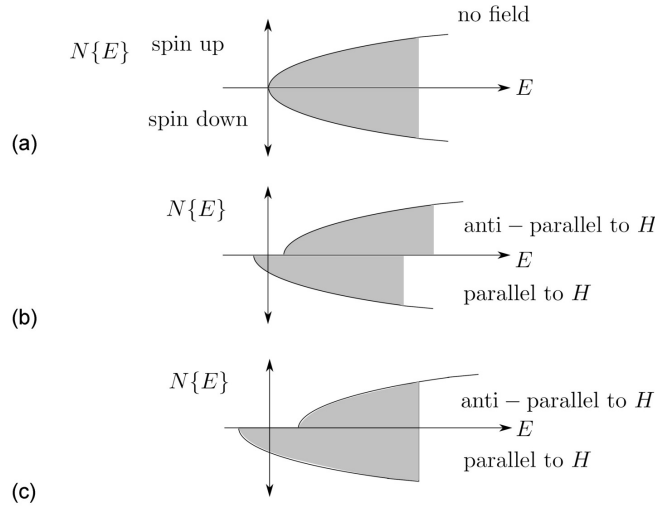


FIGURE 7.6 Mechanism of paramagnetism in a material with atoms containing unpaired electrons [17]. H is the magnetic field and $N\{E\}$ the number of electrons with energy E . (a) Density of states, with opposite spins separated for the purposes of illustration. The spin orientations illustrated are relative to an arbitrary direction. (b) Decrease in energy of those electrons with spins parallel with the applied field, and vice-versa. (c) The final energy distribution with uniform Fermi potential, leading to an imbalance in the pairing of electrons with opposite spins. After Wilkes [p.98, 17].

7.7.3 Ferromagnetism, antiferromagnetism and ferrimagnetism

Materials which are ferromagnetic, antiferromagnetic or ferrimagnetic can possess a magnetic dipole moment in the absence of any externally applied field. This is because their atoms contain electrons which are not spin-paired, making them *magnetic ions*. When these are arranged on a crystal lattice, then at low temperatures where the entropy is sufficiently small, the magnetic ions ‘order’ spontaneously (Figure 7.7).

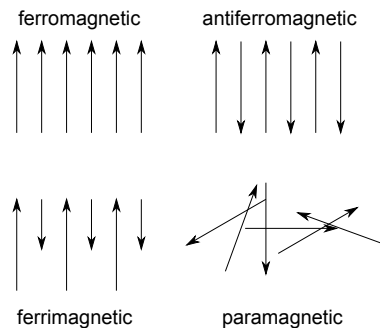


FIGURE 7.7 Variety of dipole alignments in materials containing atoms with un-spin-paired electrons.

Ferromagnetism occurs when the dipoles from the individual atoms align parallel. If neighbouring dipoles are antiparallel then there is a zero net magnetic moment resulting in an antiferromagnetic state. In a body-centred cubic antiferromagnetic crystal, the dipoles are parallel on each of the primitive cubic sub-lattices, but those on one sub-lattice are exactly anti-parallel to those on the other, resulting in a net zero magnetic moment.

The long-range ordering of magnetic ions is destroyed by thermal agitation once the Curie temperature (T_C) is exceeded in a ferromagnet. The corresponding order-disorder temperature for ferrimagnetic and antiferromagnetic materials is designated the Néel temperature. The disordered state is paramagnetic.

7.8 MAGNETIC DOMAINS

Below T_C , a ferromagnetic material spontaneously magnetises. However, it doesn't form a single, giant magnet. Instead, it breaks up into small regions called magnetic domains (*cf.* Section 3.2), Figure 7.8a. Within each domain, all the atomic magnetic moments are indeed aligned in the same direction, resulting in a strong spontaneous magnetisation for that specific domain.

The reason why the macroscopic sample splits into domains in order to minimise its own magnetic field that permeates out of the boundaries of the sample. This external magnetic field stores a significant amount of energy. To reduce this, the material divides itself into domains. This is why ordinary iron that is ferromagnetic, does not attract another piece of similar iron, because the external fields are essentially cancelled by domain formation. In this way, the external

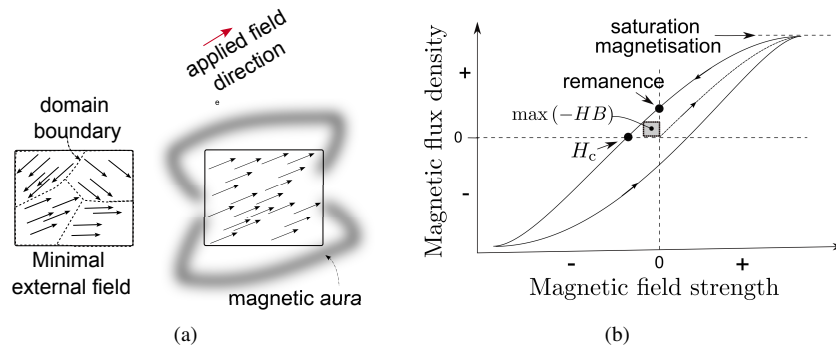


FIGURE 7.8 (a) How domain formation in a ferromagnet minimises external magnetic fields. (b) A magnetic hysteresis loop. The units of flux density B are $\text{J A}^{-1} \text{m}^{-2}$, and that of the field strength H , A m^{-1} . Notice that the product of these two terms is the energy per unit volume. The product $-HB$ is the largest rectangle that can be drawn in the second quadrant of the plot, often taken to represent how difficult it is to demagnetise the sample.

field lines can close within the material itself.

The domain boundaries represent regions where the direction of the magnetic moment changes gradually; they are mobile and so can adjust to grow or shrink if an external magnetic field is applied. When an external field is applied to an unmagnetised ferromagnetic material, the domain walls move such that those which comply best with the field grow at the expense of those that do not. The hysteresis loop in Figure 7.8b graphically depicts the non-linear and irreversible relationship between the applied field (H) and magnetisation, which increases as domains grow and even rotate until they are fully aligned and saturation magnetisation is achieved.

When the field is reduced from saturation, the magnetisation does not follow the same path back. Instead, it ‘lags’ behind the field a behaviour designated *hysteresis*. The material retains some magnetisation even when the field reaches zero; this is referred to as the *remanent* magnetisation, or remanence. The field has to be reversed to H_c (the coercivity) in order to demagnetise the material.

Every time a ferromagnetic material undergoes a full cycle of magnetisation and demagnetisation, energy is dissipated. This energy loss, primarily as heat, is due to the irreversible processes involved in domain wall movement (e.g., overcoming pinning sites like defects, impurities, or grain boundaries) and domain rotation. This is often referred to as hysteresis loss. Notice that the area in the plot has units of J m^{-3} .

The coercivity should be large in the manufacture of permanent magnets. Permanent magnets are designed to retain their magnetisation once they’ve been magnetised. A large H_c means that a strong reverse field is required to de-

magnetise them, making them robust against external fields. Such materials are referred to as hard magnetic materials. Steel, Cu-Ni-Fe, Al-Ni-Co, hexagonal BaO-(Fe₂O₃)_x are used in magnetic applications and have $-HB$ values in the range $2 \rightarrow 80 \text{ J m}^{-3}$.

On the other hand, it should be close to zero for alternating current transformers which like motors and generators, operate by constantly magnetising and demagnetising their core material. The laminations⁵ of ferromagnetic steels that are stacked together to form the core have very small H_c , i.e., are easy to magnetise and demagnetise easily. A small H_c leads to a very narrow loop associated with minimal energy loss. Samarium cobalt and Nd₂Fe₁₄B are powerful permanent magnets with $-HB = 120 \rightarrow 240 \text{ J m}^{-3}$. They obviously contain elements that are in short supply.

Example 35: Tetrataenite

Tetrataenite is an atomically ordered Fe-Ni compound with equal atomic fractions of each element. It forms in meteorites but only at temperatures below 321 °C [18, 19]. It is of interest because it has a large coercivity and at the same time should be cheap, and possibly compete against the powerful but expensive magnetic material available. Why is this not manufactured on Earth?

Solution 35

In the absence of impacts, the meteorites cool from the red-hot state ($> 1500 \text{ K}$) at 1-1000 K per million years [20]. This is why tetrataenite occurs in meteorites. Suppose we manufacture Fe-Ni by casting, it would not be tetrataenite, but rather a disordered solution of the two elements. It is impossible to heat treat it below 321 °C in order to achieve atomic ordering, because it would take 10^4 years for either Fe or Ni to execute one atomic jump [21].

5. Laminated to reduce eddy currents and associated losses.

REFERENCES

1. L. C. de Wreede: ‘Willebrord Snellius (1580-1626) – a humanist reshaping the mathematical sciences’: Ph.D. thesis, Universiteit Utrecht, The Netherlands, 1974.
2. C. Kittel: Introduction to Solid State Physics: 8th ed., New York, USA: John Wiley and Sons Inc., 2005.
3. G. Pekkan, K. Pekkan, B. Ç. Bayindir, M. Özcan, and B. Karasu: ‘Factors affecting the translucency of monolithic zirconia ceramics: A review from materials science perspective’, *Dental materials journal*, 2020, **39**, 1–8.
4. D. A. Gryvnak, and D. E. Burch: ‘Optical and infrared properties of Al_2O_3 at elevated temperatures’, *Journal of the Optical Society of America*, 1965, **55**, 625–629.
5. N. K. K. Thein, A. Htet, and T. T. Aye: ‘Optical properties of natural dye from strawberry fruits as photosensitizer for dye-sensitized solar cells application’, *University of Mandalay Research Journal*, 2020, **11**, 178–186.
6. Y. Yang, and Y. Zhang: ‘Passive daytime radiative cooling: Principle, application, and economic analysis’, *MRS Energy & Sustainability*, 2020, **7**, 1–8.
7. H. K. D. H. Bhadeshia, and H. Yan: ‘Phase transitions – an introduction with worked examples, published independently’: www.phase-trans.msm.cam.ac.uk/2022/EMS523U_book.pdf, 2024.
8. S. S. Brenner: ‘Tensile strength of whiskers’, *Journal of Applied Physics*, 1956, **27**, 1484–1491.
9. H. K. D. H. Bhadeshia: ‘High-strength steels’, In: J. A. Charles, G. W. Greenwood, and G. C. Smith, eds. *Future Developments of Metals and Ceramics*. London, U.K.: Institute of Materials, 1992:25–74.
10. F. Pockels: ‘Ueber den einfluss elastischer deformationen, speciell einseitigen druckes, auf das optische verhalten krystallinischer körper (on the influence of elastic deformations, especially unilateral pressure, on the optical behavior of crystalline bodies)’, *Annalen der Physik*, 1889, **273**, 144–172.
11. F. Pockels: Ueber den Einfluss des elektrostatischen Feldes auf das optische Verhalten piezoelektrischer Krystalle (On the influence of the electrostatic field on the optical behavior of piezoelectric crystals), vol. 39: Germany: Dieterichsche Verlags-Buchhandlung, 1894.
12. J. Kerr: ‘The Reverend Dr John Kerr, FRS’, *Nature*, 1907, **76**, 575–576.
13. J. Kerr: ‘XL. A new relation between electricity and light: Dielectrified media birefringent’, *The London, Edinburgh, and Dublin Philosophical Magazine and Journal of Science*, 1875, **50**, 337–348.
14. J. Kerr: ‘LIV. A new relation between electricity and light: Dielectrified media birefringent (second paper)’, *The London, Edinburgh, and Dublin Philosophical Magazine and Journal of Science*, 1875, **50**, 446–458.
15. J. Kerr: ‘XXVI. Electro-optic observations on various liquids’, *The London, Edinburgh, and Dublin Philosophical Magazine and Journal of Science*, 1879, **8**, 229–245.
16. J. Billaud, F. Bouville, T. Magrini, C. Villevieille, and A. R. Studart: ‘Magnetically aligned graphite electrodes for high-rate performance Li-ion batteries’, *Nature Energy*, 2016, **1**, 1–6.
17. P. Wilkes: Solid state Theory in Metallurgy: Cambridge, U. K.: Cambridge University Press, 1973.
18. J. Pauleve, D. Dautreppe, J. Laugier, and L. Néel: ‘Une nouvelle transition ordre-désordre dans Fe-Ni (50-50)’, *Journal de Physique et le Radium*, 1962, **23**, 841–843.
19. L. Swartzendruber, V. Itkin, and C. Alcock: ‘The Fe-Ni (iron-nickel) system’, *Journal of Phase Equilibria*, 1991, **12**, 288–312.
20. R. J. Lyons, T. J. Bowling, F. J. Ciesla, T. M. Davison, and G. S. Collins: ‘The effects of

- impacts on the cooling rates of iron meteorites', *Meteoritics & Planetary Science*, 2019, **54**, 1604–1618.
21. R. Scorzelli: 'A study of phase stability in invar Fe-Ni alloys obtained by non-conventional methods', *Hyperfine Interactions*, 1997, **110**(1), 143–150.

Chapter 8

Two-dimensional materials, superconductors

8.1 INTRODUCTION

8.2 HALL EFFECT

Edwin Herbert Hall, while working with Professor John Rowland at John Hopkins University, discovered in 1879 that when a magnetic field is applied perpendicular to the flow of electric current in a conductor or semiconductor, it causes a field (E_{Hall}) to develop across the material, perpendicular to both the current and the magnetic field [1].¹

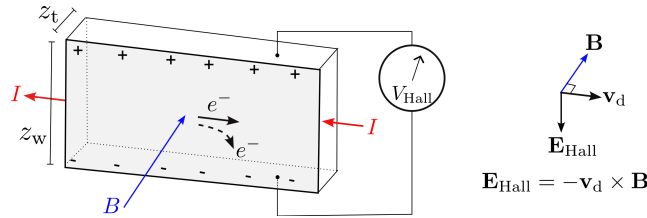


FIGURE 8.1 A magnetic field B applied normal to the metal sheet in which electrons flow from left to right, induces a Hall field E_{Hall} across the sheet in a direction that is normal to both the current flow and the magnetic field. The dashed arrow shows a transient effect, in which the magnetic field induces some electrons to migrate downwards, until the E_{Hall} that opposes this motion reaches a balance with the effect of the field. The thickness and width are labelled z_t and z_w , respectively.

In the context of the Hall effect, written using vector notation,

$$\mathbf{E}_{\text{Hall}} = -\mathbf{v}_d \times \mathbf{B} \quad (8.1)$$

where the direction of the electric field is defined as that in which a positive charge would move, \mathbf{v}_d is the drift velocity of the charge carrier and \mathbf{B} is the magnetic field.

The current $I = nAqv_d$, where n is the number of charge carriers per unit volume, q is the charge on each carrier, and A is the area across which the current flows.

1. ‘... if a strong magnetic force were made to act perpendicularly to the face of the disk a new electromotive force would be set up, which would be always perpendicular to the direction of the magnetic force and to the actual direction of flow of the electricity. . . [2].’

Since the Hall voltage $V_{\text{Hall}} = E_{\text{Hall}} \times z_w$, and given that the current flows in the $-v_d$ direction, it follows that

$$V_{\text{Hall}} = \frac{IB}{nz_t q}. \quad (8.2)$$

8.3 GRAPHENE DEVICE

It follows from Equation 8.2 that the Hall voltage detected increases as the thickness z_t is reduced. Suppose graphene (Figure 8.2) is used to make a Hall effect sensor [3], the thickness would be the smallest possible, giving greater sensitivity to magnetic fields.

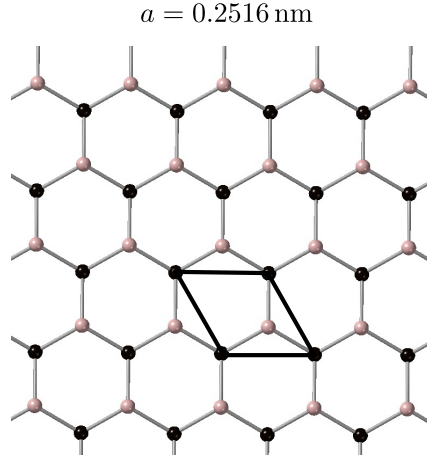


FIGURE 8.2 All the atoms in the image are carbon, but different colours indicate coordinates that are not crystallographically equivalent, because the highlighted, two-dimensional, hexagonal unit cell of graphene has a motif of two carbon atoms per lattice point.

In its perfect form, the carbon atoms are sp^2 hybridised, meaning that one s orbital and two p orbitals from the carbon atom combine to form three equivalent hybrid orbitals. This leaves one unhybridised p orbital. The sp^2 orbitals are arranged to form the 120° bonds illustrated. The unhybridised p orbitals of adjacent carbon atoms delocalise to form π -bonds. This delocalisation gives the graphene a large electrical conductivity and the charge carriers have unprecedented room temperature mobility [4] with mean-free-paths in the micrometre domain. It is possible therefore, to make Hall effect sensors that have reduced electronic noise while at the same time, able to detect minute magnetic fields.

Paragraf has developed a technology to make large area graphene, and markets graphene Hall-effect sensors. The sensors offer high sensitivity, low power consumption, and the cryogenic version of their sensor is able to function down to 10 mK. It can measure magnetic fields from microtesla to more than 7 Tesla.

Their high-field cryogenic sensor has a sensing range ± 30 T. The devices have an additional thinness-advantage in that stray field effects are absent. The ‘stray field’ refers to interference by field components that are not normal to the sensing plane of thick 3-dimensional devices, which lead to false signals. The graphene sensor in contrast, measures along a single direction.

Given the large electron mobility, graphene Hall sensors operate at a thousandth of the power of silicon Hall sensors. The device is made by depositing the graphene on to a wafer substrate using a proprietary metal-organic vapour deposition process, so that a two-dimensional single-crystal can form over a large area. The graphene is coated with a dielectric layer so that only its edges are exposed, in order to prevent contamination. It is then metallised in controlled regions and scribed into smaller segments for device fabrication.

Each wafer segment is then connected to conductors and encapsulated in ceramic such that the graphene is about 0.47 mm from the top surface of the finished device, with an active area 0.25 mm^2 , Figure 8.3. There are four pairs of pins (each pair connected to each other, e.g., 1 and 2 are connected to each other inside the package); the ohmic contacts are to the edge of the graphene layer, rather than to its surface, which has the advantage of improved current injection. Two sets on opposite sides (1-2 and 5-6) can be supplied with an input voltage and the other orthogonal set used to monitor the Hall voltage.

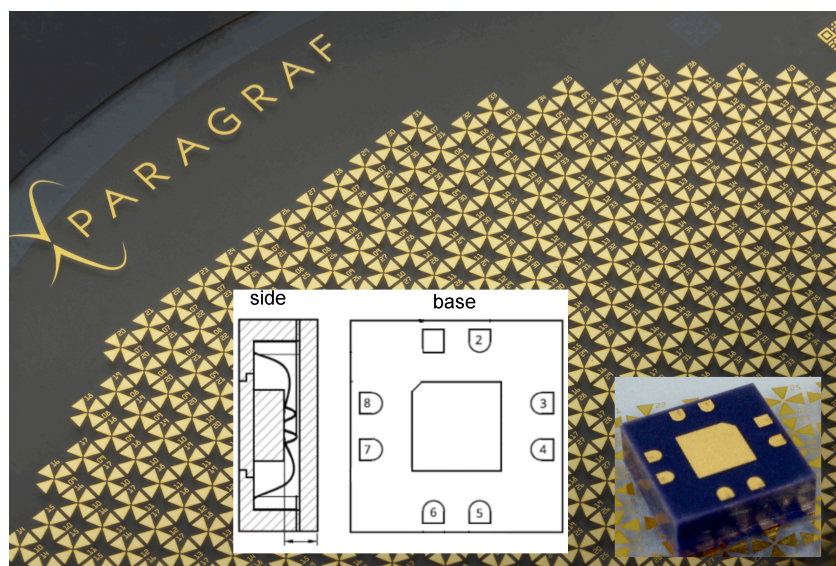


FIGURE 8.3 Showing a wafer, the finished product on the right, and a technical drawing showing the connection pins and the internal structure of the 1.1 mm thick device. Adapted from images and information courtesy of *Paragraf* via Colin Humphreys.

The general purpose graphene-sensor can measure magnetic fields in the minimum-range ± 2 T over a temperature range $-40 \rightarrow 125$ °C. Figure 8.4 shows it being tested at low temperatures. By measuring the resistance between the contacts across which the input voltage is applied, the device temperature can be determined directly. Graphene has a stable electrical resistance versus temperature relationship, in contrast to materials such as silicon, thus enhancing the accuracy of the temperature measurement over the service life of the sensor.

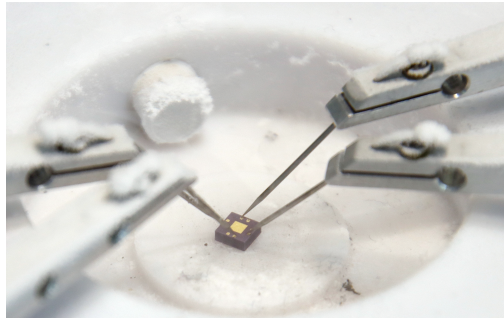


FIGURE 8.4 Testing the graphene Hall-effect sensor at low temperatures. Image courtesy of *Paragraf* via Colin Humphreys.

Example 36: Transparency of graphene

Why is graphene transparent? Could there be a use for this property?

Solution 36

Graphene does absorb visible light but the efficiency of the process is very limited, just 2.3%. The reason is the high mobility of electrons, which reduces the likelihood of scattering events that would lead to increased absorption.

Since a monolayer graphene absorbs 2.3% of incident light, many layers of graphene will absorb all the light and appear black. The ‘lead’ in pencils is a mixture of graphite and clay. When the pencil is used to write on paper, many layers of graphene are rubbed off so the writing appears black, since each layer progressively absorbs 2.3% of the incident light.

(A more complicated answer would explain the large mobility of charge carriers in graphene in terms of its band structure. There are six points in momentum space where the conduction and valence bands touch, i.e., the band gap is zero. This means that there is no barrier there, for the electrons to transition from the valence to the conduction band. This should enable the absorption of photons

in the visible spectrum. However, the rapid movement of charge carriers means that they may not remain in the vicinity of the photon long enough to interact effectively. This reduces the absorption of light, making graphene essentially transparent. Graphene is of course thin, but this is not the primary reason for transparency; for example, graphene oxide is opaque because of its different electronic structure.)

Indium tin oxide forms the transparent, conductive electrode on most touch-screen devices such as telephones and computers. Graphene too is an excellent electrical conductor, and is transparent and flexible so could form the basis of touch-screen devices. A limitation to its use in this application is the ability to deposit large areas of single-layer graphene directly on to a transparent substrate. This difficulty has been overcome commercially using metal-organic chemical vapour deposition. Figure 8.5 shows a favourable comparison of the optical transparency of the single-layer graphene against the indium tin oxide [5].

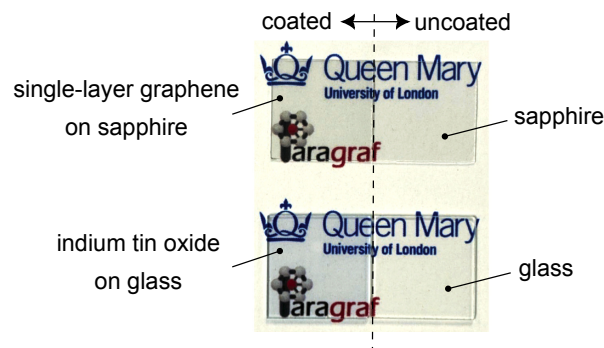


FIGURE 8.5 Showing the optical images of single-layer graphene on sapphire and indium tin oxide on glass. On the right of the dashed line are the uncoated substrates. Image courtesy of Oliver Fenwick with details in [5].

8.4 SUPERCONDUCTORS

A material is a *superconductor* when it has not just a low electrical resistance, but *no* electrical resistance below a finite low temperature T_{sc} [6]. The resistance reappears above that temperature. The word *finite* is important because prior to the discovery of superconduction, it was believed that the electrical resistance of a metal would vanish at 0 K. The phenomenon was discovered by Heiki Kamerlingh Onnes at Lyden University when in 1911 [7], he observed that solid mercury when cooled to temperatures below 4.22 K abruptly lost resistance to the passage of an electrical current, Figure 8.6.

A current established in a closed loop of superconducting wire circulates ‘in-

definitely' without the need for a power source to sustain it [8]; the duration of the persistence was limited in the old days by how long the liquid helium used to cool the metal would last. This is less of a difficulty in modern times so the current has been demonstrated to persist for at least $2\frac{1}{2}$ years, implying a resistivity of less than $10^{-21} \Omega \text{ cm}$ [p.503, 9]. It is theoretically estimated that the lifetime of the persistent current in a superconducting loop that is interrupted by single junction of a particular kind, is 10^{12} years. limited by random fluctuations [10].

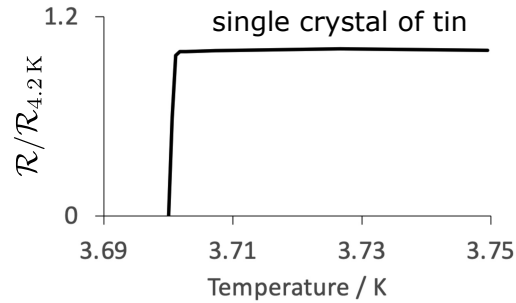


FIGURE 8.6 The rapid drop in electrical resistivity (ratio) as a function of temperature for pure tin in single-crystalline, wire form, $T_{sc} \approx 3.7^\circ \text{C}$. Adapted using selected data from de Haas, quoted in [11].

To understand the mechanism of superconductors, one must appreciate that electrons are charged particles that carry current, and that phonons represent the collective vibrations of the atoms in the lattice. Bardeen, Cooper and Schrieffer first developed a theory that explained much of the experimental behaviour of metallic superconductors [12]. One might assume that electrical conduction in metals occurs by the uncorrelated motion of valence electrons, which should repel each other given their like charges, though the repulsion is small at large separations because of the screening due to nearby electrons. When an electron moves through the lattice of positive ions, it pulls the ions in its vicinity towards itself, leading to a slightly positive charge in its neighbourhood. Another electron moving through the distorted region will experience an attractive force towards the first electron because of the positive charge created by the lattice distortion. This interaction is mediated by phonons, i.e., the interactions between the two electrons occurs through the exchange of phonons. These 'Cooper pairs' of electrons that have opposite spins and momenta, so the pair has a net zero spin, which means they do not obey the Pauli exclusion principle. Any number of pairs can occupy the same quantum state. As a result, they are able to condense with other Cooper-pairs into a single, macroscopic wave function, which enables them to move through the lattice without scattering, leading to the superconducting state.

Cooper pairs are weakly coupled, so thermal vibrations become sufficiently

energetic beyond T_{sc} to break them, leading to a loss of superconductivity. It is an obvious advantage from a practical point of view for the superconducting material to have a reasonably large T_{sc} . The niobium-tin compound Nb_3Sn has $T_{sc} = 18.3$ K and has large scale applications, for example in the superconducting magnets at the large Hadron collider (CERN) and in magnetic resonance imaging scanners in hospitals.

8.4.1 Meissner effect

In a paper published in 1933, Meissner and Ochsenfeld found that if a cylindrical, lead superconductor is placed in a homogenous magnetic field normal to its axis, the field inside the tube becomes zero below T_{sc} , i.e., the superconductor expels the field [13], Figure 8.7.

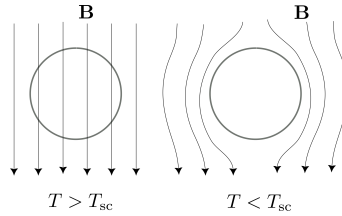


FIGURE 8.7 Shows how below T_{sc} the applied magnetic field is excluded from the superconductor.

The mechanism of the Meissner effect is related to the condensation of the Cooper pairs into a collective ground state without being scattered. When the superconductor is below T_{sc} in a magnetic field, currents are generated within a thin layer near the surface of the superconductor, that perfectly cancel the magnetic field inside the bulk of the superconductor. The applied field is therefore expelled.² The superconducting state can vanish if the applied field strength is above a critical value. Without going into detail, certain superconductors do permit magnetic flux lines to penetrate in the form of quantised vortices, which permit the superconducting properties to persist in applied fields, meaning that they can carry larger superconducting currents.

Example 37: Estimation of T_{sc}

Cooper pairs are pairs of electrons that are bound together at low temperatures, leading to superconductivity. The binding energy of Cooper pairs in Nb_3Sn

2. In normal conductivity, electrons experience resistance due to scattering. When an external magnetic field is applied or changed, induced currents would try to oppose it (Lenz's law), but these currents rapidly decay due to resistance, preventing sustained, organised surface currents required for magnetic field expulsion.

is about 3.2×10^{-22} J. Estimate the temperature below which the compound becomes superconducting.

Solution 37

It might be reasonable to assume that a Cooper pair is disrupted by thermal energy, causing the pair to become unbound. The material will cease to become superconducting when thermal agitation overcomes the binding energy. If the energy due to thermal vibrations is written $\frac{3}{2}kT$ ($\frac{1}{2}kT$ for each degree of freedom). Given $k = 1.3807 \times 10^{-23} \text{ J K}^{-1}$ then

$$T_{\text{sc}} \approx \frac{3.2 \times 10^{-22}}{1.5 \times 1.3807 \times 10^{-23}} = 15.45 \text{ K.} \quad (8.3)$$

The actual $T_{\text{sc}} = 18.3 \text{ K}$, page 135.

However, Nb_3Sn is brittle so pure niobium, which is a ductile body-centred cubic metal, is inserted into bronze (Cu-Sn solid solution), drawn out into wire form, and then heat treated so that the tin in the bronze reacts completely with the niobium wires to produce the Nb_3Sn , Figure 8.8a; the pure niobium used is illustrated in Figure 8.8b. The central core is pure copper, separated from the bronze by a diffusion barrier made of tantalum. The diffusion barrier prevents the tin in the bronze from entering the copper core. The copper core is required to control eddy currents. The outer shell of bronze contains the superconducting Nb_3Sn filament bundles made by reacting the tin in the bronze with the niobium. Note that very strong magnetic fields can lead to a break up of the Cooper pairs, but for Nb_3Sn , the limiting field is about 30 T. Superconduction also breaks down if the current exceeds a critical value, which for Nb_3Sn is of the order of $180 \rightarrow 500 \text{ A}$, depending on processing, strain, magnetic field etc.

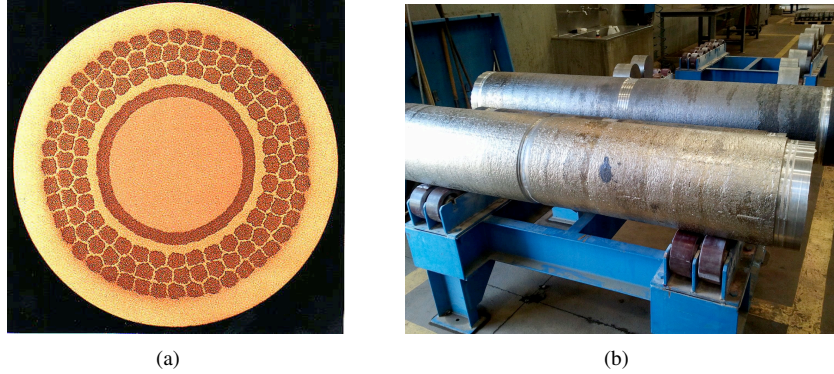


FIGURE 8.8 (a) Superconducting composite created by reacting tin within the bronze with pure niobium. A diffusion barrier prevents the tin in the bronze from entering the copper core, which is required to control eddy currents. The outer shell of bronze contains the superconducting Nb_3Sn filament bundles. Image courtesy of Jan Evetts. (b) High-purity niobium ingots produced by electron beam melting at CBMM in Brazil (www.phase-trans.msm.cam.ac.uk/2011/CBMM/index.html).

If $T_{\text{sc}} > 77 \text{ K}$, liquid nitrogen can be used to cool the superconductor rather than the much more expensive liquid-helium refrigerant. However, the Cooper pairing mechanism where small charge re-arrangements induce an attractive force between pairs of electrons, can be disrupted by lattice vibrations (phonons)³, setting $T_{\text{sc}} \lesssim 30 \text{ K}$.

High-temperature oxide superconductors such as the original LaBaCuO with $T_{\text{sc}} \approx 30 \text{ K}$ [14] and the huge efforts since then have discovered with T_{sc} reaching 140 K . It has to be said that there is no unified theory that explains the mechanism by which high superconducting transition temperatures are achieved in these materials. Bearing in mind that the oxides are brittle and difficult to work with in wire or tape form limits applications. Potential applications include devices such as magnetic bearings. Perhaps the neodymium based permanent magnets in wind turbines, can in principle be replaced by an oxide superconducting magnet assembly, that would be much smaller (Figure 8.9), though necessitating cooling systems [15, 16]. The superconductor forms the field coils in the rotor of the generator assembly.

3. Vibrational excitations of small amplitude such that every displaced ion returns to its original position.

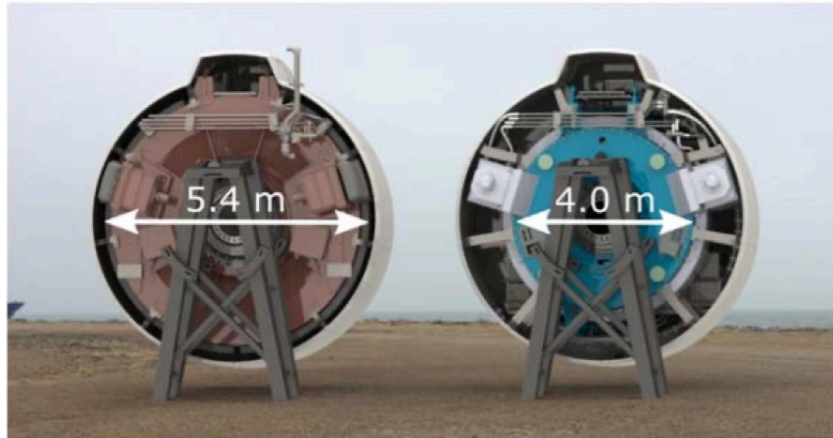


FIGURE 8.9 Conventional permanent magnet wind-turbine generator on the left, with the GdBaCO superconducting magnet generator on the right. This represents the world's first test using a 3.6 MW wind generator. The superconducting tapes are wound to the dimensions marked. Reproduced from Bergen et al. [15] under the CC BY 3.0 license, <https://creativecommons.org/licenses/by/3.0/>.

In general, the high T_{sc} superconductors have not achieved commercial exploitation [17]. Tapes of $\text{ReBa}_2\text{Cu}_3\text{O}_7$ are produced in quantity for anticipated applications in motors, generators, fault current limiters, fusion magnets and cables, but are not commercially available. The mercury based superconductors with $T_{sc} \approx 134 \text{ K}$ are toxic so their application will not be permitted.

REFERENCES

1. E. H. Hall: ‘On the new action of the magnet on electric currents’, *American Journal of Mathematics*, 1879, **2**, 287–292.
2. E. H. Hall: ‘On the new action of magnetism on a permanent electric current’, *American Journal of Science*, 1880, **3**, 161–186.
3. D. Collomb, P. Li, and S. Bending: ‘Frontiers of graphene-based hall-effect sensors’, *Journal of Physics: Condensed Matter*, 2021, **33**, 243002.
4. L. Wang, I. Meric, P. Huang, Q. Gao, Y. Gao, H. Tran, T. Taniguchi, K. Watanabe, L. Campos, D. Muller, et al.: ‘One-dimensional electrical contact to a two-dimensional material’, *Science*, 2013, **342**, 614–617.
5. Z. Weng, S. C. Dixon, L. Y. Lee, C. J. Humphreys, I. Guiney, O. Fenwick, and W. P. Gillin: ‘Wafer-scale graphene anodes replace indium tin oxide in organic light-emitting diodes’, *Advanced Optical Materials*, 2022, **10**, 2101675.
6. M. Bragg, N. Hussey, S. Sebastian, and S. Blundell: ‘Superconductivity’: Podcast: <https://www.bbc.co.uk/sounds/play/m001hfpc>, Jan 2023.
7. H. K. Onnes: ‘The resistance of pure mercury at helium temperatures’, *Communications of the Physics Laboratory, University of Leiden*, 1911, (No.120).
8. H. K. Onnes: ‘Further experiments with liquid helium. L. The persistence of currents without electromotive force in supra-conducting circuits’: In: *Through Measurement to Knowledge: The Selected Papers of Heike Kamerlingh Onnes 1853–1926*. Springer, 1991:356–362.
9. A. H. Cottrell: *An Introduction to Metallurgy*: London, U.K.: Edward Arnold, 1971.
10. A. Goldman: ‘Lifetimes of persistent currents in superconducting loops interrupted by Josephson junctions’, *Journal of Low Temperature Physics*, 1970, **3**, 55–63.
11. J. McLennan: ‘Electrical phenomena at extremely low temperatures’, *Reports on Progress in Physics*, 1934, **1**, 198.
12. J. Bardeen, L. N. Cooper, and J. R. Schrieffer: ‘Theory of superconductivity’, *Physical Review*, 1957, **108**, 1175–1203.
13. W. Meissner, and R. Ochsenfeld: ‘Ein neuer effekt bei eintritt der supraleitfähigkeit (a new effect when superconductivity occurs)’, *Naturwissenschaften*, 1933, **21**, 787–788.
14. J. G. Bednorz, and K. A. Müller: ‘Possible high t_c superconductivity in the Ba-La-Cu-O system’, *Zeitschrift für Physik B Condensed Matter*, 1986, **64**, 189–193.
15. A. Bergen, R. Andersen, M. Bauer, H. Boy, M. t. Brake, P. Brutsaert, C. Bühner, M. Dhallé, J. Hansen, H. ten Kate, et al.: ‘Design and in-field testing of the world’s first ReBCO rotor for a 3.6 MW wind generator’, *Superconductor Science and Technology*, 2019, **32**, 125006.
16. X. Song, C. Bühner, A. Mølgaard, R. S. Andersen, P. Brutsaert, M. Bauer, J. Hansen, A. V. Rebsdorf, J. Kellers, T. Winkler, et al.: ‘Commissioning of the world’s first full-scale MW-class superconducting generator on a direct drive wind turbine’, *IEEE Transactions on Energy Conversion*, 2020, **35**, 1697–1704.
17. B. Glowacki: ‘Private communication to H. K. D. H. Bhadeshia’, 2025: High T_{sc} superconductors.

8.5 RANDOM QUESTIONS

1. You are designing a safety circuit for a high-power light-emitting diode system that operates in an enclosed, unventilated space. The goal is to prevent the diodes from overheating, which can drastically reduce their lifespan and efficiency. How could this system be designed to incorporate temperature protection and to reset automatically as the temperature decreases?
2. What are the most critical remaining technical and economic challenges that lead-free piezoelectrics must overcome to realistically compete with lead zirconate titanate in a broad range of high-performance applications?
3. Why does the electrical resistivity of iron increase with temperature but that of zirconia decreases when heated?
4. An electrical engineer is designing the power input stage for a sensitive medical diagnostic device that operates in varied environments, including remote clinics with potentially unstable power grids. This device absolutely cannot tolerate significant voltage surges. How could this be achieved?
5. Despite all materials being diamagnetic, we typically categorise substances as paramagnetic, ferromagnetic, or diamagnetic. Why is diamagnetism usually so weak in most materials, and what makes materials like pyrolytic graphite exceptionally diamagnetic?
6. Why does it take a temperature of almost a million Kelvin to promote large number of electrons in a filled aluminium band into the conduction band?
7. Would you expect a metal to lose electrical conductivity as its size decreases?
8. How would you evaluate a new polymeric material intended for use as a cable insulation in an underground distribution network? The cables will operate at high voltages and are exposed to environmental stresses over decades. The manufacturer claims the material has an excellent intrinsic dielectric strength.
9. From a sustainability and resource perspective, what significant advantages would widespread industrial production of synthetic tetraenaite magnets offer compared with present day technologies?
10. You synthesise two new transition metal oxide compounds, Compound A and Compound B. Both compounds contain magnetic ions with unpaired electrons. Upon cooling, Compound A becomes a strong permanent magnet, but Compound B, despite having ordered spins, shows no measurable macroscopic magnetic moment. What can you conclude from this information?
11. How does the orientation of the applied electric field relative to the crystallographic axes affect the magnitude of the piezoelectric response (strain or polarisation) in a single crystal of barium titanate BaTiO_3 ?
12. Are there any non-metals that are really good electrical conductors?
13. Can a metal be made transparent to visible light? Justify your answer.
14. Some crystals have a structure with a centre of symmetry, others do not. How does this feature in the context of functional materials?
15. Beyond temperature, what are the two other critical parameters that can destroy superconductivity in a material?

16. What kinds of charge carriers play a role in determining the electrical conductivity of a material?
17. While both electrostriction and piezoelectricity involve the coupling of electrical and mechanical phenomena in dielectric materials, what fundamental difference in crystal structure leads to piezoelectric materials exhibiting a linear relationship between applied electric field and induced strain, whereas electrostrictive materials exhibit a quadratic relationship?
18. What are the material properties that must be optimised to achieve the very short rise times in a piezoelectric transducer?
19. Explain the primary advantage of an all-optical switch over an electronic switch, when considering the routing of data streams at speeds in excess of 100 gigabits per second.
20. Can all elements in the periodic table be made metallic, and if so, how?
21. Elaborate on two specific intrinsic properties of graphene that make it theoretically superior to conventional semiconductor materials for achieving exceptionally high sensitivity in a Hall effect sensor at room temperature.
22. You are given three, unlabelled solid samples. You determine that Sample A has no unpaired electrons, Sample B has a significant number of unpaired electrons but no long-range magnetic ordering, and Sample C has unpaired electrons with strong exchange interactions leading to magnetic domains. Classify, with justification, each sample as diamagnetic, paramagnetic, or ferromagnetic.

Subject index

Antenna, 36
Antiferroelectrics, 55
Antiferromagnetism, 125
BaBi₂Nb₂O₉, 82
Band theory, 5
BaTiO₃, 16, 27–29, 78
Bi_{0.5}Na_{0.5}TiO₃, 80
Bismuth ferrite, 50
Bohr magneton, 120
Breakdown, 1, 76
CaCu₃Ti₄O₁₂, 36
Cadmium selenide, 10
Calcium oxide, 11
Candela, 97
Capacitors, 25
Centre of symmetry, 64, 80
Conduction
 activation energy, 3
Conductivity, 1
 electronic, 2
 Ionic, 2
 ionic, 10
 Siemens, 2
 solid electrolyte, 2, 10
Curie temperature, 3, 16, 79, 120
Curie-Weiss law, 44
Diamagnetism, 121
 anisotropic, 122
Dielectric resonator, 36
Dielectric strength, 18
Dielectrics, 25
 capacitors, 25
 linear, 43
 nonlinear, 43
 silica, 25
Dipolar polarisation, 30
Domain structures, 47, 93
ferroelectric, 45
ferroelectric domains, 29
magnetic, 125
wall mobility, 47
Double hysteresis, 92
Drift velocity, 1
Electrical breakdown, 17
 field induced, 17
 temperature induced, 17
Electrical conductivity, 1
Electrical current density, 1
Electromagnetic spectrum, 110
Electromechanical
 breakdown, 17
 coupling, 69, 79
Electronic polarisation, 32
Ferrimagnetism, 125
Ferroelectric oxides, 43
Ferromagnetism, 125
Free electrons, 5
Gallium arsenide, 37
Gold, 5
Graphene, 96
 Hall effect, 131
 transparency, 133
Graphite, 122
Hall effect, 130
Hydrogen
 metallic, 5
Indium tin oxide, 134
Insulator, 5
Ionic polarisation, 27, 32
junctions, *p-n*, 12

- K_{0.5}Na_{0.5}NbO₃, 79
- Kröger-Vink notation, 11, 16
- KH₂PO₄, 119
- Layered ferroelectrics, 80
- LiNbO₃, 40, 74, 116, 119
- Lithium-ion battery, 122
- Loss tangent, 35
- Magnetism
 - antiferromagnetism, 125
 - diamagnetism, 121
 - ferrimagnetism, 125
 - ferromagnetism, 125
 - Lenz's law, 121
 - negative susceptibility, 121
 - paramagnetism, 124
- Meissner effect, 136
- Mobile telephone, 5
- Mobility of charge, 1
- Molecular ferroelectric, 95
- Multilayer capacitor, 36
- Néel temperature, 125
- Na_{0.5}K_{0.5}NbO₃, 51
- NaK_{0.5}Nb_{0.5}O₃, 48
- Ohm's law, 1
- Opacity, 110
- Optical and magnetic materials, 110
- Order-disorder transformation, 125
- Organic materials, 87
 - electrical conductivity, 97
 - LED, 97
 - polarisation, 88
 - polymer composites, 90
- Orientational polarisation, 30
- Oxides, 43
- Paraelectric, 92
- Paramagnetism, 124
- Pb(Zr_xTi_{1-x})O₃, 82
- Pb(Zr_xTi_{1-x})O₃, 58
- PbTiO₃, 28, 29, 51, 77
- PbZrO₃, 55
- Permittivity, 26
 - giant, 36
 - ice, 31
- Perovskite, 2, 10
 - layered, 80
- Pierre Curie's balance, 62
- Piezoelectrics, 61
 - efficiency, 68
- Polarisation
 - electronic, 31, 93
 - ionic, 31
- Poling, 53, 58, 64, 67, 77, 95
- Polyacetylene, 96
- Polycarbonate, 91
- Polyethylene, 92
- Polymer composite, 91
- Polyvinyl chloride, 89
- Polyvinylidene fluoride, 91
- Polyvinylidene fluoride, 58, 93
- Quantum dots, 10
- Relaxor, 93
- Relaxor ferroelectrics, 54, 58, 92
- Resistance, 1
- Rochelle salt, 41, 43, 95
- Semiconductor
 - intrinsic, 5
- Space charge, 30
- Sr₂Nb₂O₇, 3
- SrBi₄Ti₄O₁₅, 43, 44
- SrBi₄Ti₄O₁₅, 58
- Strontium niobate, 3

- Superconduction, 134
 - Cooper pairs, 135
 - Hadron collider, 135
 - Meissner, 136
 - Nb_3Sn , 137
 - oxides, 138
- Terahertz probe, 37
- Thermistors, 15
- Thermoelectrics, 100
- Two-dimensional, functional
 - materials, 130
- Varistors, 14
- Yttria, 2, 10
- Zirconia, 2, 10, 37
 - phase transitions, 10
 - stabilisation, 10

Functional materials represent those specifically designed to exhibit unique and often tuneable physical or chemical properties in response to external stimuli. They are valued for their 'function' - their ability to perform a specific task or change their behaviour under certain conditions. They can change their shape, electrical conductivity, magnetic properties, colour, or other characteristics when exposed to temperature, pressure, electric fields, magnetic fields, light, or chemical changes. Materials with electrical conductivity between that of a metal and an insulator are the basis of electronics. Long-chain molecules too have functionalities, including flexibility and charge mobility. Ordered arrangements of molecules can be useful in optics. Inorganic, non-metallic solids such as ceramics can be exploited for properties like piezoelectricity, and for elevated temperature service.



This short book serves as an introduction, providing sufficient and complete coverage of concepts suitable for a final year undergraduate course. It includes worked examples to aid understanding and is designed for third-year students across a range of disciplines, including materials science, engineering, chemical engineering, physics, chemistry, Earth sciences, and general physical sciences. For those wishing to explore the topics in greater depth, references are provided at the end of each chapter.

